UNIVERSITY OF CALIFORNIA, SAN DIEGO

New Insights Into Unconventional Splicing and Modulation of RNase Activities of IRE1, a Multifunctional UPR Component

A dissertation submitted in partial satisfaction of the
requirements for the degree Doctor of Philosophy

in

Biology

By

Arvin B. Tam

Committee in charge:

Maho Niwa, Chair
Gourisankar Ghosh
Randolph Hampton
Alexander Hoffmann
Ze'ev Ronai
Inder Verma

2011

The Dissertation of Arvin B. Tam is approved, and it is acceptable in quality and form for publication on microfilm and electronically:

_____

_____

_____

_____

_____

_____
Chair

University of California, San Diego

2011

TABLE OF CONTENTS

LIST OF FIGURES

Chapter 2

Chapter 3

VITA

Ph.D. Biology, 2011, University of California, San Diego, CA 92093

B.S. Biochemistry, with Honors, June 2000, Minor in Religious Studies, University of California, Riverside, CA 92521

PUBLICATIONS:

Ioanna Papandreou, Nicholas C. Denko, Michael Olson, Heleen Van Melckebeke, Sofie Lust, Arvin Tam, David E. Solow-Cordero, Donna M. Bouley, Fritz Offner, Maho Niwa, and Albert Koong. Identification of an Ire1alpha endoribonuclease specific inhibitor with cytotoxic activity against human multiple myeloma. Blood. Nov. 16, 2010

DuRose JB, Tam AB, Niwa M. 2006. Intrinsic Capacities of Molecular Sensors of the Unfolded Protein Response to Sense Alternate Forms of Endoplasmic Reticulum Stress. Molecular Biology of the Cell. Jul;17(7):3095-107

Zheng ZL, Nafisi M, Tam A, Li H, Crowell DN, Chary SN, Schroeder JI, Shen J, Yang Z. 2002. Plasma membrane-associated ROP10 small GTPase is a specific negative regulator of abscisic acid responses in Arabidopsis. Plant Cell. Nov;14(11):2787-97.

Szick-Miranda K, Jayachandran S, Tam A, Werner-Fraczek J, Williams AJ, Bailey-Serres J. Evaluation of Translational Control Mechanisms in Response to Oxygen Deprivation in Maize. 2003. Russian Journal of Plant Physiology. Vol 50, No 6. 774-786.

TEACHING AND MENTORING:

Teaching Assistant – Moleuclar Biology; Cell Biology; Biochemistry Techniques ; Department of Biology; University of California, San Diego

Graduate Advocate: Summer Training Academy for Research in the Sciences (STARS) Program – Summer 2006

GUIDE Peer Advocate – 2008

HONORS AND AWARDS:

Ford Foundation Graduate Fellowship 2006-2009

NSF Graduate Student Fellowship-Honorable Mention 2005

Department of Biology TA Excellence Award 2004-2005

NIH/UCSD Scholar 2003-2004

ABSTRACT OF THE DISSERTATION

New Insights Into Unconventional Splicing and Modulation of RNase Activities of IRE1, a Multifunctional UPR Component

By

Arvin B. Tam

Doctor of Philosophy

University of California, San Diego, 2011

Professor Maho Niwa, Chair

The endoplasmic reticulum (ER) is an important organelle where secreted and membrane proteins are initially folded and processed properly. Professional secretory cells are especially sensitive to changes in ER folding need and must respond by adjusting ER folding capacity for proper secretion. The Unfolded Protein Response is a pathway that senses changes in ER requirement and increases ER function appropriately mainly by activation of several transcription factors which upregulate genes such as ER chaperones which increase ER folding capacity. However, if the distress in the ER cannot be solved, then the UPR can also activate cell death

pathways. IRE1 is an ER transmembrane protein and is the most evolutionarily conserved branch of the UPR, present from yeast to humans. It is a multifunctional protein containing a cytosolic domain with both kinase and nuclease functions. Its kinase function has been implicated in activation of cellular pathways such as JNK, while its nuclease is involved in unconventional splicing of an mRNA coding for a transcription factor. Splicing of this mRNA is a key event in activation of this UPR transcription factor. Here we show new insights into IRE1's functions and roles in the cell. We show that IRE1 is required for full activation of NF-κB, a transcription factor. Furthermore, IRE1 dependent NF-κB activation is required for full activation of a subset of UPR target genes, making it an integral part of the UPR. Also, we show that IRE1 is able to differentially recognize splice sites of its substrates, giving us increased understating of IRE1's unconventional splicing ability. Finally, we show direct evidence that IRE1 is able to cleave ER localized mRNAs, indicating an alternate activation mode for IRE1's nuclease. We also demonstrate that we are able to pharmacologically manipulate IRE1's nuclease modes which may be useful in targeting IRE1 related diseases.

Chapter 1

INTRODUCTION

Secreted and membrane bound proteins are translated into the endoplasmic reticulum (ER) where they are properly processed with the help of ER resident proteins. Chaperones ensure the proper folding of proteins, while other factors ensure proper glycosylation and isomerization of disulfide bonds which are critical for maintaining the correct structure and functions of these proteins. To guarantee proper cellular function, secreted and membrane proteins need to be accurately folded and modified, and since the ER is the first organelle where these events occur, the ER has the capacity to monitor and respond to demands in protein folding capacity. Consequently, the ER is able to regulate various aspects of cellular function to ensure ER homeostasis. Conversely, conditions that disrupt ER function present a threat to cell viability.

Several conditions are known to disrupt ER function leading to ER stress. Generally, an accumulation of unfolded proteins in the ER causes stress and disrupts homeostasis. This can be achieved through pharmacological agents such as thapsigargin, tunicamycin, and dithiotheitol which disturb calcium levels in the ER, inhibit glycosylation, and break disulfide bonds, respectively. However, genetic conditions that prevent a protein from being properly folded also lead to ER stress. One example is the Akita mouse which harbors a point mutation in the insulin gene and prevents formation of one disulfide bond. These mice display stressed ER and eventually develop diabetes (Araki et al., 2003). Recently, other conditions such as a high fat diet or free fatty acids have been shown to cause ER stress (Ozcan et al., 2003; Cnop et al., 2007). Taken together, conditions that present an imbalance between ER folding capacity versus folding load leads to ER stress.

In response to stress, the ER activates a set of signaling pathways collectively called the Unfolded Protein Response (UPR) which aims to restore ER homeostatis. The UPR has wide-ranging effects on the cell including initiation of a transcriptional profile through activation of

several transcription factors, global translation repression, and activation of apoptosis (reviewed in Ron and Walter Nat Rev 2007; Rutowski and Hedge JCB 2010). The ability of the ER to sense and respond to stress is evolutionarily conserved since this pathway is present from yeast to humans. ER stress can be sensed by ER transmembrane proteins that detect the presence of unfolded proteins in the lumen of the ER and relay signals through their cytosolic domains. In higher eukaryotes, UPR signaling is initiated by three sensors, the kinase/RNase IRE1, the kinase PERK, and the transcription factor ATF6. While in yeast, only IRE1 is present.

IRE1 is a type I ER transmembrane protein containing an ER luminal stress sensing domain and a cytosolic portion containing kinase and endoribonuclease domains and is the most evolutionary conserved component of the UPR. When activated, IRE1 initiates spliceosome independent splicing of specific mRNAs encoding for basic leucine zipper transcription factors, HAC1 in yeast and XBP1 in higher eukaryotes. Under unstressed conditions in yeast, translation of HAC1 mRNA is repressed due to interaction of a secondary structure element present in the intron with the 5' untranslated region (UTR) (Ruegsegger Cell 2001). During ER stress, HAC1 mRNA is targeted to IRE foci in the ER through a targeting element in the 3' UTR (Aragon Nature 2009). IRE1 is then able to cleave HAC1 at two stem loop structures (Sidrauski Cell 1997), releasing a 252 nucleotide intron and lifting the block in translation. Ligation of the exons by tRNA ligase results in a spliced form of HAC1 which is translated into an active transcription factor. In mammalian cells, IRE1 cleaves XBP1 mRNA also at two stem loop structures (Calfon Nature 2000), but unlike HAC1, unspliced XBP1 (XBP1u) is able to be translated although it lacks transactivation potential due to a missing transactivation domain. However, splicing of XBP1 by IRE1 results in excision of a 26 nucleotide intron and results in a frameshift that eliminates recognition of the original stop codon. A new downstream stop codon can be recognized after splicing resulting in a larger protein, spliced XBP1 (XBP1s) (Yoshida Cell

2001). XBP1s now contains a potent transactivation domain which makes it a potent transcription factor.

Under unstressed conditions, BiP was found to bind to the luminal domain of IRE1 and was previously thought to block dimerization of IRE1 since dissociation of BiP correlated with activation of IRE1(Bertolotti et al., 2000). However, it was later shown that luminal mutants of yeast IRE1 not able to bind BiP still had a normal ER stress response (Kimata et al., 2004). The crystal structure of the luminal domain of yeast IRE1 shows formation of an MHC-like groove that was able to bind to unfolded proteins (Credle et al., 2005). Consequently, activation of yeast IRE1 is proposed to involve two steps, BiP dissociation and binding of unfolded proteins to the luminal domain of IRE1 which properly orients the cytosolic domains (Kimata et al., 2007).

Activation of the luminal domain allows for trans-autophosphrylation of the cytosolic domain of IRE1. In yeast IRE1, autophosphorylation occurs in the S840, S841, T844 residues of the activation loop and induces a conformational change that opens up the nucleotide binding pocket of the kinase domain (Papa et al., 2003). Crystal structures of the cytosolic portion of yeast IRE1 show the core dimer of IRE1 crystallized with the kinase domains facing away from each other (Lee et al., 2007). Interestingly, another crystal structure demonstrates that IRE1 forms higher ordered structures that allow for the kinase domains of two different core dimers to interact. Three interfaces important for forming an active nuclease were described and disruption of any interface results in a decrease in nuclease activity (Korennykh et al., 2009). Also, IRE1 has been visualized to form punctuate foci during ER stress in both yeast and mammalian cells which correlate to IRE1 activation, arguing for activated IRE1 forming higher ordered structures (Aragon et al., 2009; Li et al., 2010). Binding of ATP or ADP in the nucleotide binding pocket has been shown to induce an activating conformational change in the nuclease domain (Papa et al., 2003). Interestingly, engagement of the nucleotide binding pocket has been shown to be sufficient to activate the nuclease function of IRE1 even in the absence of a functional kinase

domain. This was demonstrated by mutating the kinase pocket to preferentially bind to a small molecule, 1NM-PP1, instead of ATP/ADP. This peudokinase activity of IRE in which a molecule is able to bind to the nucleotide pocket but unable to transfer phosphate was able to splice HAC1 in vivo and in vitro (Papa et al., 2003). Furthermore, small molecule kinase inhibitors that inhibit by binding to the nucleotide pocket such as APY29 and Sunitinib are able to activate IRE1's nuclease activity (Korennykh et al., 2009). Recently, quercetin, a flavanol, was found to act as a small molecule activator of IRE1. Crystal structures show quercetin binding to a novel site, the Q-site, a pocket formed by the dimer interface and is separate from the nucleotide binding site and the putative nuclease site (Wiseman et al., 2010). Quercetin is proposed to activate IRE1 by promoting dimerization and simulating the active conformation of IRE1. Interestingly, quercetin was able to activate the nuclease function of a kinase dead IRE1 unable to bind to ATP. Taken together, activation of IRE1 is a complex process since activation of the nuclease function can be achieved through several means which allows for specific manipulation of each mode of activation

PERK, another initiator of the UPR signal in higher eukaryotes, is a type I transmembrane kinase located in the ER. During ER stress, PERK signals result in inhibition of global translation, presumably to lessen the folding load of the ER, and activation of transcription factors that upregulate factors such as chaperones to increase ER folding capacity. Activated PERK kinase phosphorylates the alpha subunit of eIF2, a translation initiation factor, at Serine 51 preventing the exchange of GTP by its guanine exchange factor, eIF2B, resulting in a translation initiation block. Besides PERK, several other kinases are able to phoshporylate eIF2α in response to diverse cellular stresses. PKR is activated by double stranded RNA and is part of the cellular response to viral infection through the interferon response (Clemens and Elia, 1997; Samuel et al., 1997). GCN2 is a nutrient sensor and can repress global translation under conditions of amino acid deprivation (Harding et al., 2000a; Jiang and Wek, 2005). HRI, another

eIF2α kinase, is involved in heme regulation (Ernst et al., 1979). PERK is also able to reduce translation by downregulating synthesis of ribosomal RNA (rRNA) through inactivation of the RNA polymerase I basal transcription factor RRN3 (Durose et al., 2009). This mode of translational regulation seems to be dependent on phosphorylation of eIF2α, and therefore, may be applicable to the other eIF2α kinases. Also, this mode of translational regulation is independent of the mTOR pathway, a nutrient sensing translational regulatory pathway.

During PERK initiated translation inhibition, translation of the transcription factor ATF4 is paradoxically increased. The 5' UTR of ATF4 contains short inhibitory upstream open reading frames (ORFs) that prevent translation of the ATF4 ORF during unstressed conditions. PERK induced eIF2α phosphorlation result in ribosomes skipping the upstream ORFs and enable translation of the ATF4 ORF. (Lu et al., 2004). Furthermore, activated PERK can directly phosphorylate the transcription factor Nrf2. Phosphorlation of Nrf2 results in its dissociation with its inhibitor, Keap1, allowing it to enter the nucleus (Cullinan et al., 2003). Activation of Nrf2 by PERK is proposed to promote cell survival by maintenance of glutathione levels, and thereby, redox homeostasis (Cullinan et al., 2004).

ATF6, an ER membrane bound transcription factor, is the third UPR initiator in higher eukaryotes. In unstressed conditions, the transactivation domain of ATF6 is inactive since it is tethered to the ER membrane by a transmembrane segment and an ER luminal sensor domain. During ER stress, a golgi localization signal is exposed leading to translocation of ATF6 to the Golgi where the transmembrane segment is cleaved by two Golgi resident proteases, S1P and S2P. This cleavage results in release of the ATF6 cytosolic fragment containing the transactivation domain where it translocates into the nucleus and activates UPR target genes (Haze et al., 1999). Several tissue specific homologs of ATF6 have been discovered to be activated by ER stress in a similar manner as ATF6. For example, OASIS, a bZIP transcription factor of the CREB/ATF family, regulates ER stress genes in astrocytes (Kondo et al., 2005).

Also, CREB4 was to be cleaved by S1P during ER stress (Stirling et al., 2006). Other factors include LUMAN/CREB3, BBF2H7, and CREBH, and the variety of factors demonstrate the diversity of the ER stress response.

One transcription factor that has been reported to be activated by ER stress is nuclear factor-κB (NF-κB), although its role during the UPR has not been previously identified. NF-κB consists of a family of dimer forming transcription factors characterized by a Rel homology domain and include RelA(p65), p50, p52, RelB, and c-Rel. These exist as hetero- or homodimers in unstimulated cells. RelA(p65)/p50 is the canonical and most characterized form while Rel-B/p52 is activated in an alternative pathway. NF-κB can be activated by several stimuli including inflammatory signals and cell stresses such as DNA damage and UV irradiation (Huang et al., 2003; Wu et al., 2006). The variety of NF-κB subunits allows the pathway to differentiate between stimuli and allows for specificity in the response. For example, inflammatory signals such as TNFα, interleukin-1 (IL-1), and lipopolysaccharide (LPS) activate the canonical form, while other immune signals such as lymphotoxin b receptor (LTβR) and B-cell activating factor receptor (BAFFR) activate the alternative pathway (Hayden and Ghosh, 2004).

NF-κB is held inactive in the cytoplasm by its inhibitor, IκB (inhibitor of NF-κB) which needs to be degraded in order for NF-κB to be activated. IKK (IκB kinase) is a multisubunit comlex which comprises of IKKα, IKKβ and IKKγ (NEMO). Following activation, IKK phosphorylates IκBα at serines 32 and 36, resulting in its polyubiquitination and subsequent degradation by the proteasome. NF-κB is then free to translocate into the nucleus where it binds to κB elements in promoters of genes to regulate transcription. Translation repression has also been shown to activate NF-κB. Cycloheximide, a drug that inhibits global translation, is able to activate NF-κB. Also, stresses that lead to eIF2α phosphorylation and translation inhibition such

as amino acid deprivation, UV, and ER stress have been found to activate NF-κB (Jiang et al., 2003; O'Dea et al., 2008).

NF-κB targets genes are primarily thought to promote survival, making NF-κB a key player in the development of invasive tumors and metastases (Basseres and Baldwin, 2006; Hayden and Ghosh, 2004; Rayet and Gelinas, 1999), and frequently, NF-κB is constitutively active in several cancers. Genes that regulate various aspects of tumor progression have been found to be mediated by NF-κB. Vascular endothelial growth factor (VEGF) and IL-8, genes involved in angiogenesis, have been found to be regulated by NF-κB (Huang et al., 2000). Furthermore, adhesion molecules ICAM-1, VCAM-1, and ELAM-1, important for tumor metastases, involve NF-κB activation (Weber et al., 1995). Since DNA damaging and stress inducing agents have been found to activate NF-κB, its activation has been implicated in resistance to certain chemotherapeutic agents (Daniel et al., 1995; Frelin et al., 2005; Karin, 2006; Manna et al., 2007; Venkatraman et al., 2005).

Importance of UPR signaling in cellular functions and their physiological consequences are becoming increasingly clear. We have recently shown a housekeeping function for the UPR during cytokinesis in yeast. An intact UPR is required for efficient cytokinesis during unstressed conditions since cells lacking UPR signaling have problems undergoing cytokinesis in the absence of induced ER stress (Bicknell et al., 2007). This suggests that the ER can sense small changes in ER load and adjust ER folding capacity accordingly.

In addition, conditions that result in chronic ER stress have been connected to progression of several diseases, notably diabetes and cancer. Pancreatic beta cells are especially sensitive to ER folding capacity since they are responsible for insulin secretion and must constantly change ER folding capacity. This is evident in a mouse model called the Akita mouse which has a point mutation Cys96Try in insulin which abolishes one of the disulfide bonds of

insulin. Those mice spontaneously develop diabetes due of apoptosis of beta cells. This is partly due to ER stress induced apoptosis since Akita mice lacking CHOP, a pro-apoptotic factor activated during the UPR, can delay the onset of diabetes (Oyadomari et al., 2002). Also, Wolcott-Rallison syndrome of infantile diabetes is caused by a mutation in PERK and characterized by early destruction of pancreatic beta cells (Delepine et al., 2000). These indicate that maintenance of the ER and maintaining proper levels of UPR signaling are critical for survival of secretory cells.

IRE1 has also been implicated in context of insulin resistance. It was shown that a high fat diet results in chronic ER stress which resulted in IRE1 association with TRAF and subsequent JNK activation. This leads to phosphorylation of the insulin receptor substrate-1 (IRS-1) leading to its downregulation resulting in insulin resistance. (Ozcan et al., 2004) This illustrates another example of how that chronic ER stress contributes to disease progression. Based on these, the UPR is becoming an attractive target for finding treatments to diabetes. Since the UPR is involved in both insulin production by determining cell fate of pancreatic beta cells and insulin resistance through IRE1 signaling , pharmacological agents that modulate various elements of the UPR may be developed as treatments.

One area where UPR signaling plays a role is in the progression of cancer. Solid tumors grow in microenvironments that are altered from normal tissue, and one characteristic of this environment is that it is hypoxic. PERK can be activated during hypoxic conditions (Koumenis et al., 2002). Also, PERK contributes to tumor growth since cells lacking PERK form smaller tumors (Bi et al,. 2005). In fact, the PERK – eIF2α – ATF4 segment of the UPR is required for resistance to hypoxia and tumor growth since disruption of any of these components leads to sensitivity to hypoxic stress and smaller tumors (Fels et al., 2006), making this pathway useful for developing cancer therapies.

The IRE1-XBP1 branch of the UPR has also been shown to be an important factor in both solid tumors and immune cell cancers. Cells lacking XBP1 demonstrate decreased survival during hypoxic conditions, and xbp1-/- cells implanted into mice do not form tumors (Romero-Ramirez et al., 2004). Also, dominant negative IRE1 reduces survival of fibrosarcoma and pancreatic carcinoma cell lines in hypoxic conditions (Feldman et al., 2005). Similarly, XBP1 is essential for angiogenesis in pancreatic adenocarcinomas (Romero-Ramirez et al., 2009). Furthermore, activation of the IRE1/XBP1 branch of the UPR is important in the survival of multiple myeloma cells. PS-341, a proteasome inhibitor that block IRE1 activity and prevented generation of spliced XBP1, induced apoptosis in multiple myeloma cell lines (Lee et al., 2003). Also, high levels of spliced XBP1 were correlated with cases of B cell myelomas (Maestre et al., 2009). Recently, we have shown that a small molecule inhibitor of IRE1, STF-083010, showed cytotoxicity to human multiple myeloma samples (Papandreou et al., 2010). These findings demonstrate the importance of the UPR in regulating cell function since disruption of these pathways lead to disease. Conversely, this makes manipulation of specific pathways of the UPR a prime target for therapeutic development.

REFERENCES:

Aragon, T., van Anken, E., Pincus, D., Serafimova, I.M., Korennykh, A.V., Rubio, C.A., and Walter, P. (2009). Messenger RNA targeting to endoplasmic reticulum stress signalling sites. Nature *457*, 736-740.

Araki, E., Oyadomari, S., and Mori, M. (2003). Impact of endoplasmic reticulum stress pathway on pancreatic beta-cells and diabetes mellitus. Exp Biol Med (Maywood) *228*, 1213-1217.

Basseres, D.S., and Baldwin, A.S. (2006). Nuclear factor-kappaB and inhibitor of kappaB kinase pathways in oncogenic initiation and progression. Oncogene *25*, 6817-6830.

Bertolotti, A., Zhang, Y., Hendershot, L.M., Harding, H.P., and Ron, D. (2000). Dynamic interaction of BiP and ER stress transducers in the unfolded-protein response. Nat Cell Biol *2*, 326-332.

Bi, M., Naczki, C., Koritzinsky, M., Fels, D., Blais, J., Hu, N., Harding, H., Novoa, I., Varia, M., Raleigh, J., Scheuner, D., Kaufman, R.J., Bell, J., Ron, D., Wouters, B.G., and Koumenis, C. (2005). ER stress-regulated translation increases tolerance to extreme hypoxia and promotes tumor growth. Embo J *24*, 3470-3481.

Bicknell, A.A., Babour, A., Federovitch, C.M., and Niwa, M. (2007). A novel role in cytokinesis reveals a housekeeping function for the unfolded protein response. J Cell Biol *177*, 1017-1027.

Calfon, M., Zeng, H., Urano, F., Till, J.H., Hubbard, S.R., Harding, H.P., Clark, S.G., and Ron, D. (2002). IRE1 couples endoplasmic reticulum load to secretory capacity by processing the XBP-1 mRNA. Nature *415*, 92-96.

Clemens, M.J., and Elia, A. (1997). The double-stranded RNA-dependent protein kinase PKR: structure and function. J Interferon Cytokine Res *17*, 503-524.

Cnop, M., Vidal, J., Hull, R.L., Utzschneider, K.M., Carr, D.B., Schraw, T., Scherer, P.E., Boyko, E.J., Fujimoto, W.Y., and Kahn, S.E. (2007). Progressive loss of beta-cell function leads to worsening glucose tolerance in first-degree relatives of subjects with type 2 diabetes. Diabetes Care *30*, 677-682.

Cullinan, S.B., and Diehl, J.A. (2004). PERK-dependent activation of Nrf2 contributes to redox homeostasis and cell survival following endoplasmic reticulum stress. J Biol Chem *279*, 20108-20117.

Cullinan, S.B., Zhang, D., Hannink, M., Arvisais, E., Kaufman, R.J., and Diehl, J.A. (2003). Nrf2 is a direct PERK substrate and effector of PERK-dependent cell survival. Mol Cell Biol *23*, 7198-7209.

Daniel, L.W., Civoli, F., Rogers, M.A., Smitherman, P.K., Raju, P.A., and Roederer, M. (1995). ET-18-OCH3 inhibits nuclear factor-kappa B activation by 12-O-tetradecanoylphorbol-13-acetate but not by tumor necrosis factor-alpha or interleukin 1 alpha. Cancer Res *55*, 4844-4849.

Delepine, M., Nicolino, M., Barrett, T., Golamaully, M., Lathrop, G.M., and Julier, C. (2000). EIF2AK3, encoding translation initiation factor 2-alpha kinase 3, is mutated in patients with Wolcott-Rallison syndrome. Nat Genet *25*, 406-409.

DuRose, J.B., Scheuner, D., Kaufman, R.J., Rothblum, L.I., and Niwa, M. (2009). Phosphorylation of eukaryotic translation initiation factor 2alpha coordinates rRNA transcription and translation inhibition during endoplasmic reticulum stress. Mol Cell Biol *29*, 4295-4307.

Ernst, V., Levin, D.H., and London, I.M. (1979). In situ phosphorylation of the alpha subunit of eukaryotic initiation factor 2 in reticulocyte lysates inhibited by heme deficiency, double-stranded RNA, oxidized glutathione, or the heme-regulated protein kinase. Proc Natl Acad Sci U S A *76*, 2118-2122.

Feldman, D.E., Chauhan, V., and Koong, A.C. (2005). The unfolded protein response: a novel component of the hypoxic stress response in tumors. Mol Cancer Res *3*, 597-605.

Fels, D.R., and Koumenis, C. (2006). The PERK/eIF2alpha/ATF4 module of the UPR in hypoxia resistance and tumor growth. Cancer Biol Ther *5*, 723-728.

Frelin, C., Imbert, V., Griessinger, E., Peyron, A.C., Rochet, N., Philip, P., Dageville, C., Sirvent, A., Hummelsberger, M., Berard, E., Dreano, M., Sirvent, N., and Peyron, J.F. (2005). Targeting NF-kappaB activation via pharmacologic inhibition of IKK2-induced apoptosis of human acute myeloid leukemia cells. Blood *105*, 804-811.

Harding, H.P., Novoa, I., Zhang, Y., Zeng, H., Wek, R., Schapira, M., and Ron, D. (2000). Regulated translation initiation controls stress-induced gene expression in mammalian cells. Mol Cell *6*, 1099-1108.

Hayden, M.S., and Ghosh, S. (2004). Signaling to NF-kappaB. Genes Dev *18*, 2195-2224.

Haze, K., Yoshida, H., Yanagi, H., Yura, T., and Mori, K. (1999). Mammalian transcription factor ATF6 is synthesized as a transmembrane protein and activated by proteolysis in response to endoplasmic reticulum stress. Mol Biol Cell *10*, 3787-3799.

Huang, T.T., Wuerzberger-Davis, S.M., Wu, Z.H., and Miyamoto, S. (2003). Sequential modification of NEMO/IKKgamma by SUMO-1 and ubiquitin mediates NF-kappaB activation by genotoxic stress. Cell *115*, 565-576.

Huang, Y., Horvath, C.M., and Waxman, S. (2000). Regrowth of 5-fluorouracil-treated human colon cancer cells is prevented by the combination of interferon gamma, indomethacin, and phenylbutyrate. Cancer Res *60*, 3200-3206.

Jiang, H.Y., and Wek, R.C. (2005). GCN2 phosphorylation of eIF2alpha activates NF-kappaB in response to UV irradiation. Biochem J *385*, 371-380.

Jiang, H.Y., Wek, S.A., McGrath, B.C., Scheuner, D., Kaufman, R.J., Cavener, D.R., and Wek, R.C. (2003). Phosphorylation of the alpha subunit of eukaryotic initiation factor 2 is required for activation of NF-kappaB in response to diverse cellular stresses. Mol Cell Biol *23*, 5651-5663.

Karin, M. (2006). Nuclear factor-kappaB in cancer development and progression. Nature *441*, 431-436.

Kimata, Y., Ishiwata-Kimata, Y., Ito, T., Hirata, A., Suzuki, T., Oikawa, D., Takeuchi, M., and Kohno, K. (2007). Two regulatory steps of ER-stress sensor Ire1 involving its cluster formation and interaction with unfolded proteins. J Cell Biol *179*, 75-86.

Kondo, S., Murakami, T., Tatsumi, K., Ogata, M., Kanemoto, S., Otori, K., Iseki, K., Wanaka, A., and Imaizumi, K. (2005). OASIS, a CREB/ATF-family member, modulates UPR signalling in astrocytes. Nat Cell Biol *7*, 186-194.

Korennykh, A.V., Egea, P.F., Korostelev, A.A., Finer-Moore, J., Zhang, C., Shokat, K.M., Stroud, R.M., and Walter, P. (2009). The unfolded protein response signals through high-order assembly of Ire1. Nature *457*, 687-693.

Koumenis, C., Naczki, C., Koritzinsky, M., Rastani, S., Diehl, A., Sonenberg, N., Koromilas, A., and Wouters, B.G. (2002). Regulation of protein synthesis by hypoxia via activation of the endoplasmic reticulum kinase PERK and phosphorylation of the translation initiation factor eIF2alpha. Mol Cell Biol *22*, 7405-7416.

Lee, A.H., Iwakoshi, N.N., Anderson, K.C., and Glimcher, L.H. (2003). Proteasome inhibitors disrupt the unfolded protein response in myeloma cells. Proc Natl Acad Sci U S A *100*, 9946-9951.

Lee, K.P., Dey, M., Neculai, D., Cao, C., Dever, T.E., and Sicheri, F. (2008). Structure of the dual enzyme Ire1 reveals the basis for catalysis and regulation in nonconventional RNA splicing. Cell *132*, 89-100.

Li, H., Korennykh, A.V., Behrman, S.L., and Walter, P. Mammalian endoplasmic reticulum stress sensor IRE1 signals by dynamic clustering. Proc Natl Acad Sci U S A *107*, 16113-16118.

Lu, P.D., Harding, H.P., and Ron, D. (2004). Translation reinitiation at alternative open reading frames regulates gene expression in an integrated stress response. J Cell Biol *167*, 27-33.

Maestre, L., Tooze, R., Canamero, M., Montes-Moreno, S., Ramos, R., Doody, G., Boll, M., Barrans, S., Baena, S., Piris, M.A., and Roncador, G. (2009). Expression pattern of XBP1(S) in human B-cell lymphomas. Haematologica *94*, 419-422.

Manna, S.K., Manna, P., and Sarkar, A. (2007). Inhibition of RelA phosphorylation sensitizes apoptosis in constitutive NF-kappaB-expressing and chemoresistant cells. Cell Death Differ *14*, 158-170.

O'Dea, E.L., Kearns, J.D., and Hoffmann, A. (2008). UV as an amplifier rather than inducer of NF-kappaB activity. Mol Cell *30*, 632-641.

Oyadomari, S., Koizumi, A., Takeda, K., Gotoh, T., Akira, S., Araki, E., and Mori, M. (2002). Targeted disruption of the Chop gene delays endoplasmic reticulum stress-mediated diabetes. J Clin Invest *109*, 525-532.

Ozcan, U., Cao, Q., Yilmaz, E., Lee, A.H., Iwakoshi, N.N., Ozdelen, E., Tuncman, G., Gorgun, C., Glimcher, L.H., and Hotamisligil, G.S. (2004). Endoplasmic reticulum stress links obesity, insulin action, and type 2 diabetes. Science *306*, 457-461.

Papa, F.R., Zhang, C., Shokat, K., and Walter, P. (2003). Bypassing a kinase activity with an ATP-competitive drug. Science *302*, 1533-1537.

Papandreou, I., Denko, N.C., Olson, M., Van Melckebeke, H., Lust, S., Tam, A., Solow-Cordero, D.E., Bouley, D.M., Offner, F., Niwa, M., and Koong, A.C. Identification of an Ire1alpha endonuclease specific inhibitor with cytotoxic activity against human multiple myeloma. Blood.

Rayet, B., and Gelinas, C. (1999). Aberrant rel/nfkb genes and activity in human cancer. Oncogene *18*, 6938-6947.

Romero-Ramirez, L., Cao, H., Nelson, D., Hammond, E., Lee, A.H., Yoshida, H., Mori, K., Glimcher, L.H., Denko, N.C., Giaccia, A.J., Le, Q.T., and Koong, A.C. (2004). XBP1 is essential for survival under hypoxic conditions and is required for tumor growth. Cancer Res *64*, 5943-5947.

Ron, D., and Walter, P. (2007). Signal integration in the endoplasmic reticulum unfolded protein response. Nat Rev Mol Cell Biol *8*, 519-529.

Ruegsegger, U., Leber, J.H., and Walter, P. (2001). Block of HAC1 mRNA translation by long-range base pairing is released by cytoplasmic splicing upon induction of the unfolded protein response. Cell *107*, 103-114.

Rutkowski, D.T., and Hegde, R.S. Regulation of basal cellular physiology by the homeostatic unfolded protein response. J Cell Biol *189*, 783-794.

Samuel, C.E., Kuhen, K.L., George, C.X., Ortega, L.G., Rende-Fournier, R., and Tanaka, H. (1997). The PKR protein kinase--an interferon-inducible regulator of cell growth and differentiation. Int J Hematol *65*, 227-237.

Sidrauski, C., and Walter, P. (1997). The transmembrane kinase Ire1p is a site-specific endonuclease that initiates mRNA splicing in the unfolded protein response. Cell *90*, 1031-1039.

Stirling, J., and O'Hare, P. (2006). CREB4, a transmembrane bZip transcription factor and potential new substrate for regulation and cleavage by S1P. Mol Biol Cell *17*, 413-426.

Venkatraman, M., Anto, R.J., Nair, A., Varghese, M., and Karunagaran, D. (2005). Biological and chemical inhibitors of NF-kappaB sensitize SiHa cells to cisplatin-induced apoptosis. Mol Carcinog *44*, 51-59.

Weber, C., Erl, W., Pietsch, A., Danesch, U., and Weber, P.C. (1995). Docosahexaenoic acid selectively attenuates induction of vascular cell adhesion molecule-1 and subsequent monocytic cell adhesion to human endothelial cells stimulated by tumor necrosis factor-alpha. Arterioscler Thromb Vasc Biol *15*, 622-628.

Wiseman, R.L., Zhang, Y., Lee, K.P., Harding, H.P., Haynes, C.M., Price, J., Sicheri, F., and Ron, D. Flavonol activation defines an unanticipated ligand-binding site in the kinase-RNase domain of IRE1. Mol Cell *38*, 291-304.

Wu, S., Tan, M., Hu, Y., Wang, J.L., Scheuner, D., and Kaufman, R.J. (2004). Ultraviolet light activates NFkappaB through translational inhibition of IkappaBalpha synthesis. J Biol Chem *279*, 34898-34902.

Yoshida, H., Matsui, T., Yamamoto, A., Okada, T., and Mori, K. (2001). XBP1 mRNA is induced by ATF6 and spliced by IRE1 in response to ER stress to produce a highly active transcription factor. Cell *107*, 881-891.

Chapter 2

ABSTRACT

The Unfolded Protein Response (UPR) is a signaling pathway that regulates the folding capacity of the endoplasmic reticulum (ER) in response to stress by upregulating transcription of genes that contribute to ER function. NF-κB, a transcription factor central to cell survival, proliferation and inflammation, becomes activated during ER stress. However, the mechanism of activation remains unclear and the function of NF-κB during ER stress remains undefined. Here, we find that UPR-induced NF-κB plays a critical role in the up-regulation of a subset of UPR target genes. Mechanistically, we find that a combination of inputs from two UPR sensors, IRE1 and PERK, are required for maximum activation of NF-κB in response to ER stress. Furthermore, IKK (IκBα Kinase) is necessary for NF-κB activation during ER stress. However, unlike canonical NF-κB activation, IKK activity does not increase during ER stress, but rather the level of basal IKK activity is critical for determining the extent of NF-κB activation. Furthermore, a key UPR initiator, IRE1, acts to maintain IKK basal activity through IRE1's kinase, but not RNase, activity. Thus, combined signals of translation repression by PERK and basal IKK activity by IRE1 lead to maximal NF-κB activation. These interdependencies have a significant impact in cancer cells with elevated IKK/NF-κB activity such as renal cell carcinoma cells (786-0). Inhibition of IKK by an IKK inhibitor, which significantly decreases NF-κB activity, is overridden by UPR induction, arguing for the importance of considering UPR activation in cancer treatment.

INTRODUCTION

Secreted and membrane bound proteins are first synthesized in the endoplasmic reticulum (ER). To ensure proper cell function, the ER must be able to properly fold and process these proteins, so it is critical for the ER to monitor its protein folding capacity and properly respond to demands in folding capacity. In particular, the ER experiences stress when there is an accumulation of unfolded proteins in the ER. In response to stress, the ER activates a signal transduction pathway called the Unfolded Protein Response (UPR) which has wide-ranging effects on the cell including initiation of a transcriptional profile, global translation repression, and activation of apoptosis. (Harding et al., 2001; Kaufman, 2002; Mori, 2000; Patil and Walter, 2001; Ron and Walter, 2007). UPR signaling is also emerging as a contributing factor to the pathology of several human diseases including diabetes and cancer (Bi et al., 2005; Ozcan et al., 2004; Ozcan et al., 2006; Romero-Ramirez et al., 2004). The UPR contributes to the growth and survival of tumors since a reduction in tumor mass is seen when tumors lack UPR components (Bi et al., 2005; Romero-Ramirez et al., 2004). Furthermore, certain conditions conducive to solid tumor development, such as hypoxia, have been found to induce UPR signaling (Koumenis et al., 2002; Koumenis and Wouters, 2006; Ranganathan et al., 2006)

In higher eukaryotes, UPR signaling is initiated by three ER transmembrane sensors, the kinase PERK, the kinase/RNase IRE1, and the transcription factor ATF6 (reviewed in (Kaufman, 2002; Mori, 2000; Ron and Walter, 2007; Rutkowski and Kaufman, 2004)). IRE1 excises an intron from a specific mRNA, *XBP1*, which encodes a UPR transcription factor (*HAC1* mRNA in *S. cerevisiae*) (Calfon et al., 2002; Cox et al., 1993; Mori et al., 1993; Yoshida et al., 2001). This excision and subsequent splicing produces a more transcriptionally active form of XBP1. Activation of PERK induces an inhibitory phosphorylation of eIF2α translation initiation factor, leading to an overall repression of protein translation (Harding et al., 2000b; Harding et al., 1999; Shi et al., 1998). At the same time, PERK promotes transcription of UPR-specific genes by increasing translation of the transcription factor ATF4 (Wek and Cavener, 2007); (Harding et al.,

2000b); (Hinnebusch, 1997). The third UPR sensor, ATF6, is itself a transcription factor and is proteolytically released during ER stress (Haze et al., 1999; Shen et al., 2002a; Ye et al., 2000). Thus, each ER proximal sensor is ultimately responsible for activation of a transcription factor. Activation of ATF6, ATF4, and XBP1 by the UPR result in a complex pattern of gene regulation which ultimately decides cell fate (Mori, 2000; Patil and Walter, 2001; Ron and Walter, 2007; Rutkowski and Kaufman, 2004). UPR signaling first attempts to alleviate the problem of misfolded proteins in the ER by increasing protein folding capacity through up-regulation of ER chaperones such as BiP, GRP94, calreticulin, and Erdj4 (Okada et al., 2002; Shen et al., 2002b; Yoshida et al., 1998). If proper protein folding in the ER cannot be restored, the UPR up-regulates genes such as CHOP that result in activation of apoptotic pathways. (Harding et al., 2000a; Okada et al., 2002; Oyadomari and Mori, 2004; Wang et al., 1996).

In addition, activation of the highly studied transcription factor NF-κB has been reported to be a consequence of ER stress (Deng et al., 2004; Jiang et al., 2003; Pahl and Baeuerle, 1995), although its role during the UPR has yet to be determined. NF-κB consists of a family of dimer forming transcription factors that include RelA(p65), p50, p52, RelB, and c-Rel with RelA(p65)/p50 being the canonical form. Normally held in the cytoplasm in complex with an inhibitor of NF-κB (IκBα), canonical activation of NF-κB involves phosphorylation of IκBα by IκB kinase (IKK), followed by proteasome-mediated degradation of IκB. IKK, comprised of IKKα, IKKβ, and IKKγ (NEMO) subunits, phosphorylates IκBα on serines at position 32 and 36 (DiDonato et al., 1996; Zandi et al., 1998). This frees NF-κB for nuclear accumulation, binding to consensus κB promoter sites, and transcriptional activation of target genes (Ghosh et al., 1998; Hayden and Ghosh, 2004; Karin and Ben-Neriah, 2000). Genes regulated by NF-κB primarily promote survival, making NF-κB a key player in the development of invasive tumors and metastases (Basseres and Baldwin, 2006; Hayden and Ghosh, 2004; Rayet and Gelinas, 1999),

and in resistance to certain chemotherapeutic agents (Daniel et al., 1995; Frelin et al., 2005; Karin, 2006; Manna et al., 2007; Venkatraman et al., 2005)

NF-κB can be activated by several stimuli including inflammatory signals such as tumor necrosis factor α (TNFα), interleukin-1 (IL-1), and lipopolysaccharide (LPS) (Hayden and Ghosh, 2004), and internal cell stresses such as DNA damage (Huang et al., 2003; Wu et al., 2006). Signals initiated by these stimuli converge by activating the IKK complex resulting in IKK mediated degradation of IκBα. Thus, IKK activation is a key regulatory step of NF-κB activation. Recent reports reveal that the mechanism of NF-κB activation during ER stress may differ from conventional activation. Specifically, NF-κB activation was proposed to be independent of IKK activation since IκBα phosphorylation was not detected during ER stress. Additionally, NF-κB activation was reported to be a consequence of PERK-mediated phosphorylation of eIF2α (Deng et al., 2004; Jiang et al., 2003). While these reports agree on an importance for PERK and eIF2α phosphorylation, they differ in mechanistic detail. A recent report, however, has shown that ER stress-induced NF-κB activation requires IRE1 in a human breast cancer cell line (Hu et al., 2006), and that it is mediated by canonical activation of IKK. Since IKK is a master regulator of the NF-κB pathway, determining its function during ER stress is essential. Furthermore, since signals initiated by PERK and IRE1 target separate cellular pathways, we wanted to determine if these components have separate means of activating NF-κB or if a combined signal is required. To identify the individual roles of IRE1, PERK, and IKK, we used mouse embryonic fibroblasts (MEFs) knocked out for components of the pathway in order to dissect the mechanism. Our results reveal a unique means of activating NF-κB in response to signals initiated from the ER, involving a combination of inputs from IRE1 and PERK. Furthermore, we uncover an importance of basal IKK activity for determining the magnitude of NF-κB activation during the UPR. Finally, we demonstrate that NF-κB binds directly to

promoters of a subset of UPR target genes and is required for their full transcription activation during the UPR, thus revealing that NF-κB activation is an integral part of the ER stress response.

RESULTS

IKK is Required for Activation of NF-κB during UPR

To probe the mechanistic details of NF-κB activation during ER stress, in particular, the relationships between the canonical key step involving IKK-mediated IκBα phosphorylation, we examined ER stress induced NF-κB activation in wild type mouse embryonic fibroblasts (MEFs) and MEFs lacking the α and β subunits of IKK (*ikk*$^{-/-}$) (Li et al., 1999; Tergaonkar et al., 2003). NF-κB activation was measured by the well-established electrophoretic mobility shift assay (EMSA) which involves adding a radio-labeled oligonucleotide containing the NF-κB binding site to nuclear extracts (Pahl and Baeuerle, 1995). Activated NF-κB binds to the oligonucleotide causing a shift in mobility. ER stress was induced by DTT and Thapsigargin (Tg), two well established agents which activate the UPR. DTT disrupts disulfide bonds resulting in unfolded proteins, while Tg ultimately blocks ER chaperone function by disrupting ER calcium levels. Induction of the UPR by DTT or Tg in wild type MEFs resulted in NF-κB activation (Figure 1A, IKK$^{+/+}$; Figure S1). Consistent with the EMSA results, immunofluorescence detected NF-κB translocation into the nucleus during ER stress (Figure S1F). NF-κB activation was also observed with DTT and Tg in multiple cell types (Figure S2). Specificities of the complex formed were confirmed by performing the same gel shift experiments but in the presence of cold wild type or mutant κB competitor oligonucleotides (Figure S1A, S1B), or by supershift experiments in the presence of antibodies against NF-κB subunits (Figure S1C & S1D). These assays reveal that the activated form of NF-κB is p65/p50. While wild type MEFs show strong activation of NF-κB, we found that NF-κB activation was significantly diminished in *ikk*$^{-/-}$ MEFs

(Figure 1A, *ikk*$^{-/-}$), indicating a requirement for IKK during UPR induced activation of NF-κB.

To further test involvement of IKK, we tested for the requirement of IκBα phosphorylation. We took IκBα$^{-/-}$ cells and added back either wild type IκBα (IκBα-WT) or a non-phosphorylatable IκBα where two Serines at position 32 and 36 (Ser 32/36) that are normally phosphorylated by IKK were both mutated to Alanine (IκBα-SR). We confirmed that IκBα levels were equal in cells expressing IκBα-WT and IκBα-SR (Fig S3A). Cells expressing IκBα-SR showed significantly reduced NF-κB activation during the UPR (Figure 1B), providing further support for the importance of IKK mediated IκBα phosphorylation in UPR induced NF-κB activation.

These data were in contrast to the previous reports where IκBα phosphorylation was not observed (Deng et al., 2004; Jiang et al., 2003), and thus called for re-examination of IκBα phosphorylation states during the UPR. The phosphoyrlation state of IκBα was measured using an anti-P-IκBα antibody during a UPR time course. Consistent with previous reports, we saw no significant increase in P-IκBα following UPR induction (Figure 1C, P-IκBα), while there was a significant increase in P-IκBα following TNFα treatment. Furthermore, total cellular levels of IκBα decreased after UPR induction (Figure 1C, S3B), and immunoprecipitation studies found that during the UPR, IκBα present in the cell remained bound to NF-κB (Figure S3C, IP p65 western IκBα), supporting canonical activation of NF-κB. Taken together, the decrease in IκBα occurred without an increase in its phosphorylation, in agreement with the previous result. To further investigate these apparent differences in the role of IKK, we examined IKK kinase activity directly by *in vitro* kinase assays using immunoprecipitated IKK complex from un-induced and UPR-induced MEFs, incubated with recombinant IκBα substrate and [γ^{32}P]-ATP (Figure 1D, top panel). IKKα levels in the extracts were greatly reduced after anti-IKK

immunoprecipitation, demonstrating that efficient immunoprecipitation of the IKK complex had occurred (Figure 1D, bottom panel). While incubation of the IKK complex from TNFα treated cells strongly incorporated ^{32}P label into IκBα (Figure 1D, lane 3), only low levels of kinase activity equal to uninduced levels were seen from UPR-induced cells (Figure 1D, lanes 4-7). Phospho-IκBα analyses performed in CHO cells also showed no significant increase in phosphorylation of IκBα following UPR induction (Figure S3B).

Since IκBα is degraded by the proteasome upon phosphorylation (DiDonato et al., 1997; Karin, 1999), a proteasome inhibitor, MG132, was added to cells blocking any potential degradation to allow accurate measurement of P-IκBα levels. Furthermore, we used *perk*$^{-/-}$ MEFs to prevent any decrease in production of IκBα caused by PERK induced translation repression. Levels of p-IκB that accumulated in the presence of MG132 were equivalent in the absence or presence of DTT (Figure 1E), indicating that there is no further increase in IKK kinase following UPR induction. Thus, these results highlighted a distinctive nature of the mechanism used to activate NF-κB by the UPR. Specifically, IKK mediated IκBα phosphorylation is required for NF-κB activation but no increase in IKK activity or IκBα phosphorylation was seen during the UPR.

PERK-Mediated Translation Repression is Not Sufficient to Fully Activate NF-κB During UPR in Cells Lacking IRE1

Another puzzling observation is the relative contribution of IRE1 and PERK. In order to delineate the functional contributions of IRE1 and PERK in ER stress-induced NF-κB activation, we used MEFs knocked out in either IRE1 or PERK to identify individual roles of each component. To date, there is no direct molecular event that simultaneously requires both IRE1 and PERK for its activation. Previous studies have shown that PERK mediated translational

inhibition was sufficient to induce NF-κB during the UPR (Deng et al., 2004). Consequently, blocking translation repression *in perk*$^{-/-}$ MEFs (Figure 2A; shown by ^{35}S-Met/Cys incorporation) resulted in significantly diminished activation of NF-κB in *perk*$^{-/-}$ MEFs as compared to that in wild type cells (Figure 2B), in agreement with previous reports (Deng et al., 2004; Jiang and Wek, 2005).

Cycloheximide (CHX), a drug that inhibits translation, has been shown to substitute for PERK dependent translation inhibition during the UPR (Harding et al., 2000b; Scheuner et al., 2001). If translation inhibition is the contribution of PERK, CHX should be sufficient to induce NF-κB activation. Treatment of wild type MEFs with CHX resulted in efficiently activated NF-κB (Figure 2F, IRE1$^{+/+}$). Furthermore, we found that the extent of translation inhibition determines the level of NF-κB activation (Figure S4A). Using increasing CHX concentrations to modulate the levels of translation repression, we found that higher levels of translation repression resulted in higher NF-κB activation. This indicates that the contribution of PERK is translation inhibition, which is sufficient to activate NF-κB in wild type cells.

In order to determine the functional role of IRE1, we asked if PERK mediated translation inhibition was sufficient to activate NF-κB in cells lacking IRE1. Accordingly, we first determined the amount of translation inhibition in ire1$^{-/-}$ cells. We found that translation was repressed in *ire1*$^{-/-}$ MEFs at similar efficiencies to wild type MEFs by ^{35}S-Met/Cys incorporation during UPR induction (Figure 2C). This indicates that PERK represses translation normally in *ire1*$^{-/-}$ cells in response to ER stress. NF-κB activation was then measured in IRE1$^{+/+}$ and ire1$^{-/-}$ cells by EMSA. Despite the translational inhibition by PERK, we found that the overall NF-κB activity was greatly diminished in *ire1*$^{-/-}$ cells at every time point (Figure 2D, ire1$^{-/-}$), indicating that IRE1 has a functional contribution to NF-κB activation that is independent of PERK. NF-κB

activity in *ire1*$^{-/-}$ cells was restored by transfection of IRE1, showing that this effect is dependent on the presence of IRE1 and not on the difference in cell type (Figure S4B). The extent of NF-κB recovery after IRE1 transfection was directly proportional to that of IRE1-mediated XBP1 splicing (Figure S4C). Reduced NF-κB activation in ire1$^{-/-}$ cells was also in agreement with its transcription reporter assay (Figure 2E). Using a reporter carrying three copies of the canonical NF-κB binding sites fused to a luciferase gene, we measured the increase in luciferase activity as a measure of NF-κB activation. Activation of luciferase was diminished in *ire1*$^{-/-}$ cells during both DTT and Tg induced UPR, correlating with activated NF-κB levels measured by EMSA assays. Furthermore, while CHX treatment of wild type cells efficiently activated NF-κB, similar CHX treatment of *ire1*$^{-/-}$ MEFs failed to activate NF-κB to the extent similar to wild type cells (Figure 2F). These results further support the observation that repressing translation is not sufficient to activate NF-κB in ire1$^{-/-}$ cells, indicating a PERK-independent role for IRE1 in activating NF-κB during the UPR. Overall, these results indicate that loss of either IRE1 or PERK result in diminished NF-κB signaling during the UPR, suggesting combined inputs from the IRE1 and PERK signaling branches. IRE1 activation does not result in NF-κB activation in cells lacking PERK, and conversely, PERK mediated translation inhibition is not sufficient to fully activate NF-κB in cells lacking IRE1.

Basal IKK Kinase Activity is Diminished in the Absence of IRE1

Since IKK is critical to NF-κB activation during ER stress, we wanted to determine the relationships between IKK, IRE1, and PERK. Although IKK is required for NF-κB activation, IKK activity does not increase during the UPR (Figure 1). This suggests that the uninduced or *basal* IKK activity is sufficient to achieve NF-κB activation during the UPR. Recently, the importance of *basal* IKK activity in NF-κB activation by the ribotoxic stimulus UV was reported

(O'Dea et al., 2007; O'Dea et al., 2008), and thus, we tested the involvement of *basal* IKK kinase activity for UPR induced NF-κB. The conventional method for measuring IKK kinase activity which uses immunoprecipitated kinase was not sensitive enough for monitoring potential changes in basal IKK kinase activity (data not shown). Thus, accumulated P-IκBα levels were measured as readout for IKK activity. We measured the basal IKK kinase activity in *ire1*$^{-/-}$ and perk$^{-/-}$ cells in order to ask whether loss of IRE1 or PERK affected basal IKK activity. To this end, wild type, or *ire1*$^{-/-}$, *or perk*$^{-/-}$ knockout cells were incubated with MG132 without any UPR-inducing agents, and accumulation of p-IκBα was determined over time. We observed gradual P-IκBα accumulation over time in wild type cells, while in *ire1*$^{-/-}$ MEFs, p-IκBα accumulation was 2-fold lower over the time course (Figure 3A). This indicated that basal IKK activity was decreased in cells lacking IRE1 suggesting a role for IRE1 regulating IKK activity. In contrast, P-IκBα accumulation in *perk*$^{-/-}$ MEFs was identical to that of wild type cells (Figure 3B).

Since IKK-mediated phosphorylation of IκBα leads to its degradation, these results predicted that IκBα in *ire1*$^{-/-}$ cells would have a longer half-life in non-induced resting or *basal* conditions. Indeed, we found that IκBα half-life measured upon incubation with cycloheximide to prevent all new synthesis of IκBα was longer in ire1$^{-/-}$ MEFs than wild type cells (Figure 3C), further supporting the idea that IKK activity is lower when cells lack IRE1. Together these results suggested the exciting possibility that robust activation of NF-κB during the UPR requires a certain level of *basal* IKK activity, which needs to be present even prior to UPR induction. Furthermore, these results argue that IRE1 positively affects basal IKK activity.

Restoring Basal IKK Activity Can Rescue NF-κB Activation in ire1$^{-/-}$ *Cells*

To further analyze whether the decrease in NF-κB activation observed in *ire1*$^{-/-}$ MEFs is caused by alterations in basal IKK activity, we tested whether increasing the basal IKK activity

would restore efficient NF-κB induction to *ire1*$^{-/-}$ MEFs subjected to ER stress. We reasoned that increasing the concentration of IKK would increase the basal IKK activity. Thus, *ire1*$^{-/-}$ cells were transfected with extra copies of either wild type IKKα or IKKβ. Indeed, we found that expression of IKKβ, but not IKKα, in *ire1*$^{-/-}$ MEFs restored the basal level of IKK activity as measured by accumulation of p-IκBα in the presence of MG132 (Figure 3D).

Consequently, IKKβ, but not IKKα, was also able to rescue NF-κB activation in the ire1$^{-/-}$ cells, increasing NF-κB activation to wild type levels (Figure 3E). In addition, we concluded that the kinase activity of IKK is needed for activation of NF-κB by UPR, as transfection of a kinase-dead mutant of IKKβ did not rescue NF-κB activity to wild type levels in *ire1*$^{-/-}$ MEFs (Figure 3E, +IKKβ DN). Furthermore, these effects were specific to IKKβ, as transfection of IKKα was unable to restore either basal IKK activity (Figure 3D) or UPR induced NF-κB activities (Figure 3E, +IKKα). Thus, simply increasing the concentration of any kinase did not rescue NF-κB activation in *ire1*$^{-/-}$ cells. These results provide further support for the importance of IKKβ-mediated phosphorylation of IκBα to the overall output of UPR-induced NF-κB. In addition, the ability of IKKβ but not IKKα to complement *ire1*$^{-/-}$ cells suggests that IRE1 specifically influences NF-κB activation via basal IKKβ activity.

The Kinase Activity of IRE1 Is Required for NF-κB Activation During ER Stress

In order to further investigate the molecular mechanism by which IRE1 regulates basal IKKβ activity, we examined importance of IRE1 kinase and RNase activities. We transfected wild type IRE1, kinase dead IRE1 (IRE1-KD), or nuclease dead IRE1 (IRE1-ND) into ire1$^{-/-}$ MEFs and determined NF-κB activation by luciferase assay. IRE1-KD carried an alanine substitution at the catalytically important lysine for kinase activity positioned at 599 (K599A), which has previously shown to inactivate Ire1 kinase both *in vivo* and *in vitro* (Tirasophon et al.,

1998). Similarly, IRE1-ND was mutated at another lysine at 907, inactivated IRE1 RNase without affecting IRE1 kinase activity (Tirasophon et al., 2000). Western blotting shows that wild type and mutant IRE1 was successfully transfected (Figure 4A, IRE1). We found that adding back wild type IRE1 was able to rescue NF-κB activation (Figure 4A, KO+ IRE1) by luciferase assay. However, adding IRE1-KD was not able to rescue NF-κB activation. IRE1-ND allowed rescue of most, but not all of the NF-κB activity achieved by wild type IRE1 (Figure 4A). These results demonstrate that the kinase activity of IRE1 is necessary for NF-κB activation during ER stress, and suggests IRE1 may maintain basal IKK activity by phosphorylating IKK at a low, basal level. Therefore, we wanted to examine the basal phosphorylation state of IKK since IKK phosphorylation has been linked with its activity (Delhase et al., 1999). We found that levels of phosphorylated IKKβ were decreased in untreated ire1$^{-/-}$ cells as compared to wild type (Figure 4B). Furthermore, this decrease in P-IKKβ can be rescued by adding back wild type IRE1 or nuclease dead IRE1 (Figure 4B). However, kinase dead IRE1 was unable to rescue this phenotype. These results are consistent with the importance of IRE1 kinase for rescue of NF-κB activation (Figure 4A), suggesting that the basal phosphorylation state of IKKβ determines basal IKK activity. Moreover, the fact that wild type and nuclease dead IRE1, but not kinase dead IRE1, is able to rescue IKK phosphorylation suggests that IRE1 may be phosphorylating IKKβ at a basal level to regulate its activity. This is also in agreement with our observations that transfecting IKKβ but not IKKα is able to rescue both basal IKK and NF-κB activity in ire1$^{-/-}$ (Figure 3D), indicating the specific involvement of IKKβ in UPR.

A potential reason for diminished basal IKK activity in ire1$^{-/-}$ MEFs may come from an altered concentration of IKK complex components. We examined protein levels of IKKα, IKKβ, and IKKγ and found that all components of the IKK complex were equivalent in wild type and ire1$^{-/-}$ cells (Figure 4C). In addition, equivalent amounts of IKKα, IKKβ, and IKKγ were

associated with each other as each can be immunoprecipitated in wild type and ire1$^{-/-}$ cells (Figure 4D). Therefore, these results suggest that IRE1 does not affect the physical composition of the IKK complex. Another possible cause for the decreased basal IKK activity in ire1$^{-/-}$ cells is a disruption in other proteins that regulate the IKK complex. Thus, we examined protein levels of IKK regulators that may affect its basal activity including Hsp90 (Chen et al., 2002), Cdc37 (Chen et al., 2002), TAK1 (Takaesu et al., 2003), RIP (Ea et al., 2006). We found that protein levels of Hsp90, Cdc37, TAK1, and RIP were equivalent in wild type and ire1$^{-/-}$ cells (Figure 4E), suggesting that IRE1 does not affect basal IKK activity by altering protein levels of IKK regulators. A previous report has shown by immunoprecipitation that IRE1 can physically associate with the IKK complex (Hu et al., 2006). Thus, this interaction might be important for ability of IRE1 to maintain basal IKK activity. However, we were not able to detect the interaction between IRE1 and IKK despite the use of the same cell line (Figure S5A). Taken together, these results indicate that IRE1 modulates the functional capacity of the IKK complex through maintaining basal phosphorylation of IKKβ, and not through altering the physical composition of the IKK complex and its regulators.

Previously, IRE1's kinase, but not RNase activity, has been shown to be required for interaction with TRAF2, an adaptor protein that links IRE1 to c-JUN N-terminal kinase (JNK) activation (Urano et al., 2000). Since we found that the kinase activity of IRE1 is necessary for regulating basal IKK and NF-κB function, we tested a potential involvement of TRAF2 and the JNK pathway in ER stress induced NF-κB activation. To test requirement for TRAF2, we transfected a dominant negative form of TRAF2 (TRAF2-DN) missing its N terminal domain (aa 1-87) into wild type cells. This TRAF2-DN has been shown to block IKK activation of NF-κB (Habelhah et al., 2004). We found that transfecting TRAF2-DN resulted in a decreased NF-κB activity (Figure 4F) indicating that TRAF2 is required for NF-κB activation during ER stress.

Curiously, TRAF2 protein level was reduced in ire1$^{-/-}$ cells (Figure 4F). However, transfection of wild type TRAF2 in ire1$^{-/-}$ cells to increase protein levels did not rescue NF-κB activation or IKK basal activity in response to ER stress (Figure S5B). This indicates that although TRAF2 is required for NF-κB activation, maintaining wild type protein levels of TRAF2 is not sufficient for NF-κB activation. In contrast to TRAF2, however, loss of JNK (JNK1 or JNK2) did not affect NF-κB activation, as similar levels of activated NF-κB was detected by EMSA in jnk1$^{-/-}$ and jnk2$^{-/-}$ cells (Figure 4G), suggesting that IRE1 does not regulate basal IKK activity via the JNK pathway. Taken together, our data suggests that NF-κB activation during ER stress is mediated via IRE1-TRAF2 but not via JNK.

Basal IKK Activity Determines Degree of NF-κB Activation During ER Stress

These experiments reveal that *basal* IKK activity influences NF-κB activation during the UPR. In order to determine the functional importance of regulating *basal* IKK activity during the UPR, we examined the consequences of altering levels of basal IKK activity achieved by transfecting of increasing concentrations of IKKβ into *ire1*$^{-/-}$ MEFs (Figure 5A). A significant increase in basal NF-κB activity and UPR-induced NF-κB activity occurred after transfecting 1 μg of IKKβ plasmid. At this condition, kinetics and the extent of NF-κB activation were similar to those observed in wild type IRE1$^{+/+}$ cells. When a higher concentration of IKKβ plasmid (2 μg) was transfected, we observed even further elevation in the level of basal and activated NF-κB. Curiously, however, the subsequent activation of UPR did not result in further increase of NF-κB activity, but rather remained at equally high levels throughout the time course. Levels of transfected IKKβ were determined by western blot (Figure S6A). These results highlight the importance of the basal activity of IKK in mediating UPR induced NF-κB activation and may

have important consequences in conditions where elevated basal IKK activity is a contributing factor to disease such as in the case of cancer.

Certain cancer cells have been reported to display elevated basal NF-κB activity (Karin, 2006; Shishodia and Aggarwal, 2004) Therefore, we tested the renal cell carcinoma 786-0 cell line (Williams et al., 1978) previously characterized to have constitutively active NF-κB. We first wanted to confirm that the 786-O cells had high basal IKK activity. We found that the 786-O cells but not MEFs had high basal IKK activity, as measured by incorporation of ^{32}P into IκBα by immunoprecipitated IKK complexes (Figure 5B, ^{32}P-IκBα 0hr). Consistent with the high IKK kinase activity in un-induced cells, phosphorylated IκBα was detected in untreated 786-O cells, and IκBα protein levels were also significantly decreased in 786-O cells as compared to MEFs, demonstrating that high basal IKK activity the 786-O cells leads to IκBα degradation. However, IKKβ levels between MEFs and 786-O cells were equivalent indicating that the high basal IKK activity was due to activation but not overexpression of IKK.

EMSA assays of nuclear extracts revealed that basal NF-κB activity was significantly elevated in 786-0 cells (Figure 5C, 0h), confirming previous reports (An and Rettig, 2005; Jackson-Bernitsas et al., 2007; Yang and Richmond, 2001). Following UPR induction, we found that 786-0 cells with high basal NF-κB were unable to further activate NF-κB (Figure 5C). The inability of 786-0 cells to further induce NF-κB efficiently following UPR activation was consistent with *ire1*$^{-/-}$ MEFs transfected with high levels of IKKβ (Figure 5A, 2 μg), providing an additional support for the significant impact of the basal activity on the overall outcome of the signaling pathway. Lack of NF-κB activation during the UPR time course was not due to an inability of 786-0 cells to activate UPR. We found that eIF2α phosphorylation, the hallmark of

PERK activation, occurred normally upon UPR induction by DTT treatment of 786-0 cells (Figure S6B).

As high basal NF-κB contributes to the development of cancer, selective IKK inhibitors have been developed (Karin et al., 2004). This current study indicates that the UPR effectively activates NF-κB even when IKK activity is at a reduced or *basal* level. Since UPR is found to be activated in varieties of cancer, such implications will have significant consequences in outcomes of cancer treatment. Thus, we examined if the decrease in NF-κB activation by an IKK inhibitor can be overcome by UPR induction (Figure 5D, schematic). To this end, we treated 786-0 cells for 1 hr with a well-characterized IKK inhibitor, SC-514 (Kishore et al., 2003). This resulted in diminished IKK activity as determined by a decrease in phosphorylated IκBα (Figure S6D) and correspondingly diminished levels of NF-κB activity (Figure 5E, lanes 1-4). Notably, induction of UPR after SC-514 treatment allowed robust activation of NF-κB (Figure 5E, compare lanes 3 vs. 7, or 4 vs. 8), even in the presence of the IKK inhibitor. Pre-treatment of cells with SC-514 itself did not cause activation of PERK and further, DTT treatment of SC-514 pre-treated cells induced PERK normally as confirmed by eIF2α phosphorylation (Figure S6C). These results show that activation of the UPR can overcome inhibition of NF-κB by an IKK inhibitor in cancer cells with high basal IKK/NF-κB activity. Taken together, these results provide additional support for the idea that IKK *basal* activity is a critical factor in UPR induced NF-κB activation.

NF-κB Activates Transcription of the UPR Target Genes

NF-κB activation has a dramatic impact on the cellular transcriptional responses in a variety of signaling pathways. While the UPR activates canonical UPR transcription factors such as ATF6 and XBP1, the transcriptional role of NF-κB during the UPR remains undefined. Activation of NF-κB that we observed in response to classical UPR-inducing agents prompted

our further investigation of the functional significance of NF-κB activation. We reasoned that if NF-κB played a role in induction of UPR target genes, target gene expression would be diminished in UPR-induced MEFs isolated from NF-κB knockout mice. To this end, we obtained MEFs derived from "NF-κB triple knockout" (3KO) mice carrying homozygous deletions of three major NF-κB genes, p65/Rel-A, cRel and p50 (Gapuzan et al., 2005; Hoffmann and Baltimore, 2006). For confidence in our results we studied multiple isolates of wild type MEFs. As expected, we did not detect NF-κB activation during thapsigargin (Tg) treatment of 3KO MEFs (data not shown). We measured transcription levels of several established UPR target genes by quantitative PCR on cDNA prepared from cells treated with thapsigargin for up to 24 hours. UPR target genes including BiP/GRP78 (Foti et al., 1999; Li et al., 1997; Yoshida et al., 1998), CHOP (Okada et al., 2002; Oyadomari and Mori, 2004; Wang et al., 1996), HERP (Kokame et al., 2000), and ERdj4 (Shen et al., 2002b) were significantly reduced in the NF-κB knockout MEFs (Figure 6A, S7A for ERdj4). A similar reduction in UPR target gene transcription was seen in the single knockout *relA*$^{-/-}$ MEFs that lack only the p65 subunit of NF-κB (data not shown). However, not all UPR target genes are regulated by NF-κB. Expression of GRP94 (Okada et al., 2002; Yoshida et al., 1998) and calreticulin (Okada et al., 2002; Yoshida et al., 1998) during the UPR were similar in wild type and NF-κB knockout cells (Figure S9), indicating that NF-κB is not involved in activation of these genes. Furthermore, we found traditional NF-κB targets, IκBα and cIAP1, that were increased during the UPR in an NF-κB dependent manner (Figure S8). These results indicate that a subset of UPR genes require NF-κB for full activation.

Using chromatin IP (ChIP), we determined if NF-κB is able to directly bind to the promoters of these genes. We found that p65 is able to bind to the promoters of BiP/GRP78, CHOP, and HERP (Figure 6B) indicating a direct activation by NF-κB, while p65 does not bind

to the promoter of ERdj4 (Figure S7B) indicating its activation is an indirect effect of NF-κB activation. Furthermore, this binding was dependent on IRE1 and PERK since decreased promoter association was seen in *ire1*$^{-/-}$ and *perk*$^{-/-}$ cells (Figure 6B). Expression of GRP94 and calreticulin, genes not regulated by NF-κB, did not show promoter binding of p65 during the UPR (Figure S9). Taken together, NF-κB is an integral part of UPR transcription program and, moreover, a subset of the UPR target genes are direct NF-κB targets and require NF-κB for their maximum transcriptional activation.

DISCUSSION

The NF-κB transcription factor family regulates genes involved in a wide array of processes including inflammation, immune responses, apoptosis, and tumorigenesis (Basseres and Baldwin, 2006; Hayden and Ghosh, 2004; Rayet and Gelinas, 1999). NF-κB is also activated by the Unfolded Protein Response signaling pathway (Deng et al., 2004; Jiang et al., 2003; Pahl and Baeuerle, 1995). Initially, it was reported that only a subset of ER stresses activates NF-κB (Pahl and Baeuerle, 1995), although recent reports and our study clarified that NF-κB activation occurs under general UPR conditions (Deng et al., 2004; Hu et al., 2006; Jiang et al., 2003). Here, we have demonstrated that optimal activation of NF-κB during ER stress requires both IRE1 and PERK activities. In addition, we have found that NF-κB directly binds to the promoter of a subset of the canonical UPR target genes, activating their transcription in response to ER stress.

We have found, in agreement with previous reports (Deng et al., 2004; Jiang et al., 2003), that translation inhibition mediated by PERK phosphorylation of eIF2α leads to decrease in IκBα levels, but not NF-κB, due to their differential stabilities, resulting in generation of free and active NF-κB. In fact, the importance of translation inhibition has been illustrated by showing that cyclohexamide treatment of wild type cells was sufficient to activate NF-κB (Figure 2F and

(Deng et al., 2004)). However, we have found that CHX treatment alone was not sufficient to activate NF-κB in the absence of IRE1, revealing the importance of IRE1 for the activation of NF-κB. We have found that IRE1 is required for sustaining *basal* IKK activity. Furthermore, unlike most UPR induced events, IRE1 RNase function is not required but its kinase is critical for ER stress-induced NF-κB activation. Our conclusion is in contrast to the current view that NF-κB activation by PERK does not require IKK. This was derived from the observation where no significant phosphorylation of IκBα, a major target of IKK kinase, was detected in response to ER stress. While our data does agree with the lack of induced IκBα phosphorylation by the UPR (Figure 1C), we show that IKK is indeed required (Figure 1A). However, while UPR-induced increase in IκBα phosphorylation was not detectable, we have found that basal IKK activity was diminished in ire1 knockout cells. Furthermore, increasing basal IKK activity too much, as well as decreasing it too little, negatively affects the ability of the PERK signaling branch to further activate NF-κB during the UPR suggesting that there is a set range for basal IKK activity optimal NF-κB activation. By altering these inputs, the extent of NF-κB activation can be fine-tuned, allowing for a dynamic response to ER stress.

The ability of IRE1 to directly or indirectly modulate *basal* IKK activity suggests that IRE1 is never completely inactive or "OFF", even in the absence of overt ER stress, and that IRE1 has an intrinsic housekeeping function. Previously, we reported that a basal state IRE1 function is also required for efficient cytokinesis during mitosis in *S. cerevisiae* (Bicknell et al., 2007). There, we proposed that IRE1 activity is modulated in a "dimmer switch" fashion, rather than an "ON/OFF switch". Furthermore, we have reported the role of basal activity in the NF-κB pathway during the ribotoxic stimulus UV (O'Dea et al., 2007; O'Dea et al., 2008). Also, signaling mechanisms have been identified as affecting basal IKK activity as shown by PKN1 phosphorylation of TRAF1 resulting in decreased basal IKK activity (Kato et al., 2008). To date,

while inducible portions of signal transduction pathways have been the major focus of investigation, regulation of the basal activity of signal transduction components may be much more common, and a critical portion of regulating the pathways.

One of the unexpected findings here was that increasing the basal activity of IKK diminishes the ability of the PERK signaling branch to activate NF-κB, revealing a unique basal activity contribution (Figure 3 and 5). Implications of such characteristics of basal activity regulation would be specifically significant in designing strategies for treatment of certain diseases that are known to have elevated NF-κB/IKK basal activity. Increased NF-κB activity, for example, has been associated with multiple cancers and the general importance of NF-κB in cancer development has been well-established (Basseres and Baldwin, 2006; Hayden and Ghosh, 2004; Rayet and Gelinas, 1999). Therefore, drugs that suppress IKK activity are being considered for treatment (Karin et al., 2004; Nakanishi and Toi, 2005). In addition, the importance of the UPR in cancer, including the development of solid tumors and microenvironments that facilitate tumors, is becoming increasingly clear (Feldman et al., 2005; Fernandez et al., 2000; Lee and Hendershot, 2006; Ma and Hendershot, 2004; Ranganathan et al., 2006; Shuda et al., 2003). Our study has uncovered a previously un-described aspect of tumors with high basal NF-κB activity and thus may provide a key consideration for development of treatment strategies. Importance of the basal component in this system is demonstrated by the fact that UPR activation can overcome IKK suppressing drugs as tumor cells encounter UPR-inducing conditions (Figure 5). Our results suggest that the efficacy of IKK suppressing drugs may be increased when combined with drugs that inhibit the UPR.

One of the mysteries remains to be investigated is the molecular mechanism by which IRE1 regulates IKK activity at the basal condition. We have shown that the IRE1 kinase is required for specifically maintaining basal IKKβ phosphorylation (Figure 4A). While these

results suggested that IRE1 may directly associate with IKK complex or IKKβ, we have obtained no evidence that IRE1 physically associate with either IKKβ or IKK complex as no co-immunoprecipitation was detected even in the presence of reversible crosslinker (Figure S5A). The reasons why Hu et al., (2006) were able to detect such physical interaction are not clear at the moment. We have performed co-immuniprecipitation experiments using the same cell line and antibodies as those used in their study. Since IRE1 mediated regulation of IKK activity is at the basal state, the interaction between these two components or the formation of a complex that contains these may be extremely transient, and therefore, difficult to detect with conventional experimental protocols.

One of the components known to associate with IRE1 is TRAF2 and this association is thought to be a key for the activation of JNK in response to ER stress (Urano et al., 2000). Cells lacking TRAF2 function are defective in NF-κB activation during ER stress (this study, (Kaneko et al., 2003)) and more susceptible to apoptosis (Mauro et al., 2006). Our finding that IRE1 kinase but not RNase plays a role in NF-κB activation is consistent with the previous report showing the involvement of IRE1 kinase in TRAF2-JNK activation upon ER stress (Urano et al., 2000). We have also found that IRE1 regulates the stability of TRAF2 as TRAF2 levels are decreased in $ire1^{-/-}$ cells. However, the increase in levels of TRAF2 did not rescue NF-κB activation in $ire1^{-/-}$ cells, and thus significance of decrease in TRAF2 level in $ire1^{-/-}$ cells is not clear. In addition, diverging pathways from TRAF2 such as the JNK pathway do not seem to have an effect on NF-κB activation since NF-κB activation was normal in $jnk^{-/-}$ cells (Figure 4F). Taken together, our study uncovers an additional function for IRE1, expanding its role as a key regulator of stress signaling from the ER.

Our data demonstrates that NF-κB activation is an integral part of the UPR transcriptional response as a transcription factor directly binding to the promoters of certain UPR

target genes (Figure 6). Based on primary sequence analyses (Ghosh et al., 1998; Hoffmann et al., 2003; Kunsch et al., 1992), UPR target genes including those examined in our study have at least one potential NF-κB site within their promoter proximal regions. For example, the BiP/GRP78 gene contains a predicted NF-κB site between the first and second ER response element (ERSE) elements. However, predicted NF-κB sties are also found in promoters of both GRP94 and calreticulin genes despite the fact that their transcription induction during the UPR does not depend on NF-κB. Therefore, additional determinants other than the presence of an NF-κB binding site must exist for NF-κB-dependent transcriptional control. One possibility is that recruitment of NF-κB to a promoter region is facilitated by one or more transcription factors activated during the UPR. Such arrangement of the transcription enhancer elements also fits well with relatively lower activation levels of NF-κB during ER stress. While UPR activated NF-κB alone may not be sufficient to induce transcription of UPR target genes, NF-κB assists the other UPR transcription factors to achieve full activation of UPR target genes, providing a molecular ground for increasing the complexity of transcription responses. This may also explain the difference between our study and a previous study which showed that ectopic expression of NF-κB subunits was not able to activate BiP (Pahl and Baeuerle, 1995). Searches for a NF-κB site(s) placed similarly in relationships to the UPRE or the ERSE sequences within the promoter regions of homologous genes among different species may predict the UPR functional NF-κB site(s).

Our study has revealed a yet un-described aspect of transcription response during the UPR. NF-κB is an integral part of the UPR transcription response, activating transcription of a subset of the canonical UPR target genes by directly binding to their promoter. While maximal transcription of the certain canonical UPR target genes requires NF-κB, some of them, including ERdj4, do not bind directly to NF-κB to their promoter regions. One of the possibilities includes that another transcription factor(s) activated by ER stress-induced NF-κB exists, further

increasing the complexity of the UPR transcriptional response. Finally, in addition to the canonical UPR target genes, our study has also revealed that classical NF-κB target genes, such as IκBα and cIAP1, are also induced during the ER stress. Since those genes have not been identified as the UPR target genes, their transcription induction may require either NF-κB alone or no additional UPR transcription factors, such as XBP1, ATF6, and ATF4. However, not all of the canonical NF-κB target genes are activated during the UPR. For example, Bcl-2 and XIAP mRNA levels were not induced during the UPR (data not shown). Identification of the last category of genes highlights the need for future Genome-wide analyses for NF-κB dependent UPR transcription targets, which will provide more comprehensive view of the UPR transcriptome.

MATERIALS AND METHODS

Cell culture and treatment

Wild type, *ikkα/β*$^{-/-}$, *ire1*$^{-/-}$, *perk*$^{-/-}$, *jnk1*$^{-/-}$, and *jnk2*$^{-/-}$ MEFs were cultured in DMEM media (Cellgro). 786-O cells were cultured in RPMI 1640 (Cellgro). All media was supplemented with 10% fetal calf serum (Gibco), 100 U/ml penicillin, and 100ug/ml streptomycin (Mediatech). Cells were grown in 5% CO_2 at 37°C. Cells were treated with 200 nM thapsigargin (Calbiochem), 1 mM DTT (Fisher), 50 μg/ml cycloheximide (Sigma), 25μM MG-132 (Calbiochem), 100μM SC-514 (Calbiochem), or 20 ng/ml tumor necrosis factor α (TNFα) (Sigma) for the indicated amount of time.

EMSA

NF-κB activity was measured by an electrophoretic mobility shift assay (EMSA) as previously described (Werner et al., 2005). Nuclear protein was incubated at room temperature for 15 min with 0.01 pmol of ^{32}P labeled probe containing an NF-κB binding site

(AGTTGAGG**GGACTTTCC**CAGGC) in binding buffer (10mM Tris (pH 7.5), 50mM NaCl, 10% glycerol, 1% NP-40, 1mM EDTA, 0.1 µg/µl poly-dI·dC) as described detail in Pahl and Baeuerle, 1995. Complexes were separated by gel electrophoresis using a 5% non-denaturing polyacrylamide gel and visualized by autoradiography. Competition assays were performed using a single stranded probe that forms a double stranded hairpin structure containing an NF-□B binding site. The sequences of the wild type and mutant competitors are WT:(CTG**GGGACTTTCC**AGGTTAGCTTCCT**GGAAAGTCCC**CAG) and the mutant:(CTG***TCT*ACTTTCC**AGGTTAGCTTCCT**GGAAAGT*AGA***CAG). Supershift assays were performed using antibodies against p65 and p50 of NF-κB (Santa Cruz Biotech) added to the binding mixture and incubated on ice for 1 hr at 4°C, and separated by electrophoresis using a 5% non-denaturing polyacrylamide gel and visualized by autoradiography. As a control, an Oct-1 probe (TGTCGA**ATGCAAAT**CACTAGAA) was used on the same nuclear extracts to determine that total protein in the extract was similar.

Western blot

After treatment, cells were washed with ice cold PBS twice and the lysed using RIPA buffer (20 mM HEPES (pH 7.4), 150mM NaCl, 1mM EDTA, 1% NP-40, 0.25% NaDeoxycholate, 0.1% SDS, 10mM NaF, 1mM NaVO4, 1mM PMSF, 1mM PMSF, 100u/ml Aprotinin, 1.4 µg/ml Pepstatin, 1 µg/ml Leupeptin). The protein concentration was then normalized by BCA Assay (Pierce). Samples were analyzed by SDS-PAGE and transferred to nitrocellulose and probed with antibodies against NF-κB p65 subunit (Santa Cruz), p50 (Santa Cruz), IκBα (Santa Cruz), phospho-IκBα (Cell Signaling), eIF2α (Cell Signaling), phospho-eIF2α (Stressgen), IKKα (Santa Cruz), IKKβ (Biosource), IKKγ (Santa Cruz), P-IKK (Cell Signalling), TRAF2, (Santa Cruz), Cdc37 (Santa Cruz), TAK1 (Santa Cruz), RIP (Santa Cruz), HSP90 (Stressgen), P-IKK (Cell Signalling) and actin (Sigma).

^{35}S Labeling

After treatment, cell were labeled with 50 μCi/ml ^{35}S (Trans ^{35}S-Label, MP Biomedicals) for 10 min, and washed twice with cold PBS containing non radio-labeled methionine. 15 μg of total protein was separated by SDS-PAGE and visualized by staining with coomassie blue staining (CB). Cellular translation levels were measured by incorporation of radiolabeled amino acids using autoradiography.

Transfections

Cells were plated to 50% confluency in 10cm plates the day before transfection. Plasmids were transfected using the Effectene (Qiagen) system according to manufacturer's instructions for 48 hrs.

Dual Luciferase Assays

Cells were transfected with 1μg of a plasmid containing 3XκB-Luc reporter. As an internal control, cells were also co-transfected with 0.05μg of a plasmid with a *Renilla* luciferase gene driven by an SV40 promoter. Transfections were done in triplicate, and after 48h cells were treated as indicated. Luciferase assays were carried out using the Dual-Luciferase Reporter Assay (Promega) according to manufacturer's instructions. Luciferase activity was measured by luminomiter (Analytical Luminescence Laboratory, Monolight, model 2010). Values of samples were normalized to *Renilla* luciferase. Values shown are averages and standard error from at least three independent experiments.

IKK Kinase Assay

IKK activity was measured by IKK kinase assays as previously described (Werner et al., 2005) . After treatment, cells were washed twice with cold PBS, and cytoplasmic extracts were taken using Cytolplasmic Extract Buffer (10mM HEPES-KOH pH 7.9, 250mM NaCl, 1mM EDTA, 0.5% NP-40, 0.2% Tween 20, 2mM DTT, 1mM PMSF, 20mM β-glycerophosphate,

10mM NaF, 0.1mM Na_3VO_4). IKK complexes were then immunoprecipitated using an antibody against IKKγ (Pharmingen). Cytoplasmic extracts before and after immunoprecipitation were run on a western blot and probed for IKKα (Santa Cruz) to check for immunoprecipitation efficiency. IKK complexes were then incubated with 10uCi γ^{32}P-ATP, recombinant IκBα in Kinase Buffer (20mM HEPES pH 7.7, 20mM β-glycerophosphate, 100mM NaCl, 100μM Na_3VO_4, 10mM $MgCl_2$, 10mM NaF, 1mM PMSF, 2mM DTT, 20μM cold ATP) at 30C for 30 min. Samples were then run on SDS-PAGE gels and phosphorylated IκBα was visualized by autoradiography.

RNA extraction, RT, and quantitative PCR

Total RNA was prepared using RNeasy Mini Kit (Qiagen) and treated with DNase (Qiagen) according to manufacturer's instructions. One microgram of total RNA was then reverse transcribed using ThermoScript reverse transcriptase (Invitrogen) according to manufacturer's instructions to obtain cDNA. For quantitative PCR, 5 ng of input cDNA was analyzed in triplicate per sample for each primer pair. All reactions were performed using SYBR Green PCR Master Mix (Applied Biosystems) and 400nM of each primer per reaction in a total volume of 25 μl. The reaction was performed using default cycling parameters on an ABI Prism 7200 Sequence Detector. A standard curve composed of five-fold serial dilutions of concentrated cDNA was included in each qPCR run for each primer. Since the SYBR Green system is used, it is important to have a single product being amplified so a melting curve analysis was performed after each run to confirm amplification of a single product. Expression of each gene was normalized to 18S and expressed as fold induction. Values are mean±s.e.m of at least three independent experiments. The following primers were used for the qPCR reaction:

GRP78/BiP: F-CCATCCCGTGGCATAAACC, R-GGAATCAGTTTGGTCATGACACC; *CHOP*: F-GAGCTGGAAGCCTGGTATGAG, R- GTGTGACCTCTGTTGGCCC; HERP*:* F-GTGCACAAGAGATACCTGTGGTC, R- CACCTTGTGCATTCATCCG; ERDJ4*:*

F- GCTACTATGATATCTTAGGTGTGCC, R- GCTTCTGCAATCTCTCTGAA: *Calreticulin: F-* CGCTGGGTCGAATCCAAAC, R- GCTGGCCGCACAATCAGTG: *GRP94:* F- AAGAGGACCTGGGTAAAAGCC, R- GTTTCATCATCCTGTTCACTTCAGC; IκBα*:* F- CCTCAACTTCCAGAACAACCTGC, R- GCCCTGCTCACAGGCAAG; cIAP-*1:* F- TCCAAGGTGTGAGTTCTTGATACG, R- GGGTCAGCATTTTCTTCTCCTG; XIAP*:* F- CACCATATACCCGAGGAACCC, R- CCTGTGTTCTGACCAGGCAC; Bcl-*xL:* F- GCACTGTGCGTGGAAAGCG, R- CCCAGCCGCCGTTCTCC.

Chromatin Immunoprecipitation

ChIP was performed essentially as described in Rayman et al. 2000. Briefly, wild type, *ire1*$^{-/-}$, *perk*$^{-/-}$, and 3KO (*nkfb*$^{-/-}$) cells were treated with 200 nM Thapsigargin and fixed with 1% formaldehyde (Sigma). Cells were then sonicated to obtain approximately 500 bp fragments, and lysate was cleared of debris by centrifugation. Sample was then precleared with protein-G (Upstate) beads blocked with sheared salmon sperm DNA (New for 2h twice. Immunoprecipitation was done overnight at 4°C with 1μg p65 antibody (Santa Cruz Biotech). For the negative control, a mouse IgG (Bio-Rad) was used instead p65 antibody. Complexes were recovered by protein-G beads blocked with salmon sperm DNA, washed under stringent conditions, then decrosslinked at 65°C overnight. While decrosslinking, samples were also eluted with 1% SDS. Samples were then treated with Proteinase K at 55°C for 2 hrs. DNA was extracted by phenol/chloroform and PCR was performed. Primers were designed targeting the promoter regions of genes and contain at least one putative NF-κB binding site. The following primer pairs were used: *BiP/GRP78*: F- GGCGTAGCAATGACGTGAG, R- GCCACTCGCCTTATATACCC; *Herp:* F- ACTCAGGATGACGCAACCAC, R- GCCGTCTGAGACCACACAAC; *IκBα*: F- GCCAGCGTTTCCACTCTTGG, R- TGGAAAGTCCTCCCGACCAG; *CHOP:* F- TTTTCCCTTTTCCCCAGAGG, R-

GTGTGTGGGACCTGGCTTTC; *Calreticulin:* F- CGAGCCAGAGACTCTCAGCAG, R- GGATCCCAGATGGCTGATTTC; *ERdj4:* F- CCATTGTTTGGGCAGAGTGG, R- GCTGCGGTTGTTCGCTAGTC; *cIAP1:* F- GGAAAACCAGCTGCAGACTTCAC, R- GGTGAATTGACACCCTCACAGG; *GRP94:* F- CTCAGGGACCAAGGCTTCCC, R- GCGGTCCGCCCACTAAGC.

ACKNOWLEDGEMENTS

We thank Dr. Doug Cavener for providing *perk*$^{-/-}$ and PERK$^{+/+}$ MEFs, Dr. Randal Kaufman for *ire1*$^{-/-}$ and the cognate IRE1$^{+/+}$ MEFs, Dr. Randall Johnson for LLCs and 786-O cells, Dr. Inder Verma for *ikk*$\alpha/\beta^{-/-}$, IKK$\alpha/\beta^{+/+}$ MEFs, Dr. Michael Karin for the jnk1$^{-/-}$, jnk2$^{-/-}$, and JNK$^{+/+}$ MEFs, Dr. Richard Morimoto for the IKK plasmids, and Dr. Kazutoshi Mori for the Luciferase reporters. We also thank Dr. Douglass Forbes and Andrew Doedens for valuable suggestions and critical reading of the manuscript.

REFERENCES

An, J., and Rettig, M. B. (2005). Mechanism of von Hippel-Lindau protein-mediated suppression of nuclear factor kappa B activity. Mol Cell Biol *25*, 7546-7556.

Basseres, D. S., and Baldwin, A. S. (2006). Nuclear factor-kappaB and inhibitor of kappaB kinase pathways in oncogenic initiation and progression. Oncogene *25*, 6817-6830.

Bi, M., Naczki, C., Koritzinsky, M., Fels, D., Blais, J., Hu, N., Harding, H., Novoa, I., Varia, M., Raleigh, J., *et al.* (2005). ER stress-regulated translation increases tolerance to extreme hypoxia and promotes tumor growth. Embo J *24*, 3470-3481.

Bicknell, A. A., Babour, A., Federovitch, C. M., and Niwa, M. (2007). A novel role in cytokinesis reveals a housekeeping function for the unfolded protein response. J Cell Biol *177*, 1017-1027.

Calfon, M., Zeng, H., Urano, F., Till, J. H., Hubbard, S. R., Harding, H. P., Clark, S. G., and Ron, D. (2002). IRE1 couples endoplasmic reticulum load to secretory capacity by processing the XBP-1 mRNA. Nature *415*, 92-96.

Chen, G., Cao, P., and Goeddel, D. V. (2002). TNF-induced recruitment and activation of the IKK complex require Cdc37 and Hsp90. Mol Cell *9*, 401-410.

Cox, J. S., Shamu, C. E., and Walter, P. (1993). Transcriptional induction of genes encoding endoplasmic reticulum resident proteins requires a transmembrane protein kinase. Cell *73*, 1197-1206.

Daniel, L. W., Civoli, F., Rogers, M. A., Smitherman, P. K., Raju, P. A., and Roederer, M. (1995). ET-18-OCH3 inhibits nuclear factor-kappa B activation by 12-O-tetradecanoylphorbol-13-acetate but not by tumor necrosis factor-alpha or interleukin 1 alpha. Cancer Res *55*, 4844-4849.

Delhase, M., Hayakawa, M., Chen, Y., and Karin, M. (1999). Positive and negative regulation of IkappaB kinase activity through IKKbeta subunit phosphorylation. Science *284*, 309-313.

Deng, J., Lu, P. D., Zhang, Y., Scheuner, D., Kaufman, R. J., Sonenberg, N., Harding, H. P., and Ron, D. (2004). Translational repression mediates activation of nuclear factor kappa B by phosphorylated translation initiation factor 2. Mol Cell Biol *24*, 10161-10168.

DiDonato, J., Mercurio, F., Rosette, C., Wu-Li, J., Suyang, H., Ghosh, S., and Karin, M. (1996). Mapping of the inducible IkappaB phosphorylation sites that signal its ubiquitination and degradation. Mol Cell Biol *16*, 1295-1304.

DiDonato, J. A., Hayakawa, M., Rothwarf, D. M., Zandi, E., and Karin, M. (1997). A cytokine-responsive IkappaB kinase that activates the transcription factor NF-kappaB. Nature *388*, 548-554.

Ea, C. K., Deng, L., Xia, Z. P., Pineda, G., and Chen, Z. J. (2006). Activation of IKK by TNFalpha requires site-specific ubiquitination of RIP1 and polyubiquitin binding by NEMO. Mol Cell *22*, 245-257.

Feldman, D. E., Chauhan, V., and Koong, A. C. (2005). The unfolded protein response: a novel component of the hypoxic stress response in tumors. Mol Cancer Res *3*, 597-605.

Fernandez, P. M., Tabbara, S. O., Jacobs, L. K., Manning, F. C., Tsangaris, T. N., Schwartz, A. M., Kennedy, K. A., and Patierno, S. R. (2000). Overexpression of the glucose-regulated stress gene GRP78 in malignant but not benign human breast lesions. Breast Cancer Res Treat *59*, 15-26.

Foti, D. M., Welihinda, A., Kaufman, R. J., and Lee, A. S. (1999). Conservation and divergence of the yeast and mammalian unfolded protein response. Activation of specific mammalian endoplasmic reticulum stress element of the grp78/BiP promoter by yeast Hac1. J Biol Chem *274*, 30402-30409.

Frelin, C., Imbert, V., Griessinger, E., Peyron, A. C., Rochet, N., Philip, P., Dageville, C., Sirvent, A., Hummelsberger, M., Berard, E., *et al.* (2005). Targeting NF-kappaB activation via

pharmacologic inhibition of IKK2-induced apoptosis of human acute myeloid leukemia cells. Blood *105*, 804-811.

Gapuzan, M. E. R., Schmah, O., Pollock, A. D., Hoffmann, A., and Gilmore, T. D. (2005). Immortalized fibroblasts from NF-kappa B RelA knockout mice show phenotypic heterogeneity and maintain increased sensitivity to tumor necrosis factor alpha after transformation by v-Ras. Oncogene *24*, 6574-6583.

Ghosh, S., May, M. J., and Kopp, E. B. (1998). NF-kappa B and Rel proteins: evolutionarily conserved mediators of immune responses. Annu Rev Immunol *16*, 225-260.

Habelhah, H., Takahashi, S., Cho, S. G., Kadoya, T., Watanabe, T., and Ronai, Z. (2004). Ubiquitination and translocation of TRAF2 is required for activation of JNK but not of p38 or NF-kappaB. Embo J *23*, 322-332.

Harding, H. P., Novoa, I., Bertolotti, A., Zeng, H., Zhang, Y., Urano, F., Jousse, C., and Ron, D. (2001). Translational regulation in the cellular response to biosynthetic load on the endoplasmic reticulum. Cold Spring Harb Symp Quant Biol *66*, 499-508.

Harding, H. P., Novoa, I., Zhang, Y., Zeng, H., Wek, R., Schapira, M., and Ron, D. (2000a). Regulated translation initiation controls stress-induced gene expression in mammalian cells. Mol Cell *6*, 1099-1108.

Harding, H. P., Zhang, Y., Bertolotti, A., Zeng, H., and Ron, D. (2000b). Perk is essential for translational regulation and cell survival during the unfolded protein response. Mol Cell *5*, 897-904.

Harding, H. P., Zhang, Y., and Ron, D. (1999). Protein translation and folding are coupled by an endoplasmic-reticulum-resident kinase. Nature *397*, 271-274.

Hayden, M. S., and Ghosh, S. (2004). Signaling to NF-kappaB. Genes Dev *18*, 2195-2224.

Haze, K., Yoshida, H., Yanagi, H., Yura, T., and Mori, K. (1999). Mammalian transcription factor ATF6 is synthesized as a transmembrane protein and activated by proteolysis in response to endoplasmic reticulum stress. Mol Biol Cell *10*, 3787-3799.

Hinnebusch, A. G. (1997). Translational regulation of yeast GCN4. A window on factors that control initiator-trna binding to the ribosome. J Biol Chem *272*, 21661-21664.

Hoffmann, A., and Baltimore, D. (2006). Circuitry of nuclear factor kappa B signaling. Immunological Reviews *210*, 171-186.

Hoffmann, A., Leung, T. H., and Baltimore, D. (2003). Genetic analysis of NF-kappaB/Rel transcription factors defines functional specificities. Embo J *22*, 5530-5539.

Hu, P., Han, Z., Couvillon, A. D., Kaufman, R. J., and Exton, J. H. (2006). Autocrine tumor necrosis factor alpha links endoplasmic reticulum stress to the membrane death receptor pathway

through IRE1alpha-mediated NF-kappaB activation and down-regulation of TRAF2 expression. Mol Cell Biol *26*, 3071-3084.

Huang, T. T., Wuerzberger-Davis, S. M., Wu, Z. H., and Miyamoto, S. (2003). Sequential modification of NEMO/IKKgamma by SUMO-1 and ubiquitin mediates NF-kappaB activation by genotoxic stress. Cell *115*, 565-576.

Jackson-Bernitsas, D. G., Ichikawa, H., Takada, Y., Myers, J. N., Lin, X. L., Darnay, B. G., Chaturvedi, M. M., and Aggarwal, B. B. (2007). Evidence that TNF-TNFR1-TRADD-TRAF2-RIP-TAK1-IKK pathway mediates constitutive NF-kappaB activation and proliferation in human head and neck squamous cell carcinoma. Oncogene *26*, 1385-1397.

Jiang, H. Y., and Wek, R. C. (2005). GCN2 phosphorylation of eIF2alpha activates NF-kappaB in response to UV irradiation. Biochem J *385*, 371-380.

Jiang, H. Y., Wek, S. A., McGrath, B. C., Scheuner, D., Kaufman, R. J., Cavener, D. R., and Wek, R. C. (2003). Phosphorylation of the alpha subunit of eukaryotic initiation factor 2 is required for activation of NF-kappaB in response to diverse cellular stresses. Mol Cell Biol *23*, 5651-5663.

Kaneko, M., Niinuma, Y., and Nomura, Y. (2003). Activation signal of nuclear factor-kappa B in response to endoplasmic reticulum stress is transduced via IRE1 and tumor necrosis factor receptor-associated factor 2. Biol Pharm Bull *26*, 931-935.

Karin, M. (1999). How NF-kappaB is activated: the role of the IkappaB kinase (IKK) complex. Oncogene *18*, 6867-6874.

Karin, M. (2006). Nuclear factor-kappaB in cancer development and progression. Nature *441*, 431-436.

Karin, M., and Ben-Neriah, Y. (2000). Phosphorylation meets ubiquitination: the control of NF-[kappa]B activity. Annu Rev Immunol *18*, 621-663.

Karin, M., Yamamoto, Y., and Wang, Q. M. (2004). The IKK NF-kappa B system: a treasure trove for drug development. Nat Rev Drug Discov *3*, 17-26.

Kato, T., Jr., Gotoh, Y., Hoffmann, A., and Ono, Y. (2008). Negative regulation of constitutive NF-kappaB and JNK signaling by PKN1-mediated phosphorylation of TRAF1. Genes Cells *13*, 509-520.

Kaufman, R. J. (2002). Orchestrating the unfolded protein response in health and disease. J Clin Invest *110*, 1389-1398.

Kishore, N., Sommers, C., Mathialagan, S., Guzova, J., Yao, M., Hauser, S., Huynh, K., Bonar, S., Mielke, C., Albee, L., *et al.* (2003). A selective IKK-2 inhibitor blocks NF-kappa B-dependent gene expression in interleukin-1 beta-stimulated synovial fibroblasts. J Biol Chem *278*, 32861-32871.

Kokame, K., Agarwala, K. L., Kato, H., and Miyata, T. (2000). Herp, a new ubiquitin-like membrane protein induced by endoplasmic reticulum stress. J Biol Chem *275*, 32846-32853.

Koumenis, C., Naczki, C., Koritzinsky, M., Rastani, S., Diehl, A., Sonenberg, N., Koromilas, A., and Wouters, B. G. (2002). Regulation of protein synthesis by hypoxia via activation of the endoplasmic reticulum kinase PERK and phosphorylation of the translation initiation factor eIF2alpha. Mol Cell Biol *22*, 7405-7416.

Koumenis, C., and Wouters, B. G. (2006). "Translating" tumor hypoxia: unfolded protein response (UPR)-dependent and UPR-independent pathways. Mol Cancer Res *4*, 423-436.

Kunsch, C., Ruben, S. M., and Rosen, C. A. (1992). Selection of optimal kappa B/Rel DNA-binding motifs: interaction of both subunits of NF-kappa B with DNA is required for transcriptional activation. Mol Cell Biol *12*, 4412-4421.

Lee, A. S., and Hendershot, L. M. (2006). ER stress and cancer. Cancer Biol Ther *5*, 721-722.

Li, Q., Lu, Q., Hwang, J. Y., Buscher, D., Lee, K. F., Izpisua-Belmonte, J. C., and Verma, I. M. (1999). IKK1-deficient mice exhibit abnormal development of skin and skeleton. Genes Dev *13*, 1322-1328.

Li, W. W., Hsiung, Y., Zhou, Y., Roy, B., and Lee, A. S. (1997). Induction of the mammalian GRP78/BiP gene by Ca2+ depletion and formation of aberrant proteins: activation of the conserved stress-inducible grp core promoter element by the human nuclear factor YY1. Mol Cell Biol *17*, 54-60.

Ma, Y., and Hendershot, L. M. (2004). The role of the unfolded protein response in tumour development: friend or foe? Nat Rev Cancer *4*, 966-977.

Manna, S. K., Manna, P., and Sarkar, A. (2007). Inhibition of RelA phosphorylation sensitizes apoptosis in constitutive NF-kappaB-expressing and chemoresistant cells. Cell Death Differ *14*, 158-170.

Mauro, C., Crescenzi, E., De Mattia, R., Pacifico, F., Mellone, S., Salzano, S., de Luca, C., D'Adamio, L., Palumbo, G., Formisano, S., *et al.* (2006). Central role of the scaffold protein tumor necrosis factor receptor-associated factor 2 in regulating endoplasmic reticulum stress-induced apoptosis. J Biol Chem *281*, 2631-2638.

Mori, K. (2000). Tripartite management of unfolded proteins in the endoplasmic reticulum. Cell *101*, 451-454.

Mori, K., Ma, W., Gething, M. J., and Sambrook, J. (1993). A transmembrane protein with a cdc2+/CDC28-related kinase activity is required for signaling from the ER to the nucleus. Cell *74*, 743-756.

Nakanishi, C., and Toi, M. (2005). Nuclear factor-kappaB inhibitors as sensitizers to anticancer drugs. Nat Rev Cancer *5*, 297-309.

O'Dea, E. L., Barken, D., Peralta, R. Q., Tran, K. T., Werner, S. L., Kearns, J. D., Levchenko, A., and Hoffmann, A. (2007). A homeostatic model of IkappaB metabolism to control constitutive NF-kappaB activity. Mol Syst Biol *3*, 111.

O'Dea, E. L., Kearns, J. D., and Hoffmann, A. (2008). UV as an amplifier rather than inducer of NF-kappaB activity. Mol Cell *30*, 632-641.

Okada, T., Yoshida, H., Akazawa, R., Negishi, M., and Mori, K. (2002). Distinct roles of activating transcription factor 6 (ATF6) and double-stranded RNA-activated protein kinase-like endoplasmic reticulum kinase (PERK) in transcription during the mammalian unfolded protein response. Biochem J *366*, 585-594.

Oyadomari, S., and Mori, M. (2004). Roles of CHOP/GADD153 in endoplasmic reticulum stress. Cell Death Differ *11*, 381-389.

Ozcan, U., Cao, Q., Yilmaz, E., Lee, A. H., Iwakoshi, N. N., Ozdelen, E., Tuncman, G., Gorgun, C., Glimcher, L. H., and Hotamisligil, G. S. (2004). Endoplasmic reticulum stress links obesity, insulin action, and type 2 diabetes. Science *306*, 457-461.

Ozcan, U., Yilmaz, E., Ozcan, L., Furuhashi, M., Vaillancourt, E., Smith, R. O., Gorgun, C. Z., and Hotamisligil, G. S. (2006). Chemical chaperones reduce ER stress and restore glucose homeostasis in a mouse model of type 2 diabetes. Science *313*, 1137-1140.

Pahl, H. L., and Baeuerle, P. A. (1995). A novel signal transduction pathway from the endoplasmic reticulum to the nucleus is mediated by transcription factor NF-kappa B. Embo J *14*, 2580-2588.

Patil, C., and Walter, P. (2001). Intracellular signaling from the endoplasmic reticulum to the nucleus: the unfolded protein response in yeast and mammals. Curr Opin Cell Biol *13*, 349-355.

Ranganathan, A. C., Zhang, L., Adam, A. P., and Aguirre-Ghiso, J. A. (2006). Functional coupling of p38-induced up-regulation of BiP and activation of RNA-dependent protein kinase-like endoplasmic reticulum kinase to drug resistance of dormant carcinoma cells. Cancer Res *66*, 1702-1711.

Rayet, B., and Gelinas, C. (1999). Aberrant rel/nfkb genes and activity in human cancer. Oncogene *18*, 6938-6947.

Romero-Ramirez, L., Cao, H., Nelson, D., Hammond, E., Lee, A. H., Yoshida, H., Mori, K., Glimcher, L. H., Denko, N. C., Giaccia, A. J., *et al.* (2004). XBP1 is essential for survival under hypoxic conditions and is required for tumor growth. Cancer Res *64*, 5943-5947.

Ron, D., and Walter, P. (2007). Signal integration in the endoplasmic reticulum unfolded protein response. Nat Rev Mol Cell Biol *8*, 519-529.

Rutkowski, D. T., and Kaufman, R. J. (2004). A trip to the ER: coping with stress. Trends Cell Biol *14*, 20-28.

Scheuner, D., Song, B., McEwen, E., Liu, C., Laybutt, R., Gillespie, P., Saunders, T., Bonner-Weir, S., and Kaufman, R. J. (2001). Translational control is required for the unfolded protein response and in vivo glucose homeostasis. Mol Cell *7*, 1165-1176.

Shen, J., Chen, X., Hendershot, L., and Prywes, R. (2002a). ER stress regulation of ATF6 localization by dissociation of BiP/GRP78 binding and unmasking of Golgi localization signals. Dev Cell *3*, 99-111.

Shen, Y., Meunier, L., and Hendershot, L. M. (2002b). Identification and characterization of a novel endoplasmic reticulum (ER) DnaJ homologue, which stimulates ATPase activity of BiP in vitro and is induced by ER stress. J Biol Chem *277*, 15947-15956.

Shi, Y., Vattem, K. M., Sood, R., An, J., Liang, J., Stramm, L., and Wek, R. C. (1998). Identification and characterization of pancreatic eukaryotic initiation factor 2 alpha-subunit kinase, PEK, involved in translational control. Mol Cell Biol *18*, 7499-7509.

Shishodia, S., and Aggarwal, B. B. (2004). Nuclear factor-kappaB: a friend or a foe in cancer? Biochem Pharmacol *68*, 1071-1080.

Shuda, M., Kondoh, N., Imazeki, N., Tanaka, K., Okada, T., Mori, K., Hada, A., Arai, M., Wakatsuki, T., Matsubara, O., *et al.* (2003). Activation of the ATF6, XBP1 and grp78 genes in human hepatocellular carcinoma: a possible involvement of the ER stress pathway in hepatocarcinogenesis. J Hepatol *38*, 605-614.

Takaesu, G., Surabhi, R. M., Park, K. J., Ninomiya-Tsuji, J., Matsumoto, K., and Gaynor, R. B. (2003). TAK1 is critical for IkappaB kinase-mediated activation of the NF-kappaB pathway. J Mol Biol *326*, 105-115.

Tergaonkar, V., Bottero, V., Ikawa, M., Li, Q., and Verma, I. M. (2003). IkappaB kinase-independent IkappaBalpha degradation pathway: functional NF-kappaB activity and implications for cancer therapy. Mol Cell Biol *23*, 8070-8083.

Tirasophon, W., Lee, K., Callaghan, B., Welihinda, A., and Kaufman, R. J. (2000). The endoribonuclease activity of mammalian IRE1 autoregulates its mRNA and is required for the unfolded protein response. Genes Dev *14*, 2725-2736.

Tirasophon, W., Welihinda, A. A., and Kaufman, R. J. (1998). A stress response pathway from the endoplasmic reticulum to the nucleus requires a novel bifunctional protein kinase/endoribonuclease (Ire1p) in mammalian cells. Genes Dev *12*, 1812-1824.

Urano, F., Wang, X., Bertolotti, A., Zhang, Y., Chung, P., Harding, H. P., and Ron, D. (2000). Coupling of stress in the ER to activation of JNK protein kinases by transmembrane protein kinase IRE1. Science *287*, 664-666.

Venkatraman, M., Anto, R. J., Nair, A., Varghese, M., and Karunagaran, D. (2005). Biological and chemical inhibitors of NF-kappaB sensitize SiHa cells to cisplatin-induced apoptosis. Mol Carcinog *44*, 51-59.

Wang, X. Z., Lawson, B., Brewer, J. W., Zinszner, H., Sanjay, A., Mi, L. J., Boorstein, R., Kreibich, G., Hendershot, L. M., and Ron, D. (1996). Signals from the stressed endoplasmic reticulum induce C/EBP-homologous protein (CHOP/GADD153). Mol Cell Biol *16*, 4273-4280.

Wek, R. C., and Cavener, D. R. (2007). Translational control and the unfolded protein response. Antioxid Redox Signal *9*, 2357-2371.

Werner, S. L., Barken, D., and Hoffmann, A. (2005). Stimulus specificity of gene expression programs determined by temporal control of IKK activity. Science *309*, 1857-1861.

Williams, R. D., Elliott, A. Y., Stein, N., and Fraley, E. E. (1978). In vitro cultivation of human renal cell cancer. II. Characterization of cell lines. In Vitro *14*, 779-786.

Wu, Z. H., Shi, Y., Tibbetts, R. S., and Miyamoto, S. (2006). Molecular linkage between the kinase ATM and NF-kappaB signaling in response to genotoxic stimuli. Science *311*, 1141-1146.

Yang, J., and Richmond, A. (2001). Constitutive IkappaB kinase activity correlates with nuclear factor-kappaB activation in human melanoma cells. Cancer Res *61*, 4901-4909.

Ye, J., Rawson, R. B., Komuro, R., Chen, X., Dave, U. P., Prywes, R., Brown, M. S., and Goldstein, J. L. (2000). ER stress induces cleavage of membrane-bound ATF6 by the same proteases that process SREBPs. Mol Cell *6*, 1355-1364.

Yoshida, H., Haze, K., Yanagi, H., Yura, T., and Mori, K. (1998). Identification of the cis-acting endoplasmic reticulum stress response element responsible for transcriptional induction of mammalian glucose-regulated proteins. Involvement of basic leucine zipper transcription factors. J Biol Chem *273*, 33741-33749.

Yoshida, H., Matsui, T., Yamamoto, A., Okada, T., and Mori, K. (2001). XBP1 mRNA is induced by ATF6 and spliced by IRE1 in response to ER stress to produce a highly active transcription factor. Cell *107*, 881-891.

Zandi, E., Chen, Y., and Karin, M. (1998). Direct phosphorylation of IkappaB by IKKalpha and IKKbeta: discrimination between free and NF-kappaB-bound substrate. Science *281*, 1360-1363.

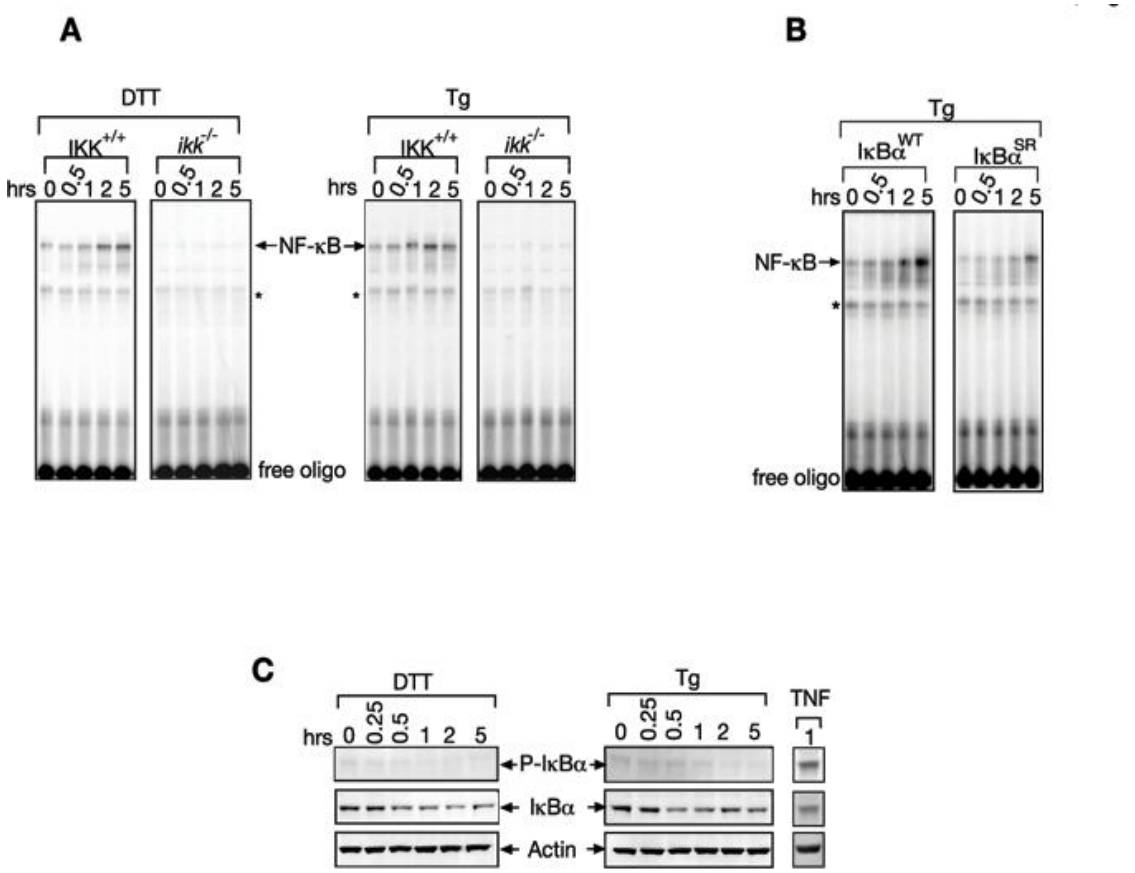

Figure 1. Basal IKK activity is required for NF-κB activation during ER stress.

(A) NF-κB cannot be activated in the absence of IKK. $IKK^{+/+}$ and $ikk^{-/-}$ (knockout for IKKα and IKKβ) cells were treated with DTT or Tg for the indicated amount of time, nuclear extracts were prepared and incubated with a radiolabelled probe that contains an NF-κB binding site (free oligo). NF-κB binding results in a shift of the mobility of the band, and indicates the amount of active NF-κB (NF-κB). The active form of NF-κB was found to be p65/p50 as determined by competition and supershift assays (Figure S1) '*' denotes a background band as determined by competition and supershift assays (Figure S1).

(B) Phosphorylation of IκBα is required for full NF-κB activation induced by UPR. IκBα WT or IκBα SR (S32A/S36A) were added back to $iκbα^{-/-}$ cells and treated with Tg for the indicated amount of time. Nuclear extracts were prepared, and activation of NF-κB was analyzed by EMSA.

(C) IκBα phosphorylation does not increase during ER stress. Wild type MEFs were treated with DTT or Tg. Levels of phosphorylated IκBα (P-IκBα) and total IκBα were analyzed by western blots using anti-phospho-specific (Ser32/36) IκBα or anti-IκBα antibodies, respectively. The level of P-IκBα upon treatment of cells with TNFα is shown for comparison. Actin was used as a loading control.

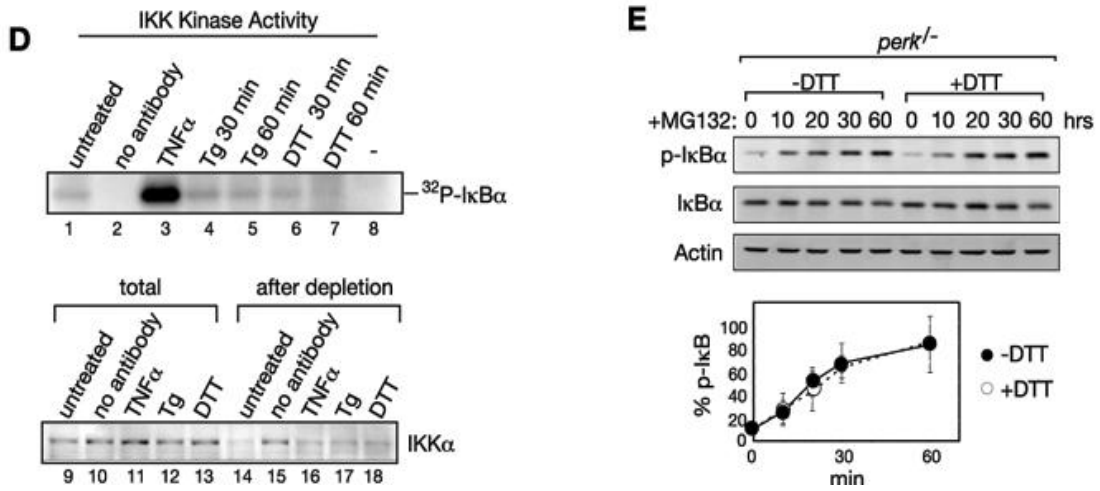

Figure 1. Continued.

(D) IKK kinase activity does not increase during ER stress. The IKK complex was immunoprecipitated from wild type MEFs treated with either Tg, DTT, or TNFα. IKK kinase activity was determined by incubation of the recombinantly expressed IκBα (IKK substrate) with immunoprecipitated IKK in the presence of [γ^{32}P]-ATP. Efficiencies of IKK immunoprecipitation using anti-IKKα antibody were shown by comparing cellular levels of IKKα in total extract before (total, lanes 9-13) and after immunoprecipitation with the antibody (after depletion, lanes 14-18), confirming that the majority of IKKα was efficiently immunoprecipitated since it was significantly reduced after depletion. No antibody denotes a negative control where no antibody was used during the immunoprecipitation procedure (lane 2). (-) shows a negative control where no kinase was added to the reaction (lane 8).

(E) IRE1 does not contribute to an increase in IKK activity during the UPR. In order to prevent the effect of the decrease in IκBα levels due to translation inhibition during the UPR, we used perk$^{-/-}$ MEFs which are unable to inhibit translation. Cells were treated with MG132 in the absence (-DTT, closed circle) or presence (+DTT, open circle) of UPR induction. Levels of P-IκBα, total IκBα, and actin were determined by western blot. Accumulation of P-IκBα after normalization is graphed. At least, three independent experiments are performed to calculate standard error.

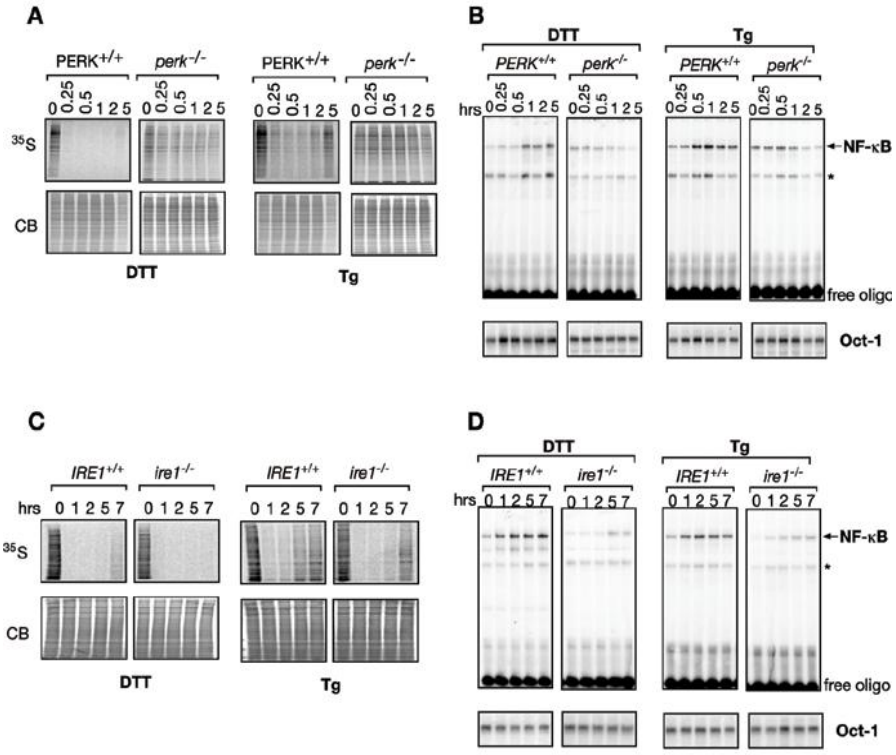

Figure 2. Translation inhibition is not sufficient to activate NF-κB in the absence of IRE1.

(A) perk$^{-/-}$ cells cannot repress global translation during the UPR. PERK$^{+/+}$ and perk$^{-/-}$ cells were treated with either DTT or Tg for the indicated amount of time and pulsed with ^{35}S labeled methionine and cystine (^{35}S-Met/Cys). Total cell extract was prepared and analyzed by SDS-PAGE. The ^{35}S panel shows autoradiography of the SDS-PAGE indicating the level of translation. Coomassie Blue (CB) staining showed that equal levels of protein were loaded in each lane.

(B) PERK is necessary for full activation of NF-κB by ER stress. PERK$^{+/+}$ and perk$^{-/-}$ cells were treated with DTT or Tg for the indicated amount of time. EMSA assays were performed on nuclear extracts to determine NF-κB activation. Oct-1 EMSA assays were performed on the same nuclear extracts as a control showing equal amounts of protein in the samples. '*' denotes a background band as determined by competition and supershift assays (Figure S1).

(C) ire1$^{-/-}$ cells can repress global translation during the UPR at the same efficiency as WT cells. IRE1$^{+/+}$ and ire1$^{-/-}$ cells were treated with either DTT or Tg for the indicated amount of time and pulsed with ^{35}S labeled methionine and cystine (^{35}S-Met/Cys). Total cell extract was prepared and analyzed by SDS-PAGE. The ^{35}S panel shows autoradiography of the SDS-PAGE indicating the level of translation. Coomassie Blue (CB) staining showed that similar levels of proteins were loaded in each lane.

(D) IRE1 is necessary for full activation of NF-κB by ER stress. IRE1$^{+/+}$ and ire1$^{-/-}$ cells were treated with DTT or Tg, nuclear extracts were prepared and EMSA assays were performed on nuclear extracts to determine NF-κB activation. Oct-1 EMSA assays were performed on the same nuclear extracts as a control showing equal amounts of protein in the samples. '*' denotes a background band as determined by competition and supershift assays (Figure S1).

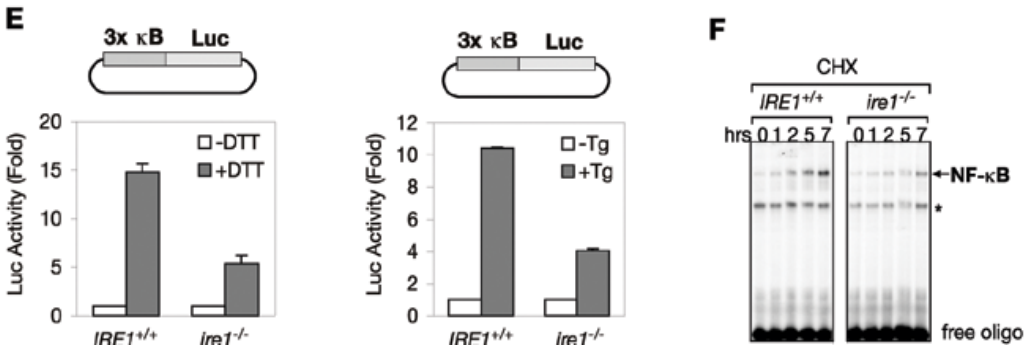

Figure 2. Continued

(E) IRE1$^{+/+}$ and ire1$^{-/-}$ cells were transfected with a luciferase reporter containing 3 NF-κB sites followed by firefly luciferase. Cells were also transfected with a Renilla luciferase reporter as a control. Cells were then treated with DTT or Tg for 12 hrs and luciferase activity was measured. Values shown were normalized based on Renilla activity.
(F) IRE1$^{+/+}$ and ire1$^{-/-}$ MEFs were treated with CHX, nuclear extracts were prepared, and activation of NF-κB was analyzed by EMSA.

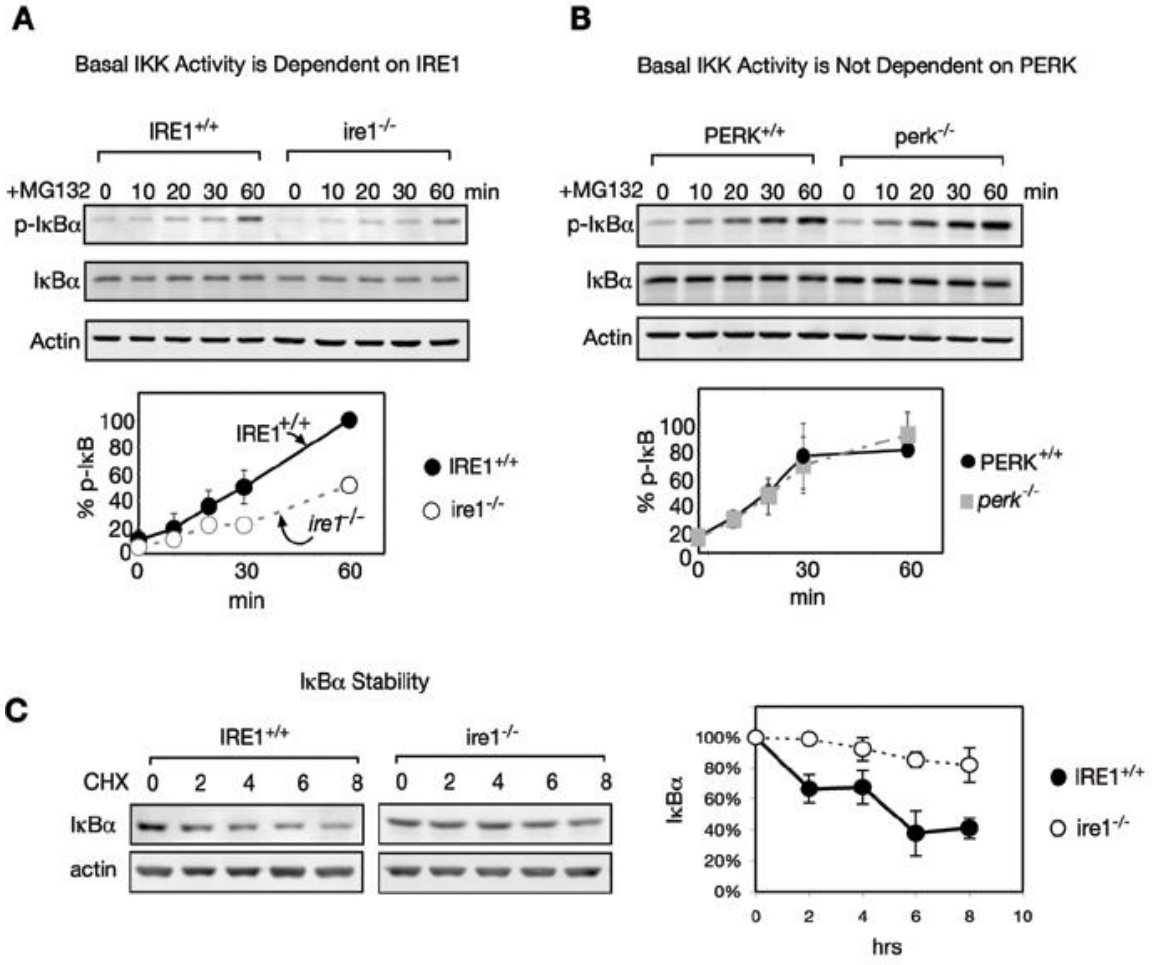

Figure 3. Basal IKK activity is decreased in cells lacking IRE1.
(A) Basal IKK activity is reduced in the absence of IRE1. IRE1$^{+/+}$ and ire1$^{-/-}$ MEFs were treated with MG132, total cell extracts were prepared, and levels of P-IκBα were determined by western blot. The rate of P-IκBα accumulation after normalization in IRE1$^{+/+}$ (closed circle) and ire1$^{-/-}$ (open circle) was used as a measure of basal IKK activity. Error bars are calculated from at least three independent experiments.
(B) Basal IKK activity was not altered in perk$^{-/-}$ cells. PERK$^{+/+}$ and perk$^{-/-}$ MEFs are treated with MG132 for the indicated amount of time. Total extracts were analyzed by western blot using antibodies against p-IκBα, total IκBα, and actin. Levels of p-IκBα were quantitated and shown as basal IKK activities in PERK$^{+/+}$ (closed circle) and perk$^{-/-}$ (closed square) cells. Error bars are calculated from at least three independent experiments.
(C) IκBα is more stable in ire1$^{-\backslash-}$ cells. IRE1$^{+\backslash+}$ (closed circle) and ire1$^{-\backslash-}$ (open circle) cells were treated with 50 μg/ml cycloheximide (CHX) for up to 8hrs. At this concentration, no synthesis of protein was detected by ^{35}S incorporation (data not shown). Decay of existing IκBα was measured by western blot. IRE1$^{+\backslash+}$ cells have a faster rate of decay of IκBα as compared to ire1$^{-/-}$. Quantitation is shown in the bottom panel and represents at least three independent experiments.

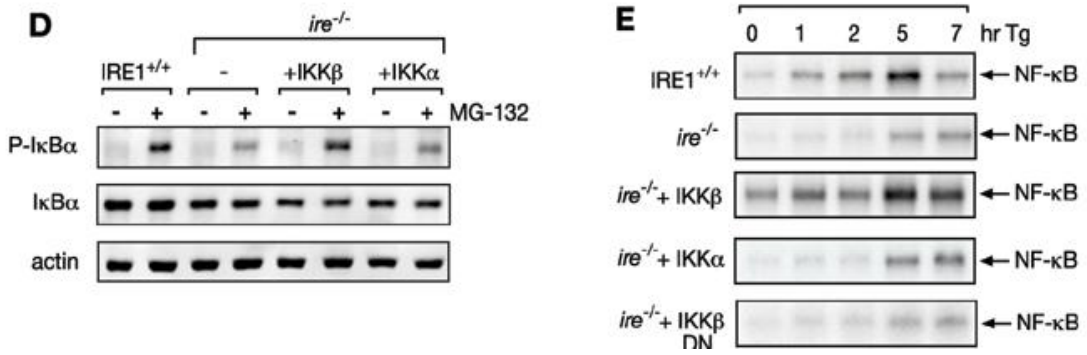

Figure 3. Continued

(D) Basal IKK activity can be rescued by expression of IKKβ. ire1$^{-/-}$ cells were transfected with IKKβ or IKKα for 48 hrs. MG132 was added to IRE1$^{+/+}$, ire1$^{-/-}$, and ire1$^{-/-}$ cells transfected with IKKβ or IKKα for 60 min. Total extracts were then prepared and probed by western blot for protein levels of P-IκBα, total IκBα, and actin.
(E) NF-κB activation can be rescued by expression of IKKβ. ire1$^{-/-}$ cells were transfected with IKKβ, IKKα, or a dominant negative form of IKKβ (IKKβ DN) for 48 hrs. IRE1$^{+/+}$, ire1$^{-/-}$, and transfected cells were treated with Tg for up to 7 hrs. Nuclear extracts were prepared and EMSA was used to determine NF-κB activity.

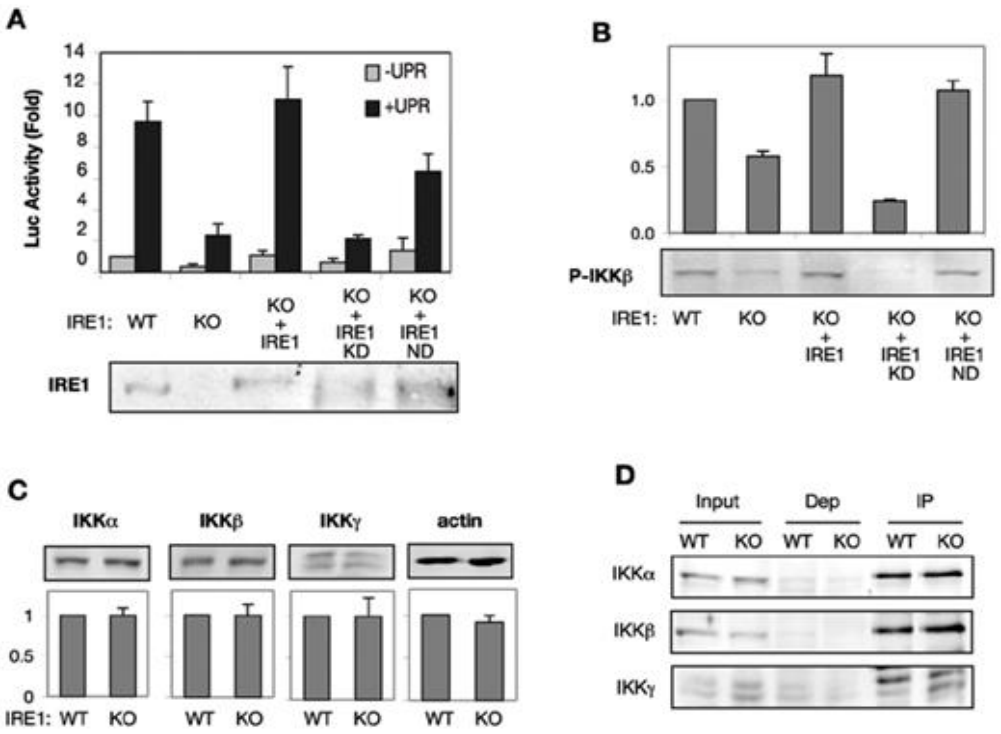

Figure 4. The kinase activity of IRE1 is required for NF-κB activation during the UPR.

(A) Kinase dead IRE1 cannot rescue NF-κB activity in ire1$^{-/-}$ cells. ire1$^{-/-}$ cells were co-transfected with either wild type IRE1, kinase dead IRE1 (KD), or nuclease dead IRE1 (ND) and luciferase reporter plasmids containing 3 NF-κB binding sites for 48 hrs. Cells were then treated with DTT for 12 hrs and luciferase assays were performed. Standard Error from at least three independent experiments is shown. Western blots were performed to demonstrate successful transfection of IRE1 (bottom panel).

(B) Basal phosphorylation of IKKβ is reduced in ire1$^{-/-}$ cells and cannot be rescued by kinase dead IRE1. ire1$^{-/-}$ cells were transfected with either wild type IRE1, kinase dead IRE1 (KD), or nuclease dead IRE1 (ND) for 48 hrs. Total cell extracts were then taken from wild type MEFs (WT), ire1$^{-/-}$ MEFs (KO) or transfected cells. P-IKK levels were then determined by western blot. Quantitations of the westerns are shown with standard error for at least three independent experiments.

(C) Protein levels of IKK subunits in ire1$^{-/-}$ cells are equal to wild type levels. Total cell extracts from WT and ire1$^{-/-}$ cells were probed for IKKα, IKKβ, and IKKγ by western blot. Quantitations of the westerns are shown with standard error for at least three independent experiments.

(D) Equivalent amounts of each IKK subunit can be immunoprecipitated in WT and ire1$^{-/-}$ cells. Untreated wild type (WT) or ire1$^{-/-}$ (KO) cells were lysed and antibody against IKKγ was used to pull down the IKK complex. Protien was then normalized and 400μg was used for the IP. Input indicates the crude lysate. After pulling down the complex, the depleted fraction (Dep) was saved to determine the efficiency of the IP. IP indicates the immunoprecipitated protein. The Input, Depleted, and IP fractions were then ran on SDS-PAGE. Western blots were performed using antibodies against IKKα, IKKβ, and IKKγ.

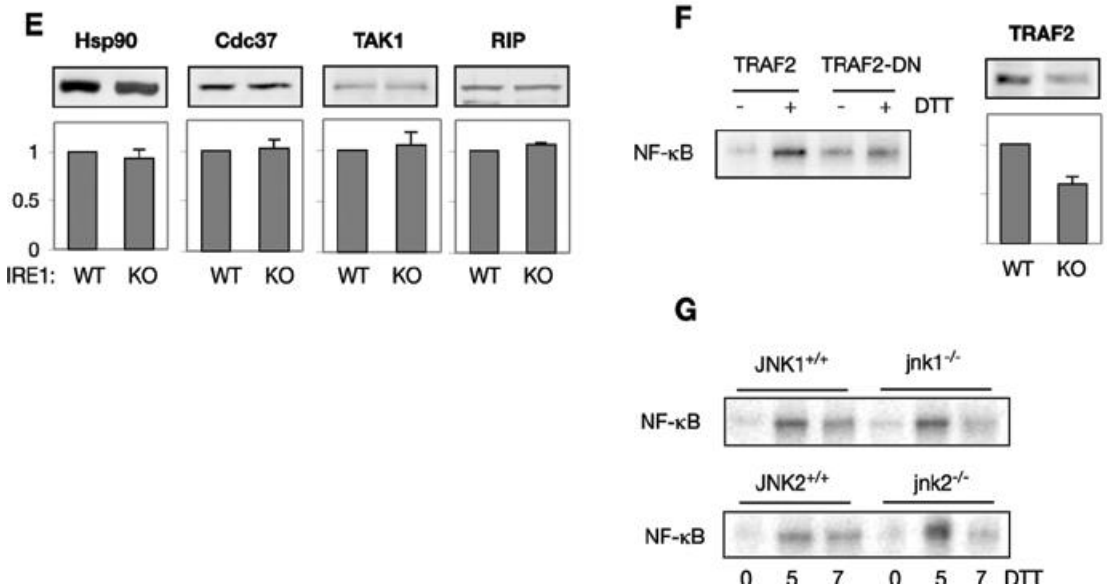

Figure 4. Continued

(E) Western blots of IKK regulators. Total cell extracts from WT and ire1$^{-/-}$ (KO) cells were probed for Hsp90, cdc37, TAK1, and RIP by western blot. Hsp90, cdc37, TAK1, and RIP have equal levels of protein in the wild type and ire1$^{-/-}$ cells. Quantitation of the westerns are shown with and standard error for at least three independent experiments.

(F) TRAF2 is required for full activation of NF-κB during ER stress. (Left panel) Wild type cells were transfected with either WT TRAF2 or dominant negative (DN) TRAF2 missing a portion of the N terminal region. Cells were then treated with DTT for 5 hrs. Nuclear extracts were prepared and EMSA was used to determine NF-κB activity. (Right panel) Total extracts from WT and ire1$^{-/-}$ (KO) were probed for TRAF2 by western blot. ire1$^{-/-}$ cells had decreased TRAF2 levels, however rescuing TRAF2 levels does not restore basal IKK activity or NF-κB activation (Figure S5).

(G) JNK is not required for NF-κB activation during ER stress. jnk1$^{-/-}$ or jnk2$^{-/-}$ cells and their cognate wild type cells were treated with DTT for up to 7 hrs. Nuclear extracts were prepared and EMSA was used to determine NF-κB activity.

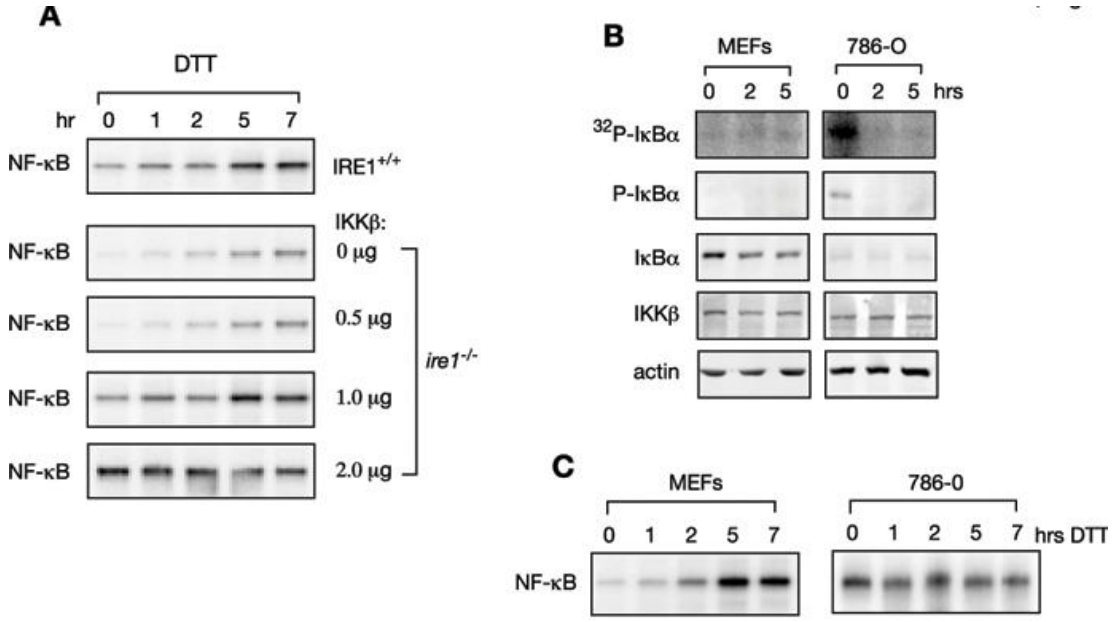

Figure 5. UPR activation can override the inhibition of NF-κB by IKK inhibitors in cancer cells.

(A) Basal IKK determines the degree of NF-κB activation during ER stress. Increasing amounts of IKKβ were transfected to ire1$^{-/-}$ cells for 48h. Cells were then treated with DTT for up to 7 hr. Nuclear extracts were prepared and EMSA was used to determine NF-κB activity. Basal NF-κB activity (0 hr) increases correlating with the amount of IKKβ transfected. NF-κB activation with 1 μg IKKβ results in a profile similar to wild type. At 2 μg IKKβ, NF-κB is high throughout the time course and cannot be further activated by UPR.
(B) Basal IKK activity is elevated in renal cell carcinoma (786-O) cells. Wild type MEFs or renal cell carcinoma (786-O) cells were induced for UPR by DTT for up to 5 hrs and kinase activity of IKK was measured by immunoprecipitation of the IKK complex and incubation with recombinant IκBα in the presence of γ-^{32}P ATP (^{32}P- IκBα). Also western blots were performed using antibodies against phospho-IκBα, total IκBα, IKKβ, and actin.
(C) Renal cell carcinoma (786-O) cells have high basal NF-κB activity. Wild type MEFs or renal cell carcinoma (786-O) cells were induced for UPR by DTT treatment up to 7 hrs, and NF-κB activity was measured by EMSA. 786-O cells have dramatically increased basal (0h) activity and are unable to further increase NF-κB activity. This is consistent with cells transfected with high levels of IKKβ (Fig 5A).

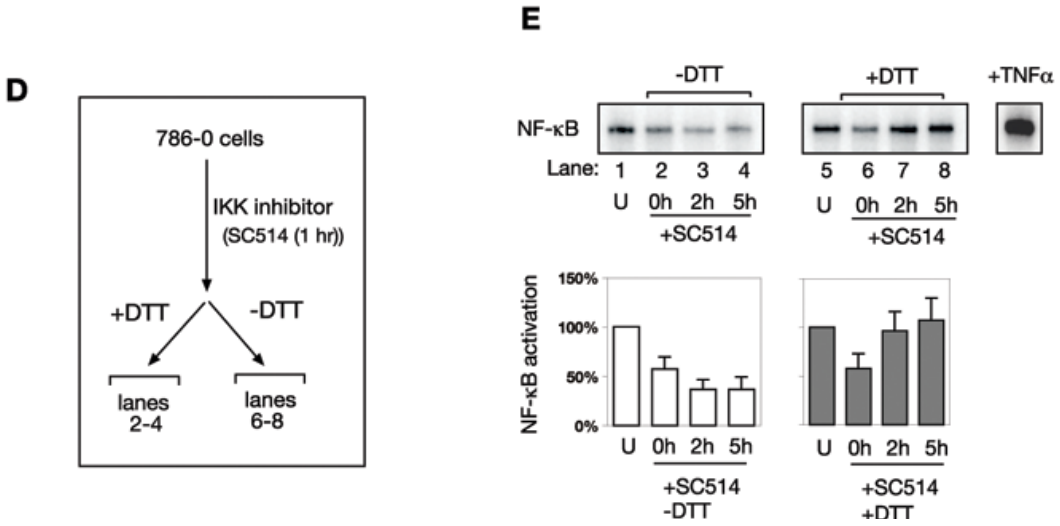

Figure 5. Continued

(D) Panel represents a schematic of the next experiment. 786-O cells with high basal NF-κB activity were treated with an IKK inhibitor (SC-514) for 1hr. Then DTT was added to cells for up to 5 hours (+DTT). –DTT indicates that no DTT was added. Both conditions still contained the IKK inhibitor.

(E) UPR activation of NF-κB in 786-0 cells while being treated with an IKK inhibitor. 786-0 cells were first incubated with SC-514, an IKK inhibitor, for 1 hr (lanes 2 and 6). After, cells were incubated with either no DTT (lane 3-4) or DTT (lanes 7-8) for up to 5 hrs still in the presence of SC-514. Nuclear extracts were taken and EMSAs were performed to measure NF-κB activity. U signifies NF-κB activity in untreated cells. Upon addition of SC-514, NF-κB activity is decreased (lanes 2 and 6). When DTT is not added, NF-κB activity continues to decrease (lanes 3-4), but when DTT is added, and increase in NF-κB activity is seen (lanes 6-8). Quantitations of the lanes are shown. In comparison to ER stress, activation of NF-κB by TNFα is shown.

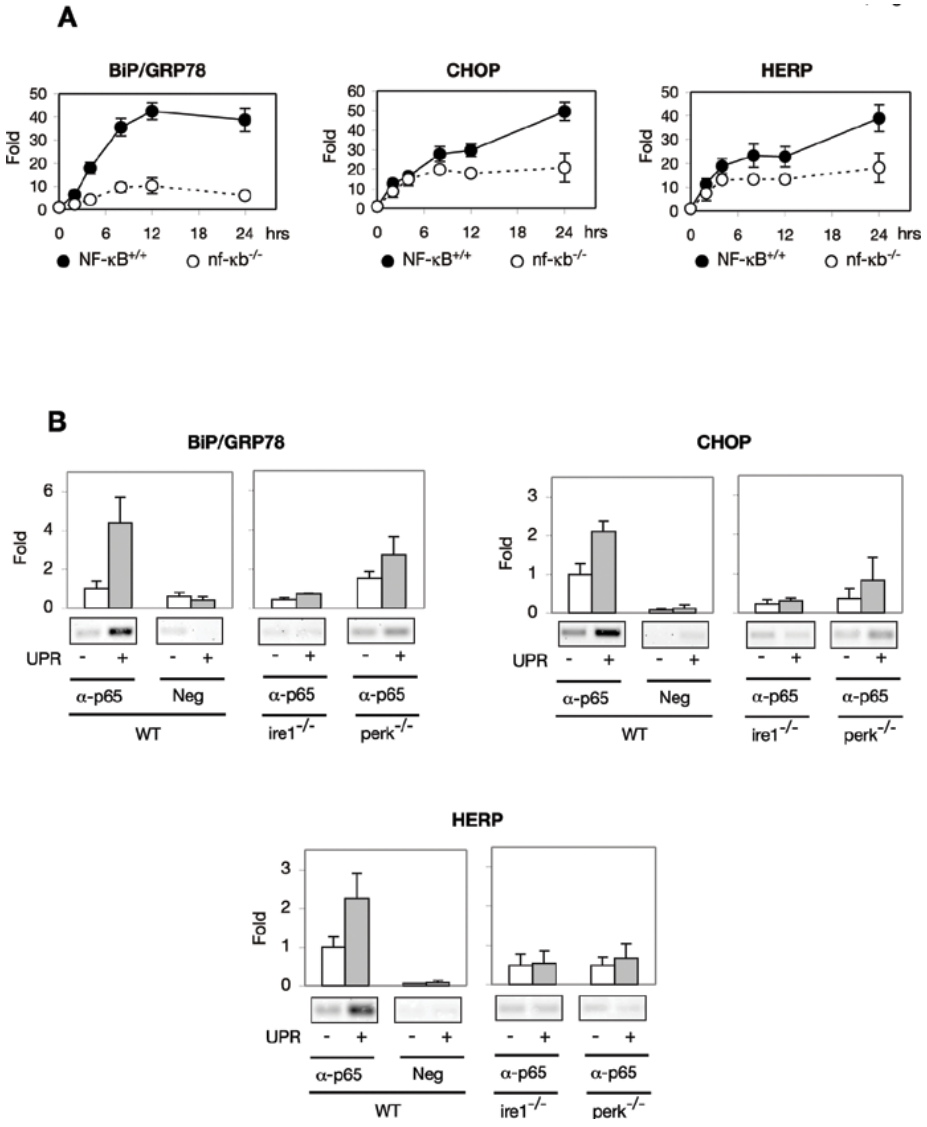

Figure. 6. Regulation of UPR Target Genes by NF-κB.

(A) NF-κB regulates UPR target genes. Wild type MEFs (closed circle) or MEFs obtained from relA, c-rel, and p50 triple knock out mouse mice (3KO – open circle) were treated with Tg for up to 24 hrs. RNA was obtained at 2, 4, 8, 12 and 24 hrs and reverse transcription was done to obtain cDNA. Quantitative real time PCR (qPCR) was done using primers against several UPR target genes. Expression of GRP78/BiP, CHOP, and HERP was reduced in the NF-κB knockout cells compared to the wild type. Standard error was calculated from at least three independent experiments.

(B) Chromatin IP showing IRE1 and PERK dependent binding of NF-κB to promoters. Wild type, *ire1*$^{-/-}$, and *perk*$^{-/-}$ MEFs were treated with Tg (UPR) for 4 hrs then fixed. DNA was sheared and p65 antibody was used for immunoprecipitation. Cells were then decrosslinked and the DNA was purified. PCR was done using primers specific for BiP/GRP78, CHOP, or HERP promoters. Neg indicates a negative control using mouse IgG instead of p65 for the IP step. Standard error was calculated from at least three independent experiments.

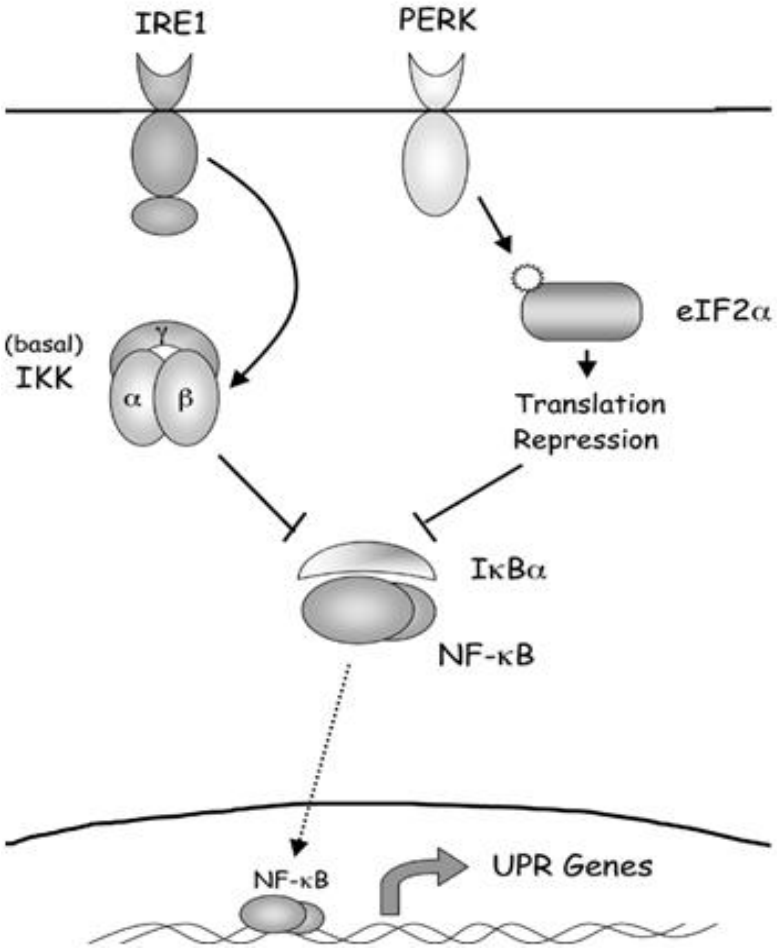

Figure. 7. Model for NF-κB activation and function during ER stress.

NF-κB activation during ER stress requires a combination of inputs from two UPR components: IRE1 and PERK. IRE1 positively influences basal IKK activity through its kinase domain by maintaining basal IKKβ phosphorylation. Cells lacking IRE1 or cell containing a kinase defective IRE1 are unable to fully induce NF-κB during ER stress. Changes in the basal activity of IKK have a major effect on the subsequent NF-κB activation. PERK activation during the UPR leads to inhibition of translation through eIF2α phosphorylation. In cells with normal basal IKK activity, translation repression is sufficient to activate NF-κB, and the increasing the level of translation inhibition increases NF-κB activation. Hence, two inputs in combination: 1) maintenance of basal IKK activity by IRE1 and 2) translation inhibition by PERK, result in optimal NF-κB activation during ER stress. Furthermore, this activated NF-κB is able to bind to promoters of a set of UPR genes contributing to their full activation.

Supplemental Materials and Methods

Immunofluorescence

After treatment, cells were washed with PBS and fixed with 4% paraformaldehyde. Cells were then permeabilized by 0.2% NP-40 and blocked with 5% BSA. p65 (Santa Cruz) was used as the primary antibody, and the secondary antibody was conjugated with FITC.

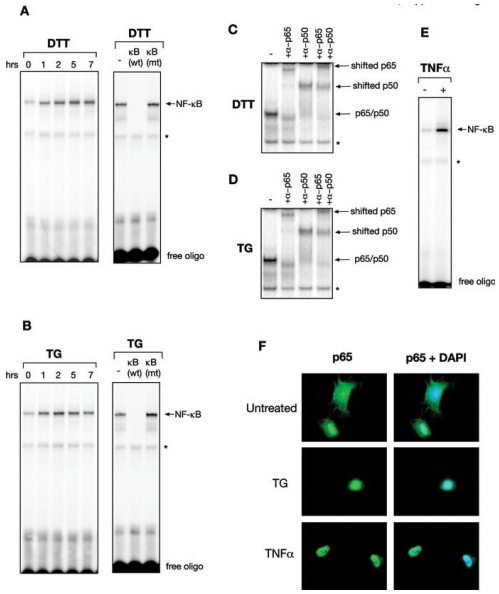

Figure S1. ER stress activated NF-κB contains p65/p50

(A) Wild type MEFs were treated with DTT for up to 7 hrs (left panel). Right panel: The 5 hr DTT sample was incubated with a non-radiolabelled oligo containing a wild type NF-κB binding site (κB wt). The correct NF-κB band is then competed out by the cold probe resulting in a loss of the signal. The band labeled (*) cannot be competed out by the cold probe containing a wild type NF-κB binding site, hence it is designated as a background band. Its identity as a background band is further confirmed by supershift assays as described below. When a cold competitor containing a mutation in critical residues of the κB binding sites are added, this does not compete out the NF-κB band indicating that NF-κB is binding to the radiolabelled wild type probe.

(B) Competition assay as described in (A) for cells treated with Thapsigarin (TG) instead of DTT. Results are similar to the DTT treated cells as described above.

(C) Supershift assays identifying the active form of NF-κB contains p65 and p50. The 5 hr DTT sample was incubated with antibodies against p65, p50 or both p65 and p50 for 1 hr. Samples were then run on a gel. Incuabation of p65 resulted in a loss of the NF-κB band, and the appearance of a higher band corresponding to the probe/p65/antibody complex which has a slower mobility on the gel (shifted p65). Incubation with p50 also resulted in disappearance of the NF-κB band and the appearance of a shifted band (shifted p50). Incubation of both p65 and p50 antibodies resulted in disappearance of the NF-κB band and appearance of two shifted bands. This indicates that the activated NF-κB contains p65 and p50. The band labeled (*) could not be shifted by either p65 or p50.

(D) Supershift assays as described in (C) using TG instead of DTT. Results are similar to the DTT treated cells as described above indicating the the NF-κB activation seen is not drug specific.

(E) TNFα activation of NF-κB. As a positive control, MEFs were treated with TNFα for 15 min and EMSA was performed to determine NF-κB activation.

(F) Nuclear localization of NF-κB during TG and TNFα treatment. Cells were treated with TG for 1 hr or TNFα for 15 min. Immunofluorescence was then done with antibodies against p65 and DAPI to detect nuclei.

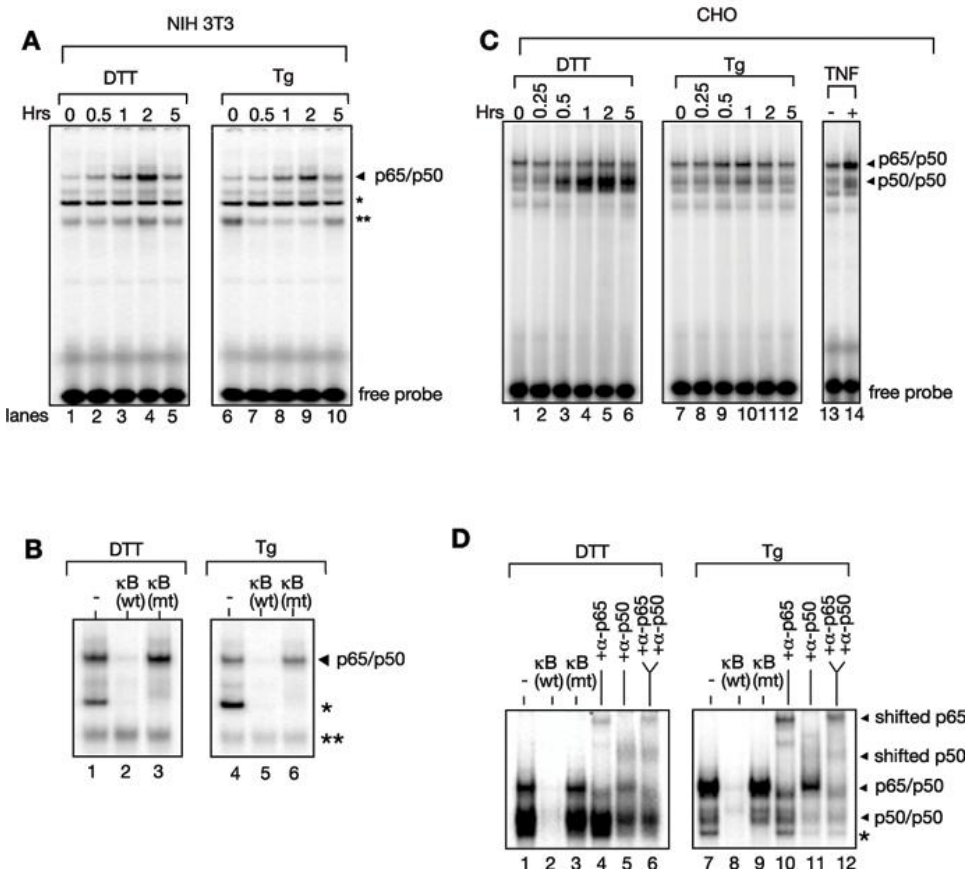

Figure S2. NF-κB activation in other cell types: NIH 3T3 and CHO

(A) NIH 3T3 cells were treated with either DTT or TG for up to 5 hrs, nuclear extracts were prepared, and EMSAs were performed to measure NF-κB activation. NF-κB was activated in treatments with both DTT and TG. (*) and (**) denote background bands as determined by competition and supershift assays.

(B) Competition assay for NIH 3T3 cells. The 2 hr sample was taken and incubated with a cold oligo containing a wild type or mutant NF-κB binding site. The p65/p50 can be competed out by the wild type competitor but not the mutant competitor demonstrating that the band is NF-κB. Although the band labeled (*) can be competed out by the wild type cold competitor, it can also be competed out by the mutant competitor signifying that it is not NF-κB. The band labeled (**) cannot be competed out by the wild type competitor demonstrating that it is a background band.

(C) CHO cells were treated with either DTT, TG, or TNFα for up to 5 hrs, nuclear extracts were prepared and EMSAs were performed to measure NF-κB activation. The main form of NF-κB activated by DTT was p50/p50 while TG activated the p65/p50 form of NF-κB.

(D) Competition and supershift assays of NF-κB activated in CHO cells. The 2 hr sample was used and incubated with a wild type or mutant cold competitor. The bands in which the wild type competitor was able to compete out the signal while the mutant was not indicate an NF-κB signal. Also, supershift assays reveal the presence of two forms of NF-κB, p65/p50 and p50/p50 as indicated. The p65/p50 band can be shifted by both p65 and p50 antibodies while the p50/p50 band can only be shifted by the p50 antibody.

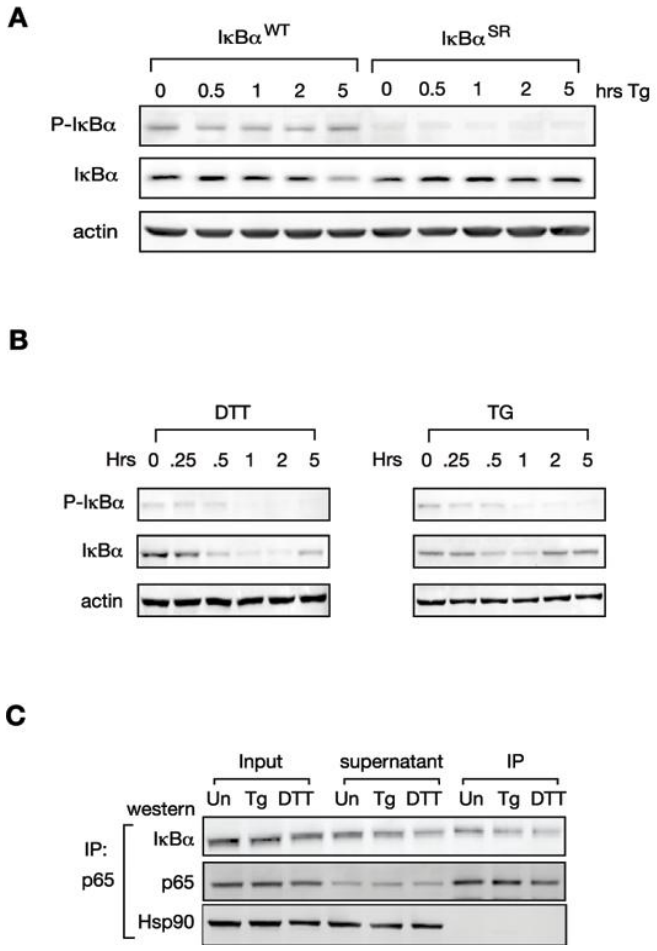

Figure S3. IκBα levels decrease during ER stress, and IκBα is still able to associate with NF-κB.

(A) IκBα-WT and IκBα-SR are expressed at the same levels when added back to IκBα$^{-/-}$ cells. IκBα WT and IκBα SR were treated with Tg for up to 5 hrs and protein was extracted. Western blots using antibody against P-IκBα cannot detect phosphorylated IκBα in IκBαSR cells. However, both have equivalent amounts of total IκBα indicating that IκBαSR cells cannot phosphorylate IκBα. Also, a decrease in IκBα levels can be detected in IκBαWT cells but not in the IκBαSR cells, consistent with NF-κB activation from Figure 2B.

(B) P-IκBα does not increase and total IκBα levels decrease during the UPR in CHO cells. CHO cells were treated with DTT or TG for up to 5 hrs and protein was extracted. Western blots show that P-IκBα levels do not increase, similar to results using MEFs. Also, IκBα levels decrease during both DTT and TG treatment similar to MEFs. Actin was used as a loading control.

(C) IκBα is bound to NF-κB during UPR activation. Wild type MEFs were treated with either Tg or DTT for 1h and cell extracts were collected (Input). Extracts were incubated with anti-p65 antibody for immunoprecipitation overnight. Protein G beads were then used to separate the depleted fraction (supernatant) from the immunoprecipitated fraction (IP). Samples were subjected to SDS PAGE and immunoblotting using antibodies against p65, IκBα, or HSP90. HSP90 was used as a control to show that the immunoprecipitation did not pull down non-specific proteins.

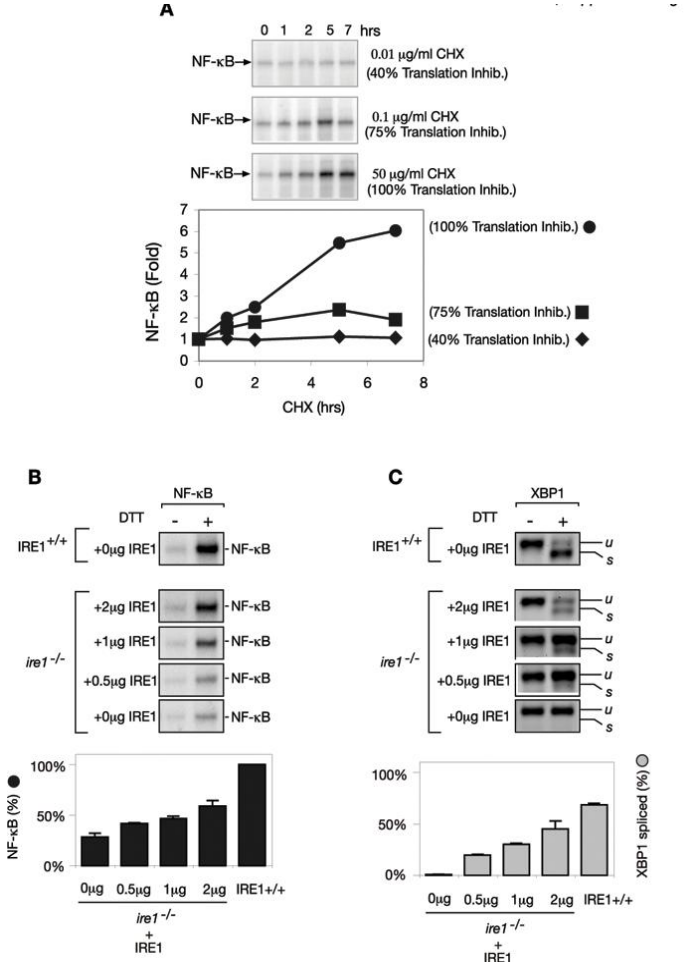

Figure S4. Translation inhibitioin determines NF-κB activation and addition of IRE1 can rescue NF-κB activation and XBP1 splicing in ire1$^{-/-}$ cells.

(A) Degree of translation inhibition determines the strength of NF-κB activation. Increasing concentrations of CHX were used to inhibit translation at different levels. The degree of translation inhibition was determined by 35S labeling at different concentrations of CHX (data not shown). We found that 0.01 μg/ml CHX will inhibit 40% of global translation, 0.1 μg/ml CHX inhibits 75% of global translation, and 50 μg/ml inhibits 100% of global translation. Wild type MEFs were then treated with these concentrations of CHX, and NF-κB activation was determined by EMSA. Increasing the degree of global translation inhibition results in increasing NF-κB activity.

(B) Adding back IRE1 can rescue NF-κB activation in ire1$^{-/-}$ cells. ire1$^{-/-}$ cells were transfected with increasing amounts of IRE1 plasmid up to 2 μg for 48 hrs. Cells were then treated with DTT for 5 hours, nuclear extracts were taken, and EMSA assays were performed to determine NF-κB activation. Transfecting increasing amounts of IRE1 led to increasing activation of NF-κB. Quantitations are shown.

(C) Adding back IRE1 can rescue XBP1 splicing in ire1$^{-/-}$ cells. ire1$^{-/-}$ cells were transfected with increasing amounts of IRE1 plasmid up to 2 μg for 48 hrs. RNA was then collected and RT-PCR was performed to determine XBP1 splicing. Unspliced (u) XBP1 contains a 26 nt intron which results in a higher band as compared to the spliced (s) XBP1.

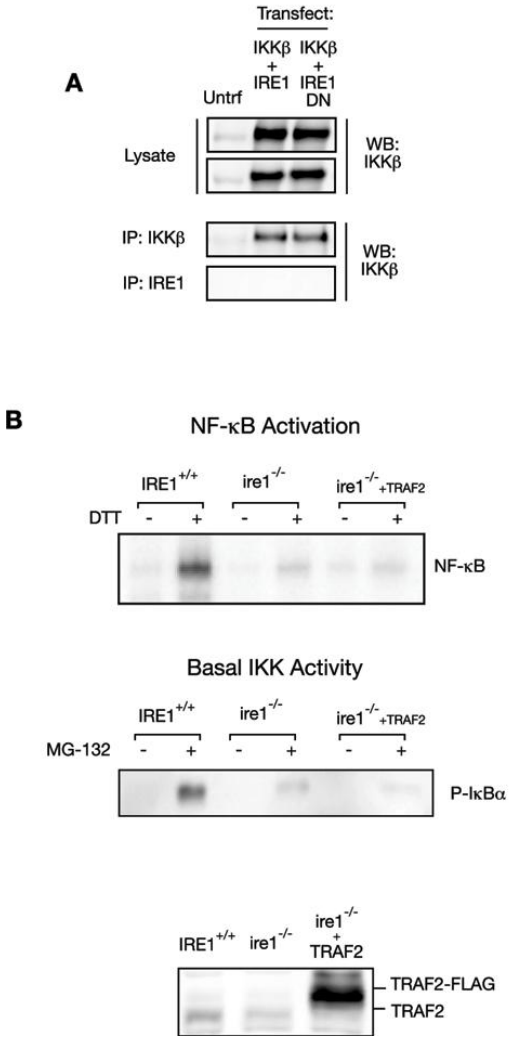

Figure S5. Increasing TRAF2 levels cannot rescue NF-κB activation and basal IKK activity in ire1$^{-/-}$ cells.

(A) IP of IRE1 and IKK. 293 cells were co-transfected with IKKβ and either IRE1 or IRE1(K599A) (IRE-DN). Antibodies against either IRE1 or IKKβ was used for the immunoprecipitation (IP). The lysate and the IP fractions were then run of a gel and transferred for western blot. Antibodies against IKKβ was used to the detect the IP. IKKβ was able to be pulled down with IKKβ antibodies, but neither IRE1 nor IRE1-DN could be pulled down.

(B) Addition of TRAF2 to ire1$^{-/-}$ cells. Top Panel: FLAG tagged TRAF2 was transfected into ire1$^{-/-}$ cells. IRE1$^{+/+}$, ire1$^{-/-}$, or ire1$^{-/-}$+TRAF2 cells were then treated with DTT and an EMSA was done to detect NF-κB activation. Addition of TRAF2 was not able to rescue the decrease in NF-κB activation. Middle Panel: Basal IKK activity was tested by adding MG132 to either IRE1$^{+/+}$, ire1$^{-/-}$, or ire1$^{-/-}$+TRAF2 for 1 hr. P-IκBα westerns then detected accumulation of phosphorylated IκBα as a measure of basal IKK activity. Increasing amounts of TRAF2 in ire1$^{-/-}$ did not result in rescue of basal IKK activity. Bottom Panel: Western blot detecting transfection of FLAG-Tagged TRAF2 in ire1$^{-/-}$ cells.

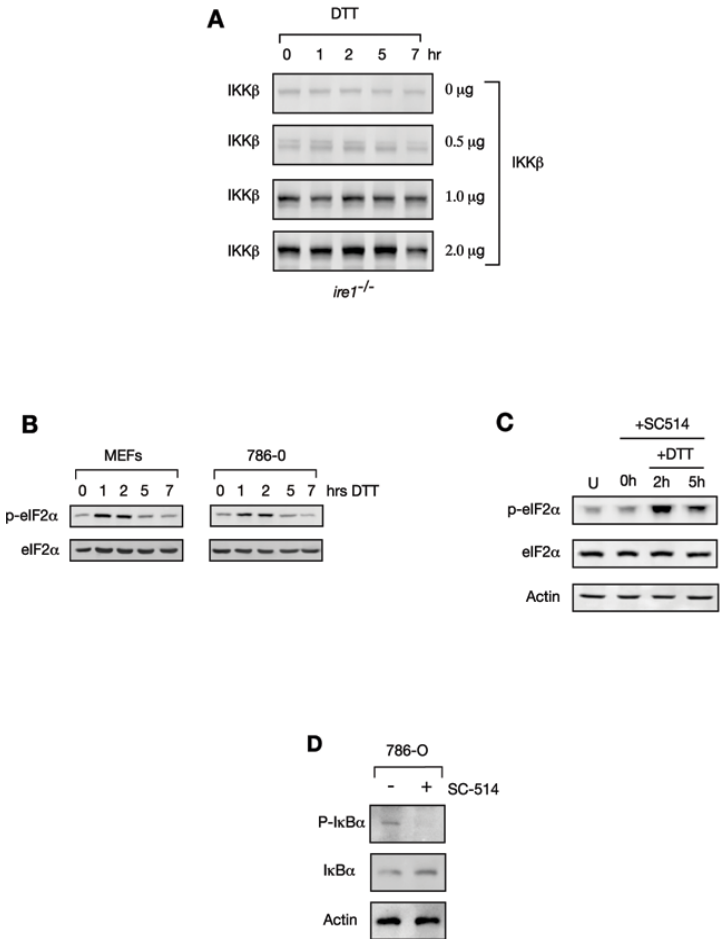

Figure S6. 786-O cells have a normal UPR response determined by PERK activation.

A) IKKβ protein levels in transfected ire1$^{-/-}$ cells. ire1$^{-/-}$ cells were transfected with increasing amounts of IKKβ up to 2 μg. Protein was then extracted and westerns were done determining levels of IKKβ.
(B) 786-O cells have normal PERK activation in response to the UPR. MEFs or 786-O cells were treated with DTT for up to 7 hrs. Protein was extracted and western blots were done for phospho-eIF2α or total eIF2α. The 786-O cells have a similar PERK activation response as measured by phospho-eIF2α as MEFs.
(C) SC-514 does not induce PERK activation. 786-O cells were treated with with SC-514 for 1 hr (+SC-514, 0h) which did not change levels of P-eIF2α as compared to untreated cells (U). However, treatement with DTT (+DTT, 2h and 5h) resulted in increased P-eIF2α. Total eIF2α remains unchanged and actin was used as a loading control.
(D) SC-514 decreases IKK activity. Since 786-O cells have increased basal IKK activity, P-IκBα can be detected in untreated conditions. When SC-514 is added, P-IκBα decreases and total levels of IκBα are stabilized indicating that IKK activity decreased. Actin was used as a loading control.

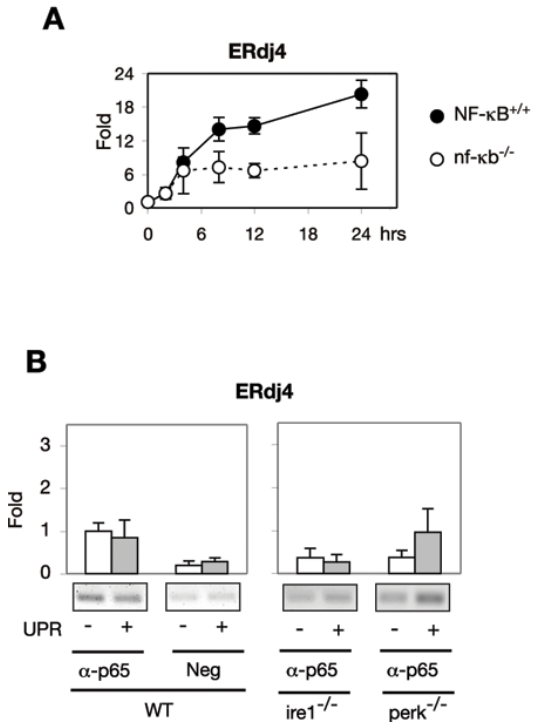

Figure S7. ERdj4 requires NF-κB activation for full transcriptional activity, however, NF-κB does not bind to its promoter.

(A) Wild type MEFs or MEFs obtained from relA, c-rel, and p50 triple knock out mouse embryos (3KO) were treated with Tg for up to 24 hrs. RNA was obtained at 2, 4, 8, 12 and 24 hrs and reverse transcription was done to get cDNA. Quantitative real time PCR (qPCR) was done using primers against ERdj4. Transcriptional activation of ERdj4 was reduced in nf-κb$^{-/-}$ cells.
(B) Chromatin IP. Wild type, ire1$^{-/-}$, and perk$^{-/-}$ MEFs were treated with Tg (UPR) for 4 hrs then fixed. DNA was sheared and p65 antibody was used for immunoprecipitation. Cells were then decrosslinked and the DNA was purified. PCR was done using primers specific for the ERdj4 promoter. Neg indicates a negative control using mouse IgG instead of p65 for the IP step. There was no increase in NF-κB binding during UPR induction indicating that induced NF-κB binding does not occur during the UPR.

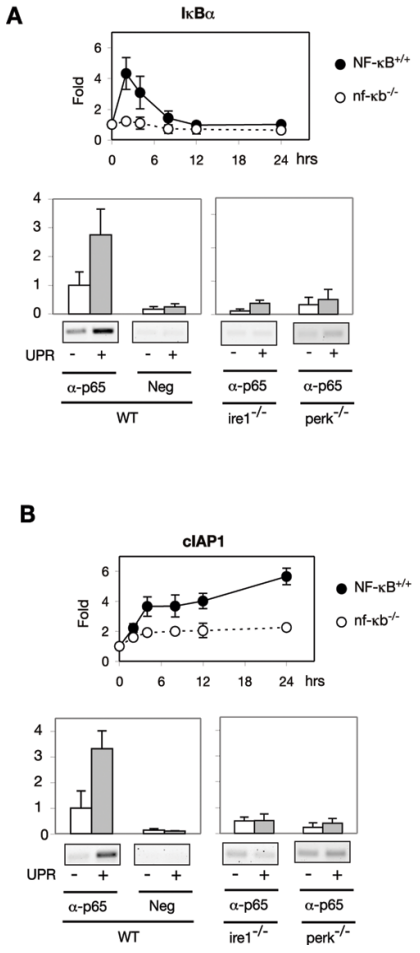

Figure S8. Canonical NF-κB targets are upregulated during the UPR.

(A) Transcription of IκBα during the UPR requires NF-κB and involves NF-κB binding to its promoter. Wild type MEFs or 3KO MEFs were treated with Tg for up to 24 hrs. RNA was obtained at 2, 4, 8, 12 and 24 hrs and reverse transcription was done to get cDNA. Quantitative real time PCR (qPCR) was done using primers against IκBα. Chromatin IP was performed on wild type, ire1$^{-/-}$, and perk$^{-/-}$ MEFs treated with Tg for 4hrs. An increase in NF-κB promoter binding can be detected in wild type cells during the UPR, but not in ire1$^{-/-}$ or perk$^{-/-}$ cells.
(B) Transcription of cIAP1 during the UPR requires NF-κB and involves NF-κB binding to its promoter. Wild type MEFs or 3KO MEFs were treated with Tg for up to 24 hrs. RNA was obtained at 2, 4, 8, 12 and 24 hrs and reverse transcription was done to get cDNA. Quantitative real time PCR (qPCR) was done using primers against cIAP1. Chromatin IP was performed on wild type, ire1$^{-/-}$, and perk$^{-/-}$ MEFs treated with Tg for 4hrs. An increase in NF-κB promoter binding can be detected in wild type cells during the UPR, but not in ire1$^{-/-}$ or perk$^{-/-}$ cells.

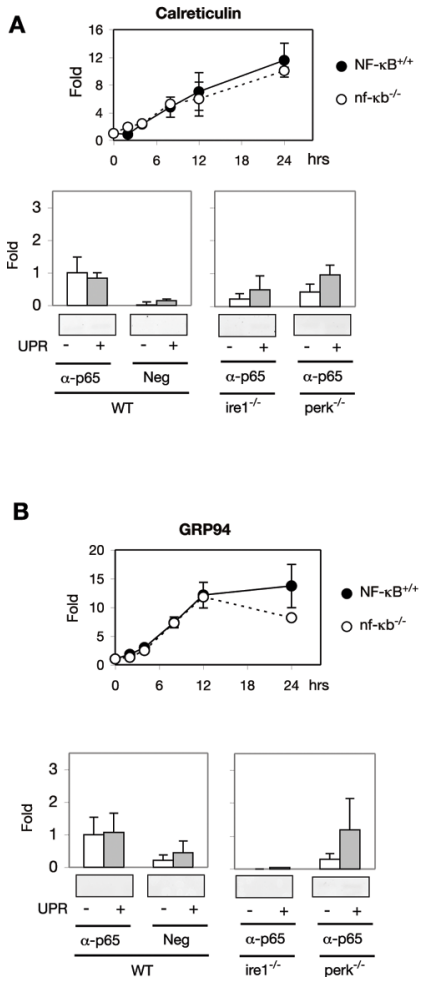

Figure S9. Not all UPR target genes require NF-κB for full activation.

(A) Transcription of calreticulin does not require NF-κB during the UPR, and NF-κB does not bind to its promoter. Wild type MEFs or 3KO MEFs were treated with Tg for up to 24 hrs. RNA was obtained at 2, 4, 8, 12 and 24 hrs and reverse transcription was done to get cDNA. Quantitative real time PCR (qPCR) was done using primers against calreticulin. Wild type MEFs and 3KO MEFs had similar transcription levels indicating that NF-κB is not required for full activation. Chromatin IP was performed on wild type, ire1$^{-/-}$, and perk$^{-/-}$ MEFs treated with Tg for 4hrs. NF-κB promoter binding cannot be deteced in wild type, ire1$^{-/-}$, or perk$^{-/-}$ MEFs.

(B) Transcription of GRP94 does not require NF-κB during the UPR, and NF-κB does not bind to its promoter. Wild type MEFs or 3KO MEFs were treated with Tg for up to 24 hrs. RNA was obtained at 2, 4, 8, 12 and 24 hrs and reverse transcription was done to get cDNA. Quantitative real time PCR (qPCR) was done using primers against GRP94. Wild type MEFs and 3KO MEFs had similar transcription levels indicating that NF-κB is not required for full activation. Chromatin IP was performed on wild type, ire1$^{-/-}$, and perk$^{-/-}$ MEFs treated with Tg for 4hrs. NF-κB promoter binding cannot be deteced in wild type, ire1$^{-/-}$, or perk$^{-/-}$ MEFs.

Chapter 3

ABSTRACT

IRE1, an endoplasmic reticulum (ER) localized transmembrane protein containing a kinase and RNase domain, is a critical component of the ER stress response that is conserved from yeast to humans, indicating its evolutionary importance as stress sensor. IRE1 functions by initiating non-splicesomal splicing of an mRNA coding for a bZIP transcription factor, Hac1 in yeast and XBP1 in higher eukaryotes, resulting in translation of an active transcription factor. When activated, IRE1 undergoes autophosphorylation and formation for higher ordered structures including dimers and oligomers. Structural studies predict that dimerization of IRE1 forms symmetric, active catalytic RNase sites suggesting IRE1 recognizes each splice site equally. Using a newly characterized inhibitor of IRE1, Irestatin, we show that IRE1 exhhibits differential specificity towards the 5' and 3' splice sites, indicating an asymmetric mode of IRE1 substrate recognition. Furthermore, we show substantial differences in substrate recognition between yeast IRE1p versus human IPE1α indicating mechanistic differences between yeast and human IRE1 activation. Specifically, human IRE1 requires a short intron for cleavage of the 3' splice site. Also, the 3' splice site structure and intron length of IRE1 substrates are not evolutionarily conserved, suggesting an evolutionary variation in IRE1's catalytic nuclease activity.

INTRODUCTION

Disruption of endoplasmic reticulum (ER) homeostatis leads to conditions of high levels of unfolded protein accumulation in the ER. Conditions such as ER calcium perturbations or decrease in ER redox capacity disrupt ER function and lead to ER stress which can be detrimental to cellular function. The cell responds to ER stress by activating a signaling pathway known as the unfolded protein response (UPR) which increases the protein folding capacity of the ER by upregulating genes such as ER chaperones. IRE1, an ER localized transmembrane protein, is a

critical component of the UPR that is conserved from yeast to humans. Anomalous IRE1 activation has been correlated with development of several diseases including diabetes and some cancers including multiple myeloma and gliomas (Oslowski et al., Curr Opin Cell Biol 2010; Auf et al., PNAS 2010; Hetz et al., Mol Cell 2009). During ER stress, IRE1 initiates spliceosome independent splicing of mRNAs encoding for basic leucine zipper transcription factors, HAC1 in yeast and XBP1 in higher eukaryotes. Splicing of these mRNAs by IRE1 allows for translation of spliced mRNA that can be translated to produce an active transcription factor.

Under unstressed conditions in yeast, translation of HAC1 mRNA is repressed due to long range base pair interaction between an elements in the 5' untranslated region (UTR) and the intron. This base pairing prevents the ribosome from scanning through the 5' UTR to form the initiation complex (Ruegsegger Cell 2001). Under conditions of ER stress, a separate targeting element located in the 3' UTR of HAC1 targets the mRNA to the ER where it is presumably spliced by IRE1 (Aragon Nature 2009). IRE1 is then able to cleave HAC1 at two stem loop structures (Sidrauski Cell 1997), releasing a 252 nucleotide intron. tRNA ligase is then responsible for ligating the exons, lifting the block in translation, resulting in translation of spliced HAC1, an active transcription factor. In mammalian cells, IRE1 cleaves XBP1 mRNA also at two stem loop structures (Calfon Nature 2000), but unlike HAC1, unspliced XBP1 (XBP1u) is translated. Translated XBP1u negatively regulates the UPR by complexing with and sequestering spliced XBP1 (XBP1s) (Yoshida et al., JCB 2006). During ER stress, IRE1 splices a 26nt intron resulting in a frame shift in the 3' exon of XBP1. The new reading frame codes for a trans-activation domain, making XBP1s a potent transcription factor (Yoshida et al., Cell 2001). IRE1 is able to cleave its substrate at two sites resulting in fragments corresponding to the 5'exon, an intron, and a 3' exon. The 5' splice site (5'ss) located at the 5' exon-intron junction and the 3' splice site (3'ss) located at the intron-3' exon junction both contain stem loop secondary structures where IRE1 cleavage occurs. Cleavage of the splice sites is thought to be

not dependent on the stem sequences since altering the sequence but maintaining the stem structure still results in cleavage (Gonzales et al., EMBO J 1999). Splice sites also contain a 7nt loop containing conserved nucleotides between the 5' splice and the 3' splice site with the sequence: nCnGnnGnn, where the indicated 'G' residue is where the cleavage occurs (Gonzales et al., EMBO J 1999; Sidrauski et al., Cell 1997). In addition, these loop residues are conserved between Hac1 and the mammalian target XBP1 (Calfon et al., Nature 2002). Mutation of these conserved residues decrease or abolish cleavage at that splice site (Gonzales et al., EMBO J 1999; Kawahara et al., JBC 1998). Similarities between splice sites suggest that IRE1 recognizes and cleaves these splice sites equally. In fact, the stem loop itself can serve as a substrate for in vitro RNase reaction (Gonzales et al., EMBO J 1999). Also, mutation of the critical 'G' residue at the 5'ss of Hac1 which abolishes cleavage at that site, still allows for cleavage of the 3'ss, and conversely mutation of the 3'ss critical 'G', still allows for cleavage of the 5'ss (Sidrauski et al., Cell 1997). This indicates that cleavage of Hac1 splice sites does not require an obligate order supporting equal recognition of the 5' and 3'ss. Also, switching the 5' and 3' loop sequences of Hac1, but not the stem sequences, still allows for cleavage in yeast (Kawahara et al., JBC 1998). The stem loops are stable structurally as IRE1 can recognize even when they are presented in the different surrounding sequences, providing a basis for generating an in vivo IRE1 activity reporter (Papandreou et al., Blood 2010). Altogether, these suggest equal recognition of splice sites by IRE1.

Crystal structures of the cytosolic domain of yeast IRE1 show that the putative nuclease catalytic site is formed by dimerization located at a concave surface at the bottom of IRE1's nuclease domain (Lee et al., Cell 2008). This site was proposed based on IRE1's homology to the active site of a related nuclease, RNase L. RNase L is similar to IRE1 based on its structure which contains a pseudokinase domain and a nuclease domain. However, unlike IRE1, the pseudokinase domain of RNase L is not active as a kinase and the nuclease substrates of RNase L

and IRE1 are unrelated and mutually exclusive (Dong et al., RNA 2001). Mutations of residues in IRE1's predicted catalytic nuclease site abolished RNase activity (Lee et al., Cell 2008). Interestingly, the catalytic centers formed by dimerization of IRE1 monomers show two-fold rotation symmetry (Lee et al., Cell 2008), suggesting that cleavage of the RNA substrate occurs in a symmetrical manner and further suggests equally recognition of substrates, though no experimental evidence has been shown.

It is thought that IRE1 catalytic RNase activity between yeast and human IRE1 are mechanistically comparable due to similarities of splice sites. In fact, substrates are being used interchangeably in IRE1 functional assays, for example, XBP1 stem loops are being used to test yeast IRE1 activity (Korennykh et al., Nature 2009; Wiseman et al., Mol Cell 2010). However, previous studies show different cleavage pattern of Hac1 between human and yeast IRE1, where cleavage of Hac1 by human IRE1 results fragments corresponding to the 5'exon alone and inton-3'exon, indicating cleavage of only the 5' splice site (Tirasophon et al., Genes Dev 2000; Niwa et al., Cell 1999). Furthermore, IRE1 was shown to cleave full length RNA more efficiently than stem loop constructs in in vitro nuclease assays indicating that the flanking RNA sequences does play a role in catalytic activity (Gonzales et al., EMBO J 1999). Here, we show that IRE1 is able to differentiate between the 5' and 3' splice sites, indicating that IRE1 does not recognize substrates equally. In addition, we show that the full length RNA plays a role in determining substrate specificity since altering placement of the stem loop splice sites in relation to the whole RNA substrate also alters specificity. In addition, Irestatin, a newly characterized IRE1 inhibitor differentially inhibits cleavage of the 5' and 3' splices sites of Hac1. We propose an asymmetric mode of IRE1 activation where splice site is treated as a distinct substrate. Additionally, we show differential substrate recognition between yeast and human IRE1, suggesting evolutionarily diverging catalytic mechanisms of IRE1RNase activation.

RESULTS

IRE1's splicing of RNA as a means to activate a transcription factor in response to ER stress is evolutionarily conserved between yeast and human. Cleavage of yeast and human substrates, Hac1 and XBP1 respectively, have been thought to be equivalent due to conservation of the splice site loop present in both the 5' and 3' splice sites (ss) of both substrates. However, previous studies show that when human IRE1α is used to cleave Hac1 in an in vitro assay, a preference for cleavage of the 5'ss of Hac1 is seen (Tirasophon et al., Genes Dev 2000; Niwa et al., Cell 1999), suggesting that IRE1 is capable of differential recognition of substrate splice sites. To clearly show this effect, we used an in vitro system comparing purified yeast IRE1p (yIRE1) and human IREα (hIRE1) cleavage of a previously characterized Hac1 RNA substrate containing 508nt (Fig. 1A) (Sidrauski et al., Cell 1996). We determined cleavage of Hac1 by either yIRE or hIRE over time, starting at very early time points. Cleavage of Hac1 by yIRE has been shown to not require an obligate order (Sidrauski et al., Cell 1997) indicating that either the 5' cleavage or the 3' cleavage can occur. As expected, yIRE1 was able to cleave the 5'ss and 3'ss of Hac1 508 resulting in a typical banding pattern which corresponds to intermediates and products of both the 5' cleavage and the 3' cleavage (Fig. 1B) (Sidrauski et al., Cell 1999). Cleavage of the 5'ss and 3'ss occurs either simultaneously or differences between splice sites occur faster than 30 seconds since intermediates from both *Primary cleavages* (Fig. 1A), but no intron resulting from a *Secondary cleavage*, can be detected (Fig. 1A and 1B). This also indicates that Hac1 is cleaved in a sequential fashion with either *Primary cleavage* (5' cut or 3' cut) occurring first at the 5' and 3' junctions, then the intermediates are cleaved in a *Secondary cleavage* event resulting in release of the intron. When we used human IRE1, we found that only intermediates form the 5'ss cleavage was detected at all time points (Fig. 1B), demonstrating that hIRE1 cleaves the 5'ss but not the 3'ss. This indicates that yIRE and hIRE1 exhibit differential substrate specificity for Hac1 since

yIRE1 cleave both splice sites, while hIRE1 only cleaves the 5'ss. This further suggests that yeast and human IRE1 may have different catalytic mechanisms of substrate cleavage.

Since cleavage of wild type (WT) Hac1 consists of two cleavage events, we wanted to isolate the 5'ss and 3'ss cleavage events individually to verify the specificity we see in hIRE. To do this, we mutated the critical 'G' residue in the loop which blocks splicing at that splice site (Sidrauski et al., Cell 1996). If we mutated the 3'ss, we can specifically examine the 5' cleavage event, and conversely, mutating the 5' ss results in cleavage of only the 3'ss (Fig. 1C, schematic). Consistent with previous reports, yIRE1 was to cleave both the 3'ss and the 5'ss mutants (Fig. 1C) (Sidrauski et al., Cell 1997). When we tested hIRE1, we found that hIRE1 was only able to cleave the 5'ss (Hac1-5'cut) but not cleave the 3'ss (Fig. 1C), consistent with its activity toward wild type Hac1 (Fig. 1B). These results further support the mechanistic differences in substrate recognition and Hac1 cleavage between yeast and human IRE1. Furthermore, differential recognition of the 5'ss and 3'ss of Hac1 by hIRE1 indicate an unequal recognition of substrates and suggests an asymmetric mode of IRE1 recognition.

Recently, we have reported a novel small molecule inhibitor of IRE1, STF-083010 (Irestatin) able to inhibit IRE1 activity in vivo (Papandrou et al., Blood 2010). Our initial characterization of this inhibitor included testing its ability to inhibit IRE1 in vitro to determine if this small molecule can directly inhibit the IRE1 protein. We also initially tested this inhibitor with yeast and human IRE1 to test if this inhibitor is effective for IRE1 from different species. We added increasing concentrations of irestatin to our in vitro reactions and determined ability of either yIRE1 or hIRE to cleave Hac1. Surprisingly, we found that Irestatin inhibition led to differential cleavage of the 5' and 3'ss of Hac1 by yIRE1. Specifically, at higher concentrations irestatin inhibited cleavage of only the 5'ss, but not the 3' splice site (Fig. 2A). Since one splice site is preferentially cleaved while another is not, this indicates that IRE1 does not recognize its substrates equally. Since we see specificity of the 5'ss vs. the 3'ss cleavage is dependent of

irestatin concentration, and since cleavage of WT Hac1 involves two separate events, we wanted isolate each cleavage event using the loop point mutants and see if we retain the concentration dependent specificity. Thus, we added increasing amounts of irestatin in a reaction with yIRE1 and the 5' or 3' mutant substrates (Fig. 2B). We found that the concentration dependent specificity was similar to WT Hac1 since the 3'ss cleavage still occurred at higher concentrations than the 5'ss cleavage (Fig. 2B).

Since irestatin was able to alter yIRE1's specificity toward its substrate, we tested if the specificity of hIRE1 would also be altered. When we added increasing concentrations of irestatin, we found that hIRE1 was more sensitive to the inhibitor since inhibition occurred at a lower concentration (Fig. 2C). Also, irestatin did not alter specificity of hIRE1, so only the 5'ss of Hac1 was cleaved. This effect was confirmed using the Hac1 point mutants. hIRE was still unable to cleave the 3'ss of Hac1 even in the presence of irestatin, and the 5'ss showed inhibition at concentration ranges similar to WT Hac1 (Fig. 2D). Taken together, these findings suggest multiple modes of IRE1 substrate recognition which can be altered pharmacologically. yIRE1 normally cleaves both the 5'ss and 3'ss of Hac1, however addition of irestatin allows yIRE1 to adopt an activation mode that only recognizes the 3'ss. Furthermore, we see species specific recognition of substrates since hIRE1 can only recognize the 5'ss of Hac1, indicating that there are mechanistic differences between yIRE1 and hIRE1 activation.

We have identified conditions of differential specificity of the 5'ss and 3'ss of Hac1. hIRE1 is unable to cleave the 3'ss of Hac1, while irestatin inhibition results in preferential cleavage of the 3'ss of Hac1 by yIRE1. This suggests that IRE1 is able to differentiate between splice sites of Hac1. Since the RNA flanking the splice sites has been shown to positively affect RNA cleavage by IRE1 (Gonzales et al., EMBO J 1999), we wanted to determine the positional effects of the complete stem loop splice sites in relation to the overall RNA sequence. To this end, we created altered Hac1 substrates to test which elements of the substrate are

important for catalysis by either yIRE1 or hIRE1 (Fig. 3A). Since IRE1 differentially recognizes Hac1 splice sites, we hypothesized that altering the positions of the stem loops will also alter the specificity of IRE1. In order to test if the positions of the stem loops in the RNA are critical, we switched the sequences of the 5' and 3' stem loops (Fig. 3A, Hac1-3'5'). When we incubated yeast IRE1 with Hac-3'5', we found that yIRE1 only cleaves the 3' portion of the RNA which now contains the 5'ss sequence (Fig 3B, yIRE1:Hac3'5'). indicating that yeast IRE1 is unable to recognize the 3'ss sequence at the 5' portion of the RNA. This result suggests an asymmetric mode of yIRE1 activation where one element of active IRE1 recognizes the 5' portion of the RNA while a separate element recognizes the 3' portion. When we examined human IRE1 with Hac1-3'5', we found that this resulted in loss of all cleavage (Fig. 3B, hIRE1:Hac1-3'5'). hIRE1 is only able to cleave the 5'ss of Hac1, however, if the 3'ss sequence is moved to the 5' portion of the RNA, hIRE1 cannot recognize that site. Furthermore, moving the 5'ss sequence, which hIRE1 can recognize at the 5' portion of the RNA, results in the inability of hIRE1 to recognize that site. Again, this suggests an asymmetric mode of hIRE1 activation where one element recognized the 5'ss and another recognizes the 3'ss. intriguingly, these suggests that hIRE1 and yIRE1 have distinct recognition elements which have different specificities.

Since yIRE1 and hIRE1 show different specificities towards splice site stem loop sequences, we wanted to further characterize the positional context of the 5'ss and 3'ss in relation to the yIRE1 and hIRE1 recognition elements. To this end, we created substrates that contained two 5' stem loop sequences (Fig. 3A - Hac1-5'5') or two 3' sequences (Fig. 3A - Hac1-3'3') instead of the wild type sequences. This allows for the RNA to present two structurally similar substrates, but with different positional environments. When we tested substrate containing two 5'ss (Hac1-5'5') with yIRE1, we found that substrate acted similar to wild type Hac1 where yIRE1 was able to cleave both sites (Fig. 3B, yIRE1:Hac-5'5'). This indicates that yIRE1 element that recognizes the 3' portion of the RNA is also able to recognize the 5'ss sequence at

that site. However, when we tested the substrate containing two 3'ss (Hac1-3'3'), we found that yIRE1 was only able to cleave the 3' portion of the RNA containing the 3'ss sequence (Fig. 3B). This indicates that the 5' recognition element cannot cleave that splice site if there is a 3'ss sequence at that site. Overall these results demonstrate that yIRE1 is only able to recognize the 5' portion of Hac1 if it contains the proper splice site sequence. However, the 3' portion of the RNA can be recognized with either the 5'ss or the 3'ss sequences. This supports an asymmetric mode of IRE1 substrate recognition and cleavage, where one element of IRE1 recognizes the 5'ss at the 5' part of the RNA while a separate element recognizes the 3' part of the RNA and can cleave either the 5'ss or 3'ss stem loop.

We then tested hIRE1 with these presenting similar substrates at different positions, hIRE1 can only cleave the 5' portion of the RNA of Hac1-5'5' (Fig. 3B, hIRE1:Hac-5'5'). This phenotype is similar to wild type Hac1 since hIRE1 is unable to cleave a stem loop sequence at the 3' portion of the RNA. When a stem loop sequence that hIRE1 can normally recognize (5'ss) is placed at the 3' portion of the RNA, hIRE1 loses its ability to cleave that sequence. Furthermore, when we tested hIRE1 with Hac1-3'3', we found that neither site was cleaved (Fig. 3B, hIRE1:Hac-3'3'), suggesting that hIRE1 cannot recognize the 3'ss of Hac1 at any position. These data indicate that hIRE1 preferentially recognizes the 5' portion of the RNA, and cannot recognize any stem loop sequence placed at the 3' portion of the RNA. Overall, these results support the idea that IRE1 contains asymmetric 5' and 3' recognition elements, and yIRE1 and hIRE1 contain discrete recognition elements with distinct specificities.

HAC1 and XBP1, cellular targets of yIRE1 and hIRE1, respectively, differ in intron size since Hac1 contains a 252nt intron while XBP1 only contains a 26nt intron. Since we see differential recognition between the 5' and 3'ss which are separated by the intron, we wanted to determine if intron length affects specificity of the 5'ss and 3'ss. To test this, we created a substrate that has a dramatically shortened intron (26nt) which matched the length of the human

substrate (Hac1-SI). When we shorted the intron of Hac1 to match the length of Xbp1(Hac1-SI), we found that yIRE1 was still able to cleave both sites (Fig. 3C), indicating that intron length is not a factor for yIRE1 recognition and cleavage. To determine if the yIRE1recognition elements are affected by the intron length, we added increasing amounts of irestatin to a reaction with yIRE1 cleaving Hac1-SI. If intron length does not affect recognition by the yIRE1 5' and 3' recognition elements, we should still see differential cleavage of the 5'ss and 3'ss with irestatin. In fact, that is what we see (Fig. 3D), indicating that for yIRE1, intron length does not affect recognition for yIRE1. However, hIRE1 was only able to cleave the 5'ss but not the 3'ss of Hac1-SI (Fig. 3C), showing that hIRE1 cannot cleave the 3'ss sequence even when the intron is short. The inability of hIRE1 to cleave the 3'ss of Hac1-SI was surprising since the cellular target of hIRE1 is XBP1, which contains a short intron. This fact challenges the current model of a symmetric IRE1 having equal recognition of substrates, and supports an asymmetric model where IRE1 differentially recognizes distinct splice sites.

Since we saw significant differences in the recognition between yIRE and hIRE1 using the yeast substrate, Hac1, we decided to test the mammalian substrate, XBP1. XBP1 is structurally different from Hac1 in that it only contains as 26nt intron as compared to a 252nt intron for Hac1, so we wanted to determine if this has an effect on 5' vs 3'ss specificity. To this end, we constructed a radiolabelled XBP1 444 RNA (Fig 4A) and incubated this substrate with either yIRE or hIRE. Interestingly, we found that yeast and human IRE can cleave XBP1 in a similar manner (Fig 4B). Both yIRE1 and hIRE1 were able to cleave both splice sites of XBP1 equally. We then tested inhibition by irestatin since we saw differences in substrate recognition with Hac1. However, we found that irestatin was able to inhibit cleavage of both 5'ss and 3'ss of XBP1 (Fig. 4C). This was in contrast to inhibition of Hac1 which showed differences between 5'ss and 3'ss cleavage. Furthermore, the concentration range of inhibition by irestatin matched the inhibition range of Hac1, where hIRE1 was more sensitive to irestatin than yIRE1. These

data showing that IRE1 exhibits differential specificity between Hac1 and XBP1 further indicate that IRE1 has distinct recognition elements. In addition, the fact that different phenotypes are seen between Hac1-SI and XBP1, both containing short introns, suggests that the stem loop sequence of the 3' splice site is important for the recognition of hIRE1.

Our findings suggest that two factors may be important for determining recognition of IRE1's substrate: position of stem loops in relation to the RNA and intron length. Specifically, we see that hIRE1 is able to cleave XBP1 RNA which contains a short intron, however, cannot cleave Hac1-SI which also has a short intron. We wanted to dissect contributions of intron length and stem loop sequence on splice site recognition. To this end, we constructed a substrate that consists of Hac1 but switched the stem loop sequences to XBP1 stem loop sequences respective to its position and retained the long intron of Hac1 (Fig. 5A, Hac1-Xss-LI). We then shortened the intron of this construct to match the length of the XBP1 intron of 26 nt (Fig. 5A, Hac1-Xss-SI). We reasoned that hIRE1 is able to recognize the XBP1 3'ss, but not the Hac1 3'ss, when the intron is short. We wanted to test if hIRE1 can recognize the XBP1 3'ss when the intron is long, corresponding to Hac1. We then tested cleavage of these substrate by both yIRE1 and hIRE1. yIRE1 is able to cleave both the Hac1 3'ss and XBP1 3'ss, so we hypothesized that yIRE1 should be able to cleave both substrates. Indeed, we found that yIRE1 was able to cleave Hac1-Xss-LI similar to WT Hac1, and Hac-Xss-SI similar to WT XBP1 (Fig. 5B), indicating that yIRE1 recognizes the XBP1 stem loops in a similar manner as Hac1 stem loops. When we examined human IRE1, we found that hIRE1 was not able to efficiently cleave the 3'site containing the sequence of the 3' XBP1 stem loop (Fig. 5B, Hac1-Xss-LI), however, when the intron was shortened to match XBP1, hIRE1 is now able to cleave the 3'ss (Fig. 5B, Hac1-Xss-SI, h-IRE). This shows that hIRE1 requires a short intron to efficiently cleave the 3'ss. Taken together, these results indicate that yIRE1 is able to recognize XBP1 stem loops regardless of intron length. However, hIRE1 can only cleave the 3' XBP1 stem loops if the intron is short.

The previous experiment was done using XBP1 stem loops in context of the Hac1 RNA. Since we find that positional context plays a role in specificity, we wanted to test intron length in context of both Hac1 and XBP1 RNA. To this end, we constructed either Hac1 or XBP1 substrates that contains only one stem loop sequence at both the 5' and 3' splice sites (Fig. 5A). We selected the Hac 5' stem loop and XBP1 3' stem loop since both can be recognized and cleaved by both yIRE1 and hIRE1in all tested positional contexts. We placed the 5' stem loop sequence of Hac1 in both splice sites of either Hac1 (Hac1-H5'5') or XBP1 (XBP1-H5'5'). We also placed the 3' stem loop sequence of XBP1 in both splice sites of either Hac1 (Hac1-X3'3') or XBP1 (XBP1-X3'3'). We found that yIRE1 was able to cleave both splice sites of Hac1-H5'5' and XBP1-H5'5' (Fig. 5C). Similarly, yIRE1 was able to cleave both splice sites of Hac1-X3'3' and XBP1-X3'3', confirming that yIRE1 is able to recognize and cleave both the 5'ss and 3'ss regardless of intron length. When we tested hIRE1 with these substrates, hIRE was only able to cleave the 5'ss of substrates with a long intron, Hac1-H5'5' and Hac1-X3'3', and unable to cleave the 3'ss (Fig. 5C). However, hIRE1 was able to cleave both splice sites of substrates with short introns, XBP1-H5'5' and XBP1-X3'3' (Fig. 5C and 5D). This indicates that a short intron is required for cleavage of the 3' portion of the RNA by hIRE1.

DISCUSSION

Although the function of IRE1 as an ER stress senor has been conserved from yeast to humans, we have shown that the manner in which it recognizes and cleaves its substrate shows mechanistic differences. Based on our findings, we propose a model for IRE1 nuclease activity involving asymmetric recognition of the substrate splice sites (Fig. 6). Specifically, our data indicates that active IRE1 nulcease contains at least two distinct splice site recognition units. One unit recognizes the junction between the 5'exon and intron (IRE1-5') while a distinct unit recognizes the intron-3'exon junction (IRE1-3'). The yIRE1-5' recognition unit can only cleave

the stem loop of the 5'ss of Hac1 and not the 3' Hac1 stem loop, while the yIRE1-3' recognition unit can cleave both. The hIRE1-5' recognition unit can cleave either the 5' or 3' stem loops of XBP1, however, the hIRE1-3' unit can only cleave any stem loop if the intron is short. Furthermore, neither hIRE1 recognition units do not recognize the 3'ss stem loop of Hac1. Also, irestatin inhibits the yIRE1-5' unit more than the yIRE1-3' unit when cleaving Hac1.

So what constitutes the IRE1 recognition units? Presently, crystal structure of the cytosolic domain of yeast IRE1 shows a symmetrical putative RNase catalytic site (Lee et al., Cell 2008). However, our findings indicate that IRE1 is able to differentially recognize different substrates, suggesting a structural asymmetry in the conformation of the protein. This asymmetry may come from binding to the RNA itself. Current crystal structures show 'active' IRE1 without any substrate, and our results suggest that the location of the stem loop in context of the RNA is critical for cleavage. Perhaps RNA binding to the protein may alter its conformation and allow it to adopt an asymmetric conformation which then exhibits differential specificity towards the 5' and 3' splice sites. Another factor that can introduce asymmetry to IRE1 is in its ability to form higher orderd structures. Another crystal structure shows IRE1 forming higher ordered structures with three distinct interfaces, IF1c, IF2c, and IF3c (Korennykh et al., Nature 2009), where IF1c was found to be the interface that forms the symmetric putative RNase site. The discovery of additional interfaces may allow for asymmetric nuclease sites to form which would have structurally distinct catalytic RNase sites. Formation of structurally different RNase sites gives rise to the possibility of differential substrate recognition. Mutational analysis that disrupts only one interface but maintains the others will help ascertain any new catalytic RNase sites.

Overall, our analysis of IRE substrates reveals that the differences in substrate recognition between yIRE1 and hIRE1 center around cleavage of the 3' splice site. For yIRE1, moving the 3'ss sequence to the 5' portion of Hac1 prevents cleavage of that site (Fig. 3B). Also, hIRE1 is not able to recognize the 3'ss of Hac1 even if the sequence is moved to the 5' portion of

the RNA (Fig. 3B), or if the intron is long (Fig. 5). However, both yIRE and hIRE can cleave both 5'ss of Hac1 or XBP1. Taken together, this suggests a divergence in the 3' recognition element between yIRE1 and hIRE1, further suggesting that the 3' splice site of the RNA may be divergent. We examined the sequences of IRE1 substrates from several yeasts up to higher eukaryotes including humans (Fig. 6A). Interestingly, we found other yeast species with Hac1 containing short introns (C. albicans, Y. lipolytica, and T. reesei) which resemble XBP1 introns. Also, upon alignment of 5' and 3' splice sites, we found that the sequence and structure of the 5' splice site loop was conserved even between S. cerevisiae Hac1 and H. sapiens XBP1 (Fig. 6A - 5' splice site, light grey). However, when we examined the 3' splice sites, we found that although the residues critical for cleavage were conserved, the overall sequence was not (Fig. 6A – 3' splice site). We found conservation between metazoans and yeasts with Hac1 containing a short intron. However, the 3' splice site of S. cerevisiae was unique among the species studied. Secondary structure predictions of the 3'ss of each group show drastically different stem loop structures, however, all maintain the structure of the catalytic loop (Fig. 6B). Altogether, these data indicate that IRE1 recognizes its substrate in an asymmetric manner and that IRE1 contains an element that recognizes the 5'ss and a separate element that recognizes the 3'ss. Also, we show divergent recognition of the 3'ss between yIRE1 and hIRE1, specifically, hIRE1 requires a short intron for cleavage of the 3'ss but not the 5'ss. Furthermore, we find divergent secondary structures of the 3' splice site in IRE1 substrates, suggesting diverse IRE1 cleavage mechanisms across species.

The function of IRE1 in splicing of a specific RNA in response to ER stress is evolutionalrily conserved. However, we find differences in substrate recognition between yIRE1 and hIRE1, indicating that the catalytic mechanism of IRE1 cleavage may be evolutionarily divergent. We analyzed this by aligning the primary sequence of IRE1 in parallel with IRE1 substrates found in several organisms. Our findings show that two factors are important in

determining specificity of substrate: positional location of stem loops and intron length. One explanation for the importance of the positional location of stem loops is that each stem loop is structurally different and separate units of IRE1 recognize different shaped stem loops. This would be an explanation for the fact that hIRE1 can cleave the XBP1 stem loop, but not the Hac1 3' stem loop in a substrate with a short intron. Because of this, we analyzed the predicted structre of the 5' and 3' stem loops across species (Fig. 7). Interestingly, we found that the structures of the 3' splice sites across species were structurally dissimilar. This could explain why yIRE1 cannot recognize the 3'ss stem loop at the 5' portion of the RNA since the unit that cleaves the 5'ss cannot recognize the structure of the 3' stem loop. Also, we find that several yeast species contain Hac1 with a short intron similar to XBP1 (Fig. 7) however, these yeast species also have a 3'splice site with a shorter stem and larger loop, suggesting that specificities of IRE1 in these organisms is also different from either S. cerevisiae or metazoans. Determining sequence similarities between each group may determine structural components of IRE1 that contribute to specificity to cellular substrates. We found parts of IRE1 that are conserved within each group, S. cerevisiae, yeast containing Hac1 with a short intron, and metazoans, which may structurally determine substrate recognition (Fig. 8). Switching these areas into another group may also switch substrate specificity.

Comparing the known crystal structure of yeast IRE1 (Han et al., Cell 2008; Korennykh et al., Nature 2009) to the predicted structure of human IRE1 may give hints as to what is causing differences in specificities. Specifically, human IRE1 cannot recognize the Hac1 3' stem loop, and cannot cleave the 3' splice site if the intron in long. Based on the known yeast IRE1 crystal structure and the alignment between yeast and human IRE1, we used a prediction program (Quckphyre) to predict the monomeric structure of human IRE1. Based on the predicted crystal structure, there are three distinct loops that are show structural differences between yeast and humanIRE1 that are in close proximity to the putative nuclease domain (Fig. 8B). These loops

may regulate access to the active site of the core dimer and dictate specificity of this particular site. The sequence of Loop1 was conserved between different yeast IRE1, however, that region in metazoan IRE1 was not as conserved (Fig. 9 – Red box), indicating that loop may be important for yeast IRE1 function. Loop2 contains an amino acid with reversed charges between yeast and human IRE1 which may affect RNA binding (Fig. 8B). Loop3 shows bulky residues extending out in predicted human IRE1 structure, while yeast IRE1 shows a more compact loop (Fig 7B). Reversing the properties of these loops between yeast and human may also reverse specificities. However, a crystral structure is human IRE1 is ideal for determining factors that affect substrate specificity.

MATERIALS AND METHODS

Constructs and Cloning

Hac1 508 substrate (pCF187) was used from Sidrauski et al (1997). XBP1 444 substrate was made by amplification of cDNA using a forward primer with a T7 promoter. (F) TAATACGACTCACTATAGGGAGAAGAACCAGGAGTTAAGACAGCGC; (R) TAAGACTAGGGGCTTGGTATATATGTG. The point mutations of the Hac1 stem loop were used as previously described in Sidrauski et al., (1997). pCF191: Hac1 5’ splice site point mutant. pCF201: Hac1 3’ splice site point mutant. The mutant substrates were constructed using overlapping PCR using the following sequences: Hac1 5’ stem loop: CGTAATCCAGCCGTGATTACG; Hac1 3’ stem loop: CTTGTACTGTCCGAAGCGCAGTCAGG; XBP1 5’ stem loop: CTGAGTCCGCAGCACTCAG; XBP1 3’ stem loop: TGCACCTCTGCAGCAGGTGCA.

In vitro Nuclease Assay

In vitro transcription of the ^{32}P labeled Hac1 508 substrate has been described previously (Sidrauski, 1997). For the nuclease assay, hIRE1 or yIRE1 protein (1μg) was incubated with the indicated amount of Irestatin, Quercetin, or DMSO in the nuclease reaction mix: Kinase buffer (100mM Hepes, 50mM MgAcetate, 250mM KOAc, 10mM DTT), RNAse out (Invitrogen), 2mM ADP), and 20,000 cpm of ^{32}P labeled Hac1 508 substrate. The reaction was incubated for 30 min at 30°C or for the indicated amount of time. After, the RNA was extracted with phenol/chloroform, ethanol precipitated and analyzed on a denaturing 6% Urea acrylamide gel. Bands were visualized by autoradiography.

Alignment and Structure Analysis

Protein and RNA alignment was done using ClustalW (www.ebi.ac.uk/clustalw/) and Quickphyre. RNA secondary structure was done using Mfold (http://mfold.rna.albany.edu/). Protein crystal structure was visualized using Rasmol

REFERENCES

Auf, G., Jabouille, A., Guerit, S., Pineau, R., Delugin, M., Bouchecareilh, M., Magnin, N., Favereaux, A., Maitre, M., Gaiser, T., von Deimling, A., Czabanka, M., Vajkoczy, P., Chevet, E., Bikfalvi, A., and Moenner, M. Inositol-requiring enzyme 1alpha is a key regulator of angiogenesis and invasion in malignant glioma. Proc Natl Acad Sci U S A *107*, 15553-15558.

Calfon, M., Zeng, H., Urano, F., Till, J.H., Hubbard, S.R., Harding, H.P., Clark, S.G., and Ron, D. (2002). IRE1 couples endoplasmic reticulum load to secretory capacity by processing the XBP-1 mRNA. Nature *415*, 92-96.

Dong, B., Niwa, M., Walter, P., and Silverman, R.H. (2001). Basis for regulated RNA cleavage by functional analysis of RNase L and Ire1p. Rna *7*, 361-373.

Gonzalez, T.N., Sidrauski, C., Dorfler, S., and Walter, P. (1999). Mechanism of non-spliceosomal mRNA splicing in the unfolded protein response pathway. Embo J *18*, 3119-3132.

Han, D., Upton, J.P., Hagen, A., Callahan, J., Oakes, S.A., and Papa, F.R. (2008). A kinase inhibitor activates the IRE1alpha RNase to confer cytoprotection against ER stress. Biochem Biophys Res Commun *365*, 777-783.

Hetz, C., and Glimcher, L.H. (2009). Fine-tuning of the unfolded protein response: Assembling the IRE1alpha interactome. Mol Cell *35*, 551-561.

Kawahara, T., Yanagi, H., Yura, T., and Mori, K. (1998). Unconventional splicing of HAC1/ERN4 mRNA required for the unfolded protein response. Sequence-specific and non-sequential cleavage of the splice sites. J Biol Chem *273*, 1802-1807.

Korennykh, A.V., Egea, P.F., Korostelev, A.A., Finer-Moore, J., Zhang, C., Shokat, K.M., Stroud, R.M., and Walter, P. (2009). The unfolded protein response signals through high-order assembly of Ire1. Nature *457*, 687-693.

Lee, K.P., Dey, M., Neculai, D., Cao, C., Dever, T.E., and Sicheri, F. (2008). Structure of the dual enzyme Ire1 reveals the basis for catalysis and regulation in nonconventional RNA splicing. Cell *132*, 89-100.

Niwa, M., Sidrauski, C., Kaufman, R.J., and Walter, P. (1999). A role for presenilin-1 in nuclear accumulation of Ire1 fragments and induction of the mammalian unfolded protein response. Cell *99*, 691-702.

Oslowski, C.M., and Urano, F. The binary switch that controls the life and death decisions of ER stressed beta cells. Curr Opin Cell Biol.

Papandreou, I., Denko, N.C., Olson, M., Van Melckebeke, H., Lust, S., Tam, A., Solow-Cordero, D.E., Bouley, D.M., Offner, F., Niwa, M., and Koong, A.C. Identification of an Ire1alpha endonuclease specific inhibitor with cytotoxic activity against human multiple myeloma. Blood.

Ruegsegger, U., Leber, J.H., and Walter, P. (2001). Block of HAC1 mRNA translation by long-range base pairing is released by cytoplasmic splicing upon induction of the unfolded protein response. Cell *107*, 103-114.

Sidrauski, C., and Walter, P. (1997). The transmembrane kinase Ire1p is a site-specific endonuclease that initiates mRNA splicing in the unfolded protein response. Cell *90*, 1031-1039.

Tirasophon, W., Lee, K., Callaghan, B., Welihinda, A., and Kaufman, R.J. (2000). The endoribonuclease activity of mammalian IRE1 autoregulates its mRNA and is required for the unfolded protein response. Genes Dev *14*, 2725-2736.

Wiseman, R.L., Zhang, Y., Lee, K.P., Harding, H.P., Haynes, C.M., Price, J., Sicheri, F., and Ron, D. Flavonol activation defines an unanticipated ligand-binding site in the kinase-RNase domain of IRE1. Mol Cell *38*, 291-304.

Yoshida, H., Matsui, T., Yamamoto, A., Okada, T., and Mori, K. (2001). XBP1 mRNA is induced by ATF6 and spliced by IRE1 in response to ER stress to produce a highly active transcription factor. Cell *107*, 881-891.

Yoshida, H., Oku, M., Suzuki, M., and Mori, K. (2006). pXBP1(U) encoded in XBP1 pre-mRNA negatively regulates unfolded protein response activator pXBP1(S) in mammalian ER stress response. J Cell Biol *172*, 565-575.

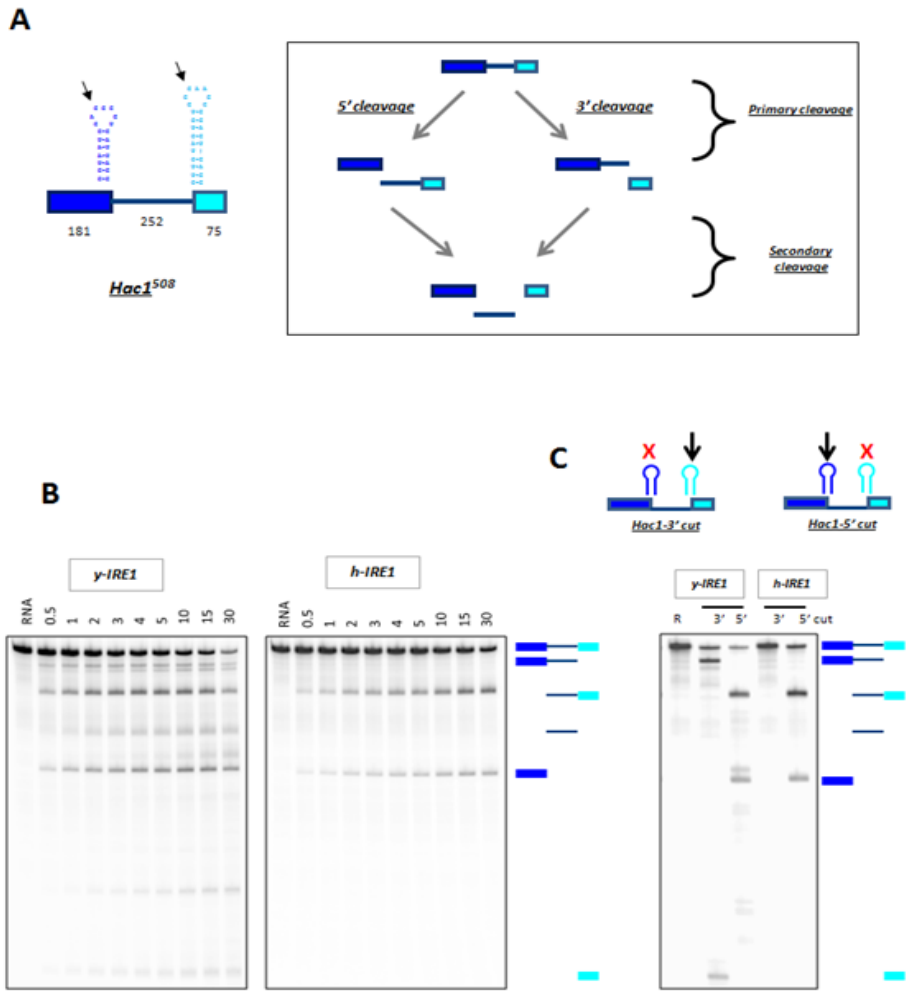

Figure 1. Hac1 RNA is differentially recognized by yeast and human IRE1.

(A) Hac1 RNA substrate containing stem loops indicating the 5' splice site (Dark Blue) and the 3' splice site (Light Blue). Right panel: Schematic of Hac1 cleavage by IRE1. The 5'ss and 3'ss are first cleaved simultaneously (Primary cleavage), then in a secondary cleavage, the remaining splice site is cleaved resulting in release of the intron.
(B) Time course of Hac1 cleavage by yeast IRE1 (y-IRE1) and human IRE1 (h-IRE1). Radiolabelled Hac1 was incubated with y-IRE1 or h-IRE1 for the indicated amount of time. y-IRE1 was able to perform primary and secondary cleavages resulting in release of the intron. h-IRE1 was only able to perform the primary cleavage of the 5'ss.
(B) Point mutations in a critical G residue of Hac1 were made to prevent cleavage of that splice site. Mutation of the 5'ss results in a substrate that can only be cleaved at the 3'ss (Hac1-3'cut), conversely, mutation of the 3'ss results in only 5'ss cleavage (Hac1-5' cut). Yeast IRE1 is able to cleave both 5'ss and 3'ss, while human IRE1 only cleaves the 5'ss of Hac1.

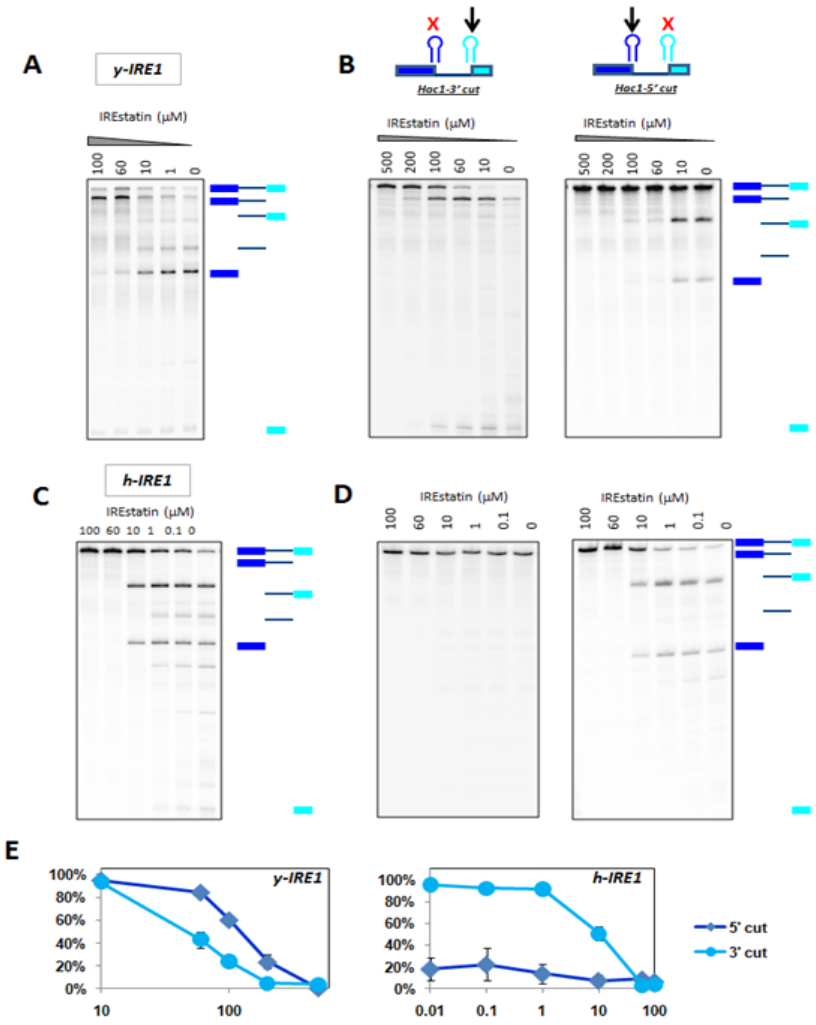

Figure 2. Asymmetric recognition of Hac1 splice sites by Irestatin.

(A) Irestatin exhibits differential inhibition of the 5' and 3' splice sites by yeast IRE1. y-IRE1 was incubated with radiolabelled Hac1 and increasing amounts of Irestatin. At higher concentrations of irestatin, only the 5'ss was inhibited.
(B) Increasing amounts of irestatin were incubated with y-IRE1 and either Hac1-3' cut or Hac1-5' cut. Irestatin was able to inhibit the 5' cleavage more than the 3' cleavage.
(C) Irestatin does not alter hIRE1's recognition of Hac1. h-IRE1 was incubated with increasing concentrations of irestatin. Irestatin is able to inhibit cleavage by h-IRE1 at a much lower concentration than y-IRE1. Also, only the 5'ss was cleaved by IRE1 and addition of irestatin did not cause the 3' to be recognized.
(D) Increasing amounts of irestatin were incubated with h-IRE1 and either Hac1-3' cut or Hac1-5' cut.
(E) Quantitation of (B) for y-IRE1 and (D) for h-IRE1.

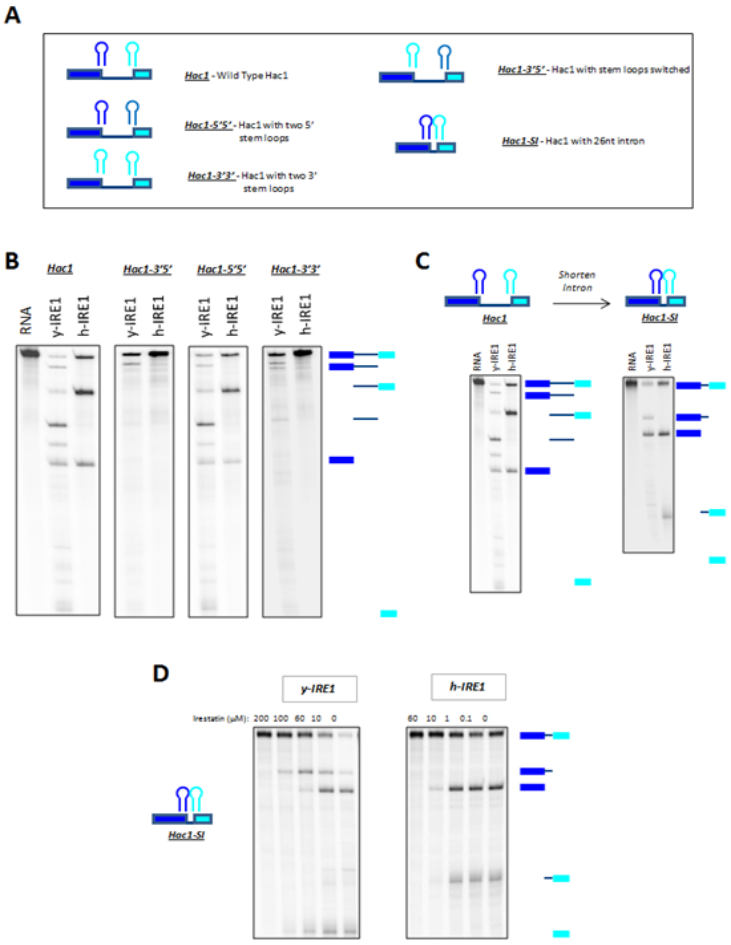

Figure 3. Positional importance of the splice sites of Hac1.

(A) Schematic of substrates used. In order to examine the positional significance of the stem loop structures, we made mutant substrates of Hac1. We replaced the stem loop at the 5' splice junction with the sequence of the 3'ss stem loop, and conversely, we took the 3' splice junction and replaced the stem loop with the sequence of the 5'ss (Hac1-3'5'). We also replaced the stem loops at both splice junctions with the sequence of the 5'ss stem loop (Hac1-5'5') or the sequence of the 3'ss stem loop (Hac1-3'3'). We also shortened the intron of Hac1 to 26 nt to match the length of XBP1, the mammalian substrate of IRE1 (Hac1-SI).
(B) IRE1 can differentially recognize the 5' and 3' splice sites. Either y-IRE1 or h-IRE1 was incubated with Hac1-3'5', Hac1-5'5', or Hac1-3'3' and run on a denaturing acrylamide gel. y-IRE1 is not able to cleave the 5' splice junction when it contains the sequence of the 3'ss stem loop. Furthermore, h-IRE1 is not able to cleave the 3' splice junction even when the 5'ss stem loops sequence is present at that location.
(C) Either y-IRE1 or h-IRE1 was incubated with wild type Hac1 or Hac1 containing a shortened intron (Hac-SI). Even with a shortened intron, h-IRE1 is still unable to cleave the 3' stem loop of Hac1.
(D) y-IRE1or h-IRE1 was incubated with Hac1-SI, and increasing amounts of Irestatin was included. Even with a shortened intron, the 5' and 3' splice sites of Hac1 were still differentially inhibited by irestatin.

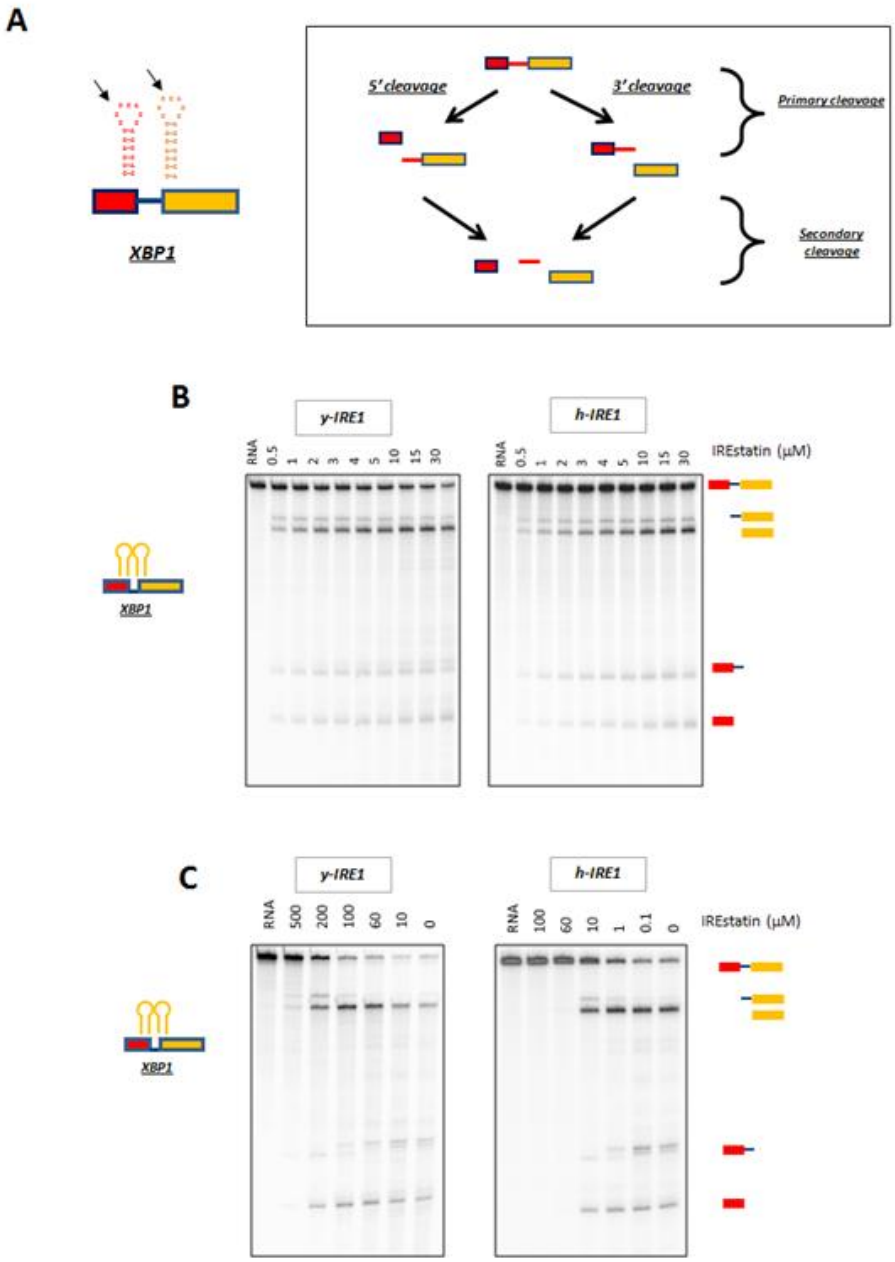

Figure 4. Yeast and human IRE1 cleaves XBP1 similarly.

(A) XBP1 substrate also containing two stem loops at the splice sites.
(B) Time course of XBP1 cleavage by y-IRE1 and h-IRE1. y-IRE1or h-IRE1 were incubated with XBP1 substrate and cleavage was determined over time. Both y-IRE1 and h-IRE1 were able to recognize both splice sites equally.
(C) Effect of irestatin on y-IRE1 and h-IRE1. Increasing concentrations of Irestatin was to inhibit XBP1 splicing for both yeast and human IRE1 in the same manner. Furthermore, the concentration of inhibiton was similar to the ones seen in the Hac1 studies.

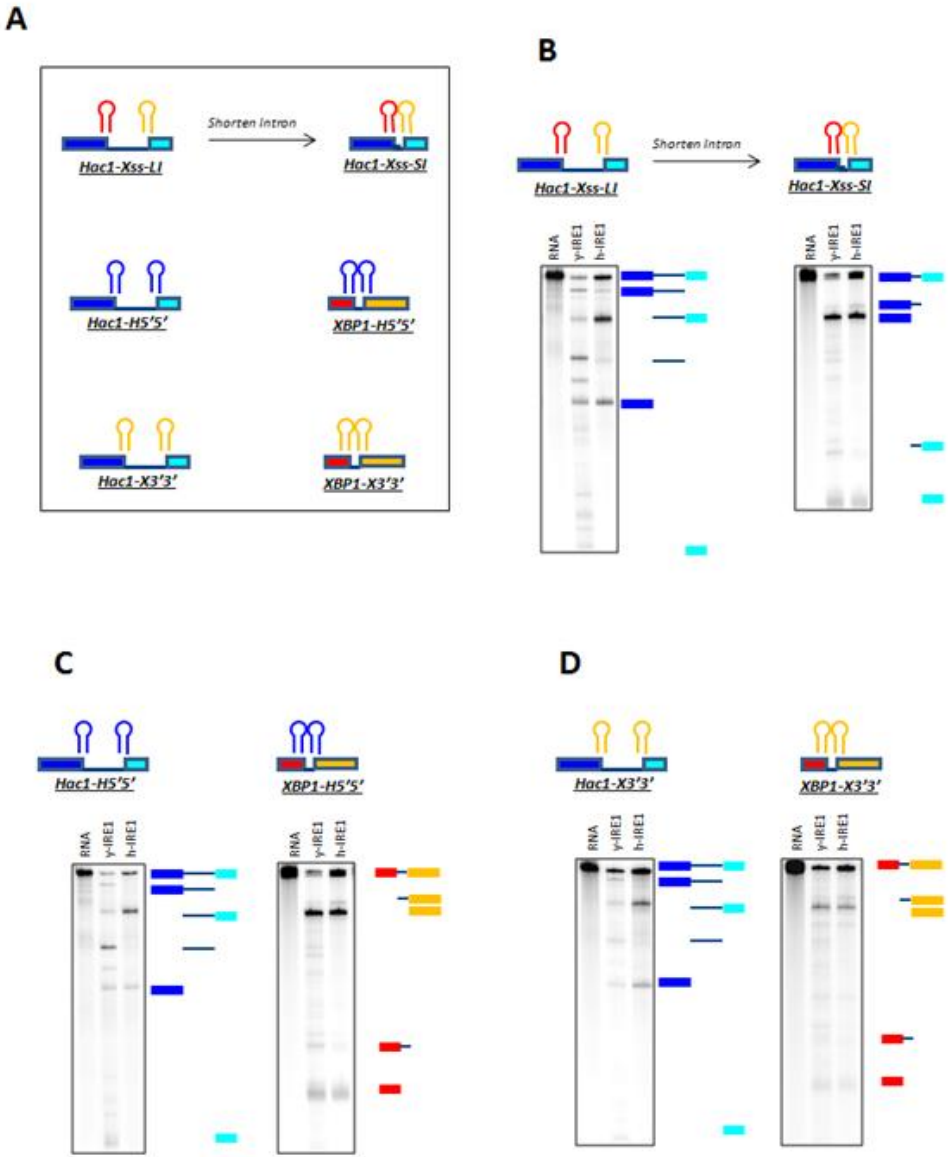

Figure 5. Intron length is critical for cleavage of the 3' splice site by human IRE1.

(A) Schematic of substrates used. In order to determine importance of the intron length, we replaced the stem loop sequences of Hac1 with the stem loops of XBP1 (Hac1-Xss-LI). We then shortened the intron to match the length of XBP1 (Hac1-Xss-SI). We also made Hac1 and XBP1 substrates containing the same stem loop sequences recognized by both yeast and human IRE1 at the 5' and 3' splice sites. We replaced the stem loops with either the Hac1 5' stem loop sequence (Hac1-H5'5' and XBP1-H5'5') or the XBP1 3' stem loop sequence (Hac1-X3'3' and XBP1-X3'3').
(B) Human IRE1 requires a short intron to cleave the 3' splice site. Yeast or human IRE1 was incubated with either Hac1-Xss-LI or Hac1-Xss-SI.
(C) Yeast or human IRE1 was incubated with either Hac1-H5'5' or XBP1-H5'5'.
(D) Yeast or human IRE1 was incubated with either Hac1-H5'5' or XBP1-H5'5'

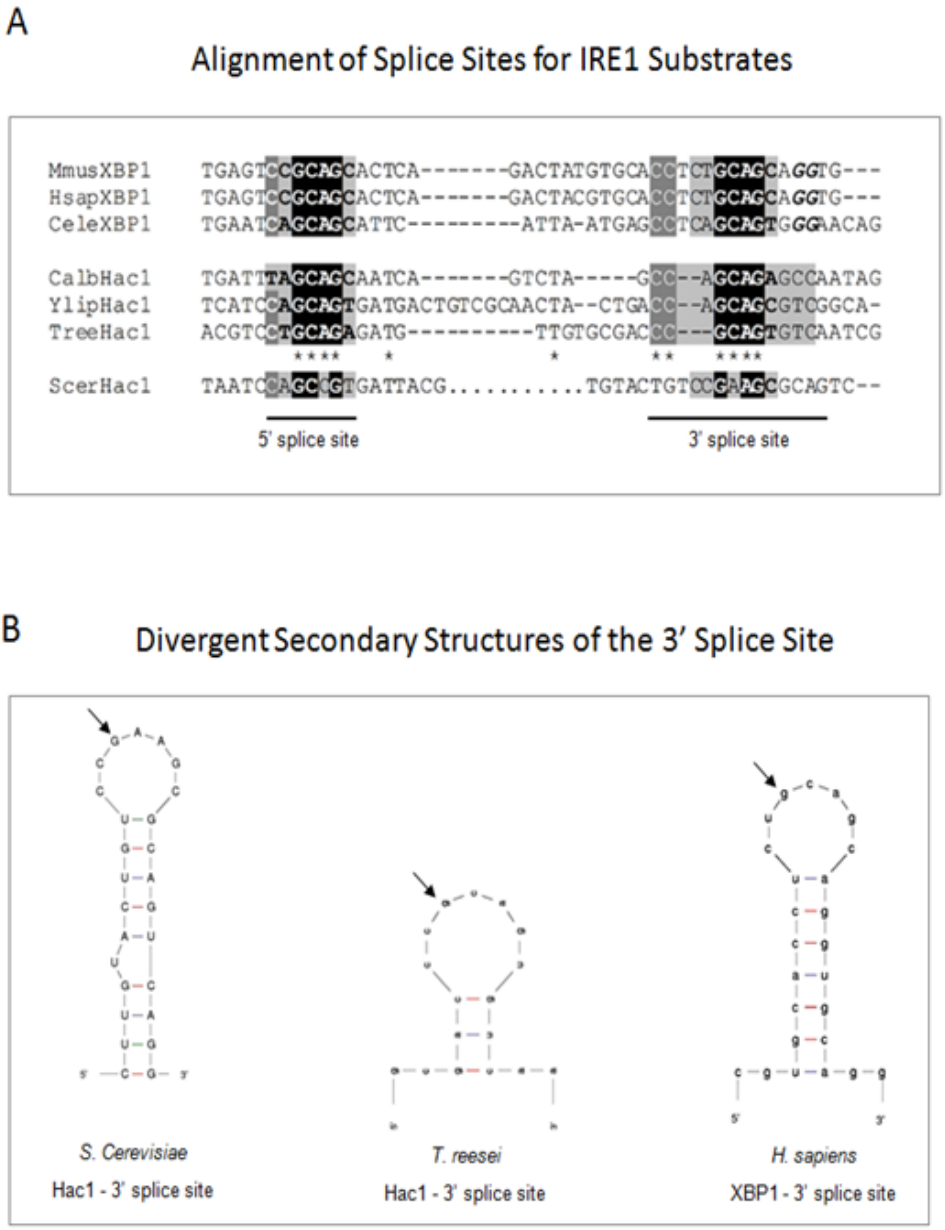

Figure 6. Alignment of IRE1 substrates show divergent 3' splice site structures

(A) IRE1 substrates from several organisms were aligned showing the 5' and 3' splice sites. 5' splice sites were conserved but not the 3' splice sites. Light grey shading – predicted catalytic loop structures. Black shading – conservation in all species. Grey – conservation in most species. * indicates conservation in all but S. cerevisiae. MmusXBP1 – mouse XBP1; HsapXBP1 – human XBP1; CeleXBP1 – C. elegans XBP1; CalbHac1 – C. Albicans Hac1; YlipHac1 – Y. lipolytica Hac1; TreeHac1 – T. reesei Hac1; ScerHac1 – S. cerevisiae Hac1.
(B) Predicted secondary structure of the 3' splice sites from each group. The 3' splice sites show divergent structures. Arrow – cleavage site.

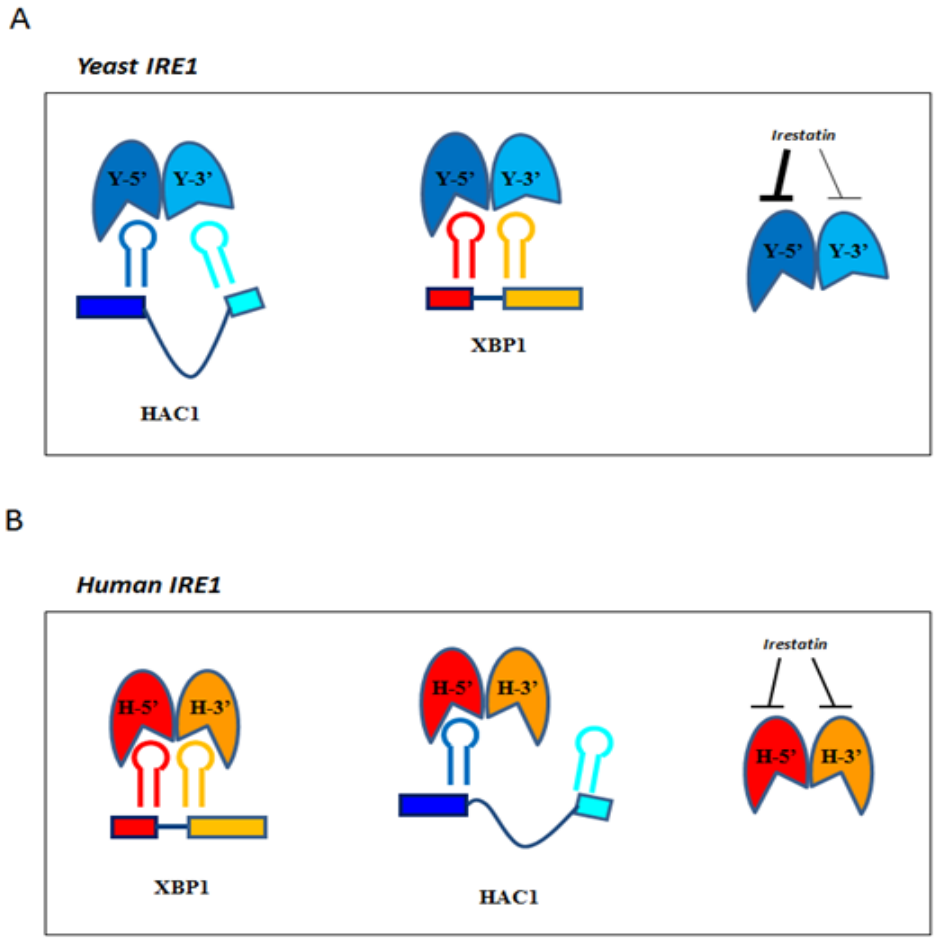

Figure 7. Model of IRE1 Activation.

(A) Yeast IRE1. Yeast IRE1 contains two recognition units. Y-5' recognizes and cleaves the 5' splice site of Hac1, and Y-3' recognizes the 3' splice site of Hac1. Y-5' cannot recognize the 3' splice site of Hac1, however Y-3' can recognize the 5' splice site of Hac1. Both units can recognize and cleave the corresponding site of XBP1. Irestatin is able to strongly inhibit Y-5' but weakly inhibits Y-3'.
(B) Human IRE1. Human IRE1 contains two recognition units. H-5' recognizes the 5'ss of XBP1, while H-3' recognizes the 3'ss of XBP1. H-3' cannot cleave unless the intron is short. Also, H-3' cannot recognize the Hac1 3' stem loop even if the intron is short. Irestatin inhibits both units equally.

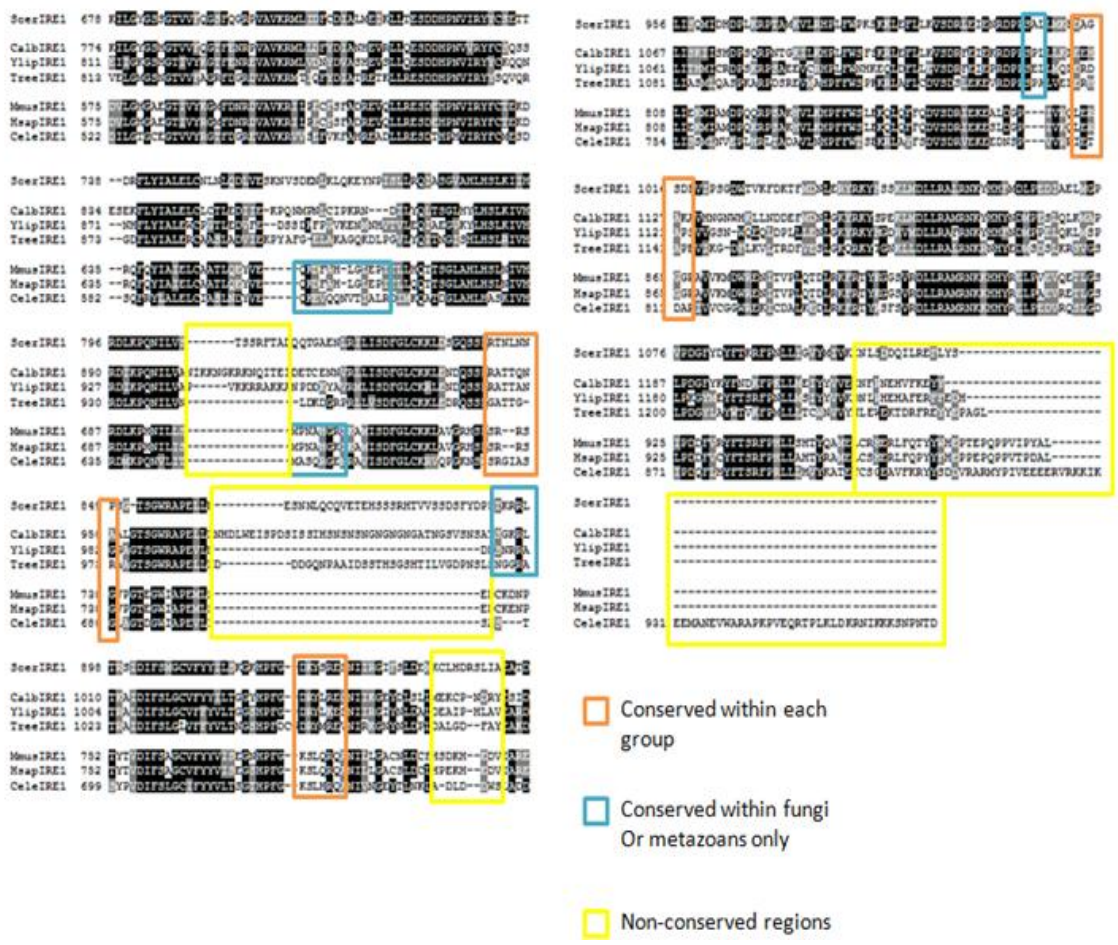

Figure 8. Alignment of Yeast and Metazoan IRE1

(A) Cytoplasmic regions of IRE1 from several species were aligned using ClustalW highlighting differences in sequence. Yeast species included S. cereviciae, C. albicans, Y. lipolytica, and T. reesei. Other species included C. elegans, M. musculus (mouse), and H. sapiens (human). Orange boxes indicate conserved regions within each group but divergent among groups. Blue boxes indicate conservation within one group. Yellow boxes indicate divergent regions among all groups.

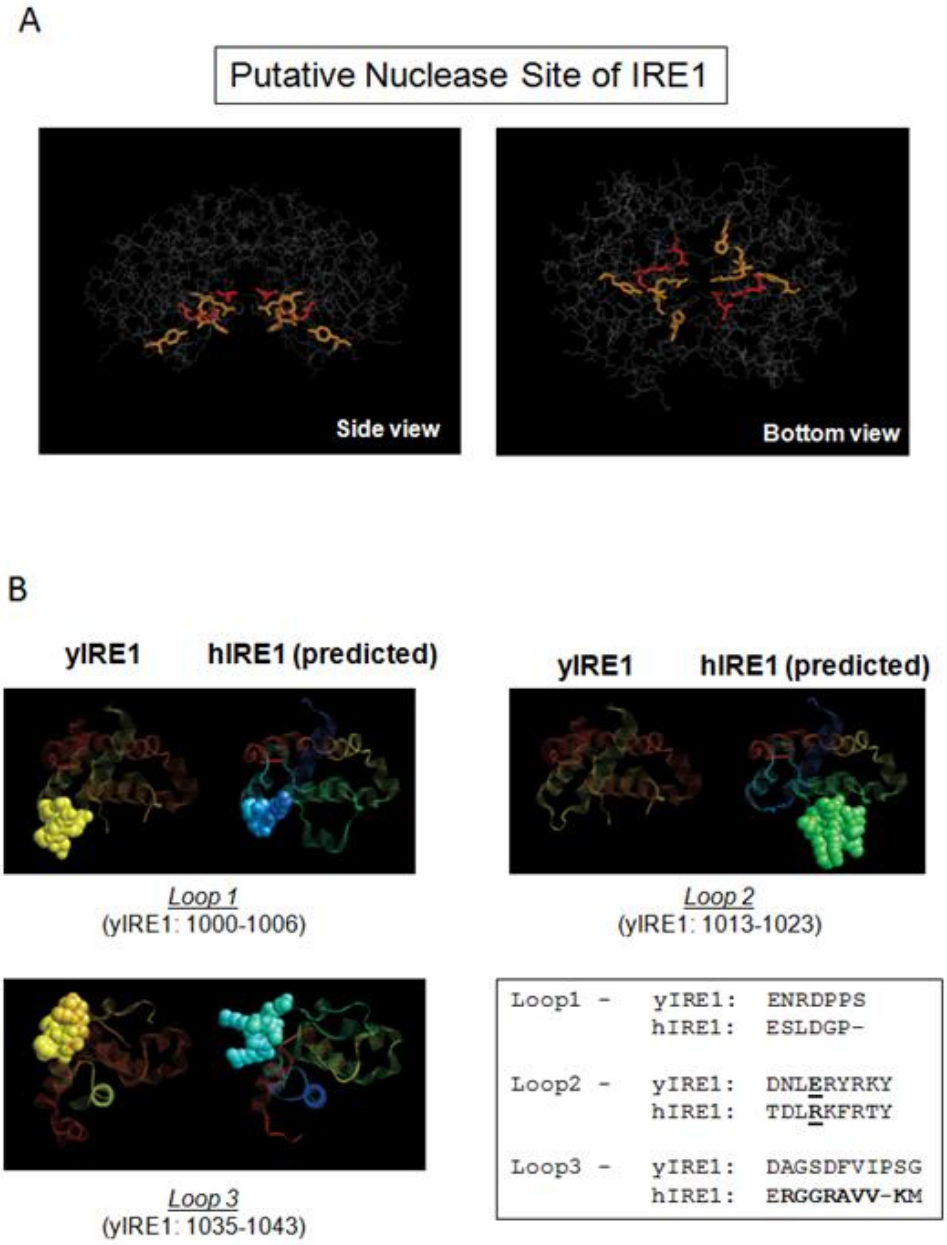

Figure 9. Structural differences between yeast IRE1 and predicted human IRE1

(A) Putative nuclease site of IRE1. Red residues align with the nuclease active site of RNaseL, a related nuclease. Yellow residues lose nuclease activity when mutated.
(B) Three loops that have predicted structural differences between yeast and human. These loops are in close proximity to the putative nuclease site and may restrict access to the nuclease site. Alignment of the segments are shown.

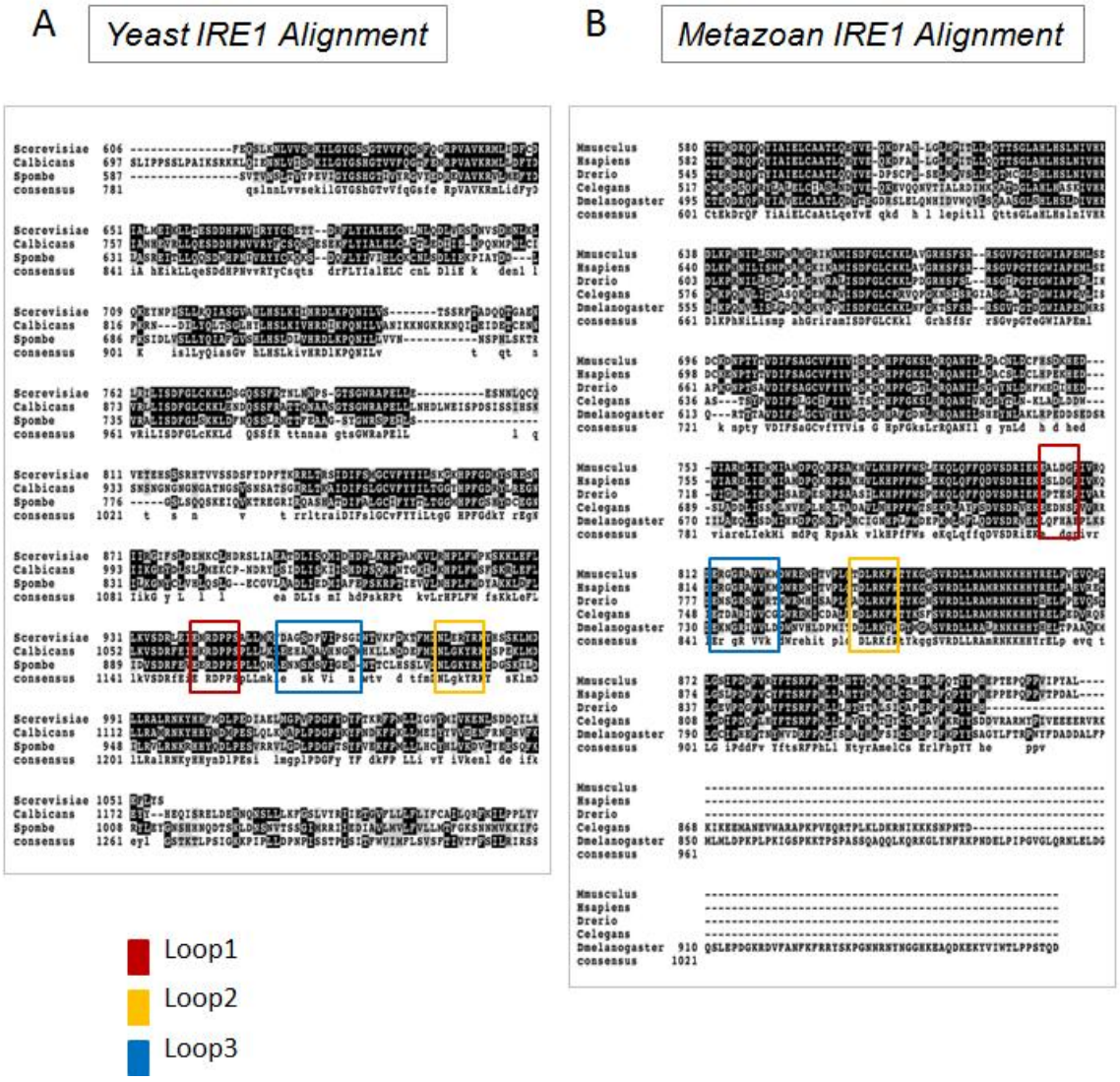

Figure 10. Alignment of IRE1

(A) Alignment of cytoplasmic regions of IRE1 in yeasts and B) in metazoans. Loop1 is indicated in red, Loop2 in yellow, and Loop3 in blue. Loops are identified in both alignments for comparison.

Chapter 4

ABSTRACT

Conditions that disrupt homeostasis of the endoplasmic reticulum (ER) reduce its protein folding capacity and leas to ER stress and activate the unfolded protein response (UPR). IRE1, a multifunctional ER transmembrane protein containing both kinase and endoribonuclease activities, is the most evolutionary conserved branch of the UPR from yeast to humans. During ER stress, IRE1 initiates non-conventional splicing of a cytosolic mRNA encoding for a bZIP transcription factor, Hac1 in yeast and XBP1 in higher eukaryotes. Recent studies report that, in addition to unconventional splicing, the UPR induces a decrease in mRNA associated with the ER membrane via a UPR activated endonucleolytic activity, thus, providing underlying proposal that IRE1 itself is responsible for their cleavage. Here, using the cell free *in vitro* reaction, we unambiguously show that IRE1 directly cleaves ER localized mRNAs, demonstrating that the IRE1 nuclease can engage in two modes of RNase activities, with or without the subsequent RNA ligation. Furthermore, using a combination of pharmacological and genetic means, we are able to specifically differentiate between these two distinct nuclease modes, allowing us specifically activate either XBP1 splicing or ER localized mRNA cleavage without activating the other. Furthermore, IRE1 mediated ER localized RNA cleavage is evolutionarily conserved since we found that it occurs with yeast IRE1 both *in vivo* and *in vitro*. Finally, we show that an IRE1specific RNase inhibitor, irestatin, is able to block ER localized RNA cleavage if IRE1's nuclease was activated via its kinase domain. Activation of XBP1 splicing has been correlated with survival during the UPR, while decrease in ER localized RNAs was proposed to correlate with UPR-induced cell death. Both the direct involvement and the pharmacological ability to distinguish two IRE1 RNase modes present a unique opportunity for development of new therapeutic strategies against human diseases caused by deregulation of IRE1.

INTRODUCTION

When the folding demand on the ER exceeds capacity, a signaling pathway called the unfolded protein response (UPR) is activated and responds by activating several transcription factors that result in activation of a transcriptional profile that increases the folding capacity of the ER to re-establish ER function. However, if ER homeostasis cannot be achieved, the UPR triggers cell fate decisions leading to apoptosis. IRE1 is an evolutionarily conserved component of the UPR and is present from yeast to humans. While higher eukaryotes posses other ER stress sensors such as PERK and ATF6, the UPR only consists of IRE1 in yeast.

IRE contains an ER luminal domain that senses the presence of unfolded proteins and oligomerizes upon ER stress (Aragon et al., Nature 2009; Credle et al., PNAS 2005). The cytoplasmic region of IRE1 contains both kinase and nuclease domains. Oligomerization of the luminal domains results in juxtaposition of the cytosolic domains allowing for trans-autophosphorylation between separate IRE1 dimers (Korennykh et al., Nature 2009). This activates the RNase activity of the nuclease domain where it initiates splicing of a cytosolic mRNA encoding for a bZIP transcription factor, Hac1 in yeast and XBP1 in higher eukaryotes. Yeast IREp (yIRE) cleaves Hac1 at two splice sites containing stem loops structures. Excision of a 252nt intron and subsequent ligation by tRNA ligase results in a spliced form of Hac1 RNA, which when translated, is an active transcripton factor. IRE1α in mammalian cells cleave XBP1 at two splice sites also containing stem loop structures. This results in excision of a 26nt intron and a shift in the reading frame resulting in translation of spliced XBP1 containing a trans activation domain, making spliced XBP1 a potent transcription factor. Genes upregulated by these transcription factors bind to a UPR responsive element located in promoters of target genes that increase ER folding capacity (Acosta-Alvear et al., Mol Cell 2007).

Besides trans-autophosphorylation activated by ER stress, other means of activating IRE1 have been discovered. This was initially determined by a mutation of IRE1 which expands the

kinase pocket and prevents ATP binding. However, addition of 1NM-PP1, a small adenine homologue with no sugar and phosphates moieties molecule that fits into the new pocket but lacks phosphotransfer activity, was able to activate Hac1 splicing (Papa et al., Science 2003), suggesting that engagement of the kinase pocket, but not ability to transfer phosphate, is sufficient to activate IRE1's splicing ability. Consistent with this, kinase inhibitors that are able to bind in the kinase pocket also result in activation of the nuclease domain (Korennykh et al., Nature 2009). These suggest that the structural conformation of IRE1 with a bound kinase pocket corresponds to an active nuclease domain.

Recently, Quercetin (Qr), a naturally occurring flavanol, was identified as an activator of IRE1 (Wiseman et al., Mol Cell 2010). Qr binds to a novel pocket in the protein called the Q-Site which is formed in the interface between two monomers. Quercetin was proposed to activate IRE1 by stabilizing dimer formation which was found to be a prerequisite for nuclease activity (Lee et al., Cell 2008). A kinase dead mutant of IRE1, which is also RNase inactive, is RNase active with Qr treatment (Wiseman et al., Mol Cell 2010) indicating that activation of IRE1 by Qr bypasses the requirement for kinase activation. This allows for a pharmacological means of uncoupling the requirement of kinase activation with nuclease activation. Consequently, Quercetin allows for targeted activation of IRE1 instead of the entire UPR.

Recent reports have demonstrated evidence that mRNAs localized to the ER are degraded during the UPR in drosophila and mammalian cells (Hollien et al., JCB 2009; Hollien et al., Science 2006; Han et al., Cell 2009). This degradation of ER localized mRNAs seems to occur in parallel with XBP1 splicing, and this activity is abolished in cells lacking IRE1 but not XBP1, suggesting IRE1 as a key component (Han et al., Cell 2009). ER localized mRNA degradation is separable from XBP1 splicing since expression of the IRE1 mutant with the extended kinase pocket in conjunction with its ligand, 1NM-PP1, resulted in only XBP1 splicing, but not degradation of ER localized RNA (Hollien et al., JCB 2009; Han et al., Cell 2010), suggesting

that an active IRE1 kinase is required for ER localized RNA decay. Furthermore, immunoprecipitated IRE1 from mammalian cells was able to cleave insulin RNA, a target of ER localized mRNA decay, in a cell free system (Han et al., Cell 2009), demonstrating that ER localized RNAs are endonucleolytically cleaved, possibly by IRE1. However, since IRE1 is known to associate with multiple cellular proteins, the exact identity of the endoribonulcease that cleaves ER localized RNA during ER stress has been a subject of heated debate.

Using an *in vitro* RNase reaction of IRE1, we show direct evidence that IRE1 is able to cleave ER localized mRNAs. Furthermore, IRE1 does not cleave actin mRNA, a non-ER localized RNA coding for a soluble cytosolic protein. These experiments have revealed IRE1 involvement in two modes of RNase activities: XBP1 RNA cleavage followed by ligation of cleaved RNA fragments and cleavage of ER-associated RNA without ligation. Furthermore, we show that yeast IRE1 is able to cleave ER localized RNA, indicating evolutionary conservation of this activity. Furthermore, using pharmacological methods, we are able to modulate the two distinct modes of IRE1 activation by activating only Hac1/XBP1 splicing or ER localized mRNA decay alone, without activating the other. The correlation of the separate activities to cell fate has implications in their role in cellular physiology, so determining contributions of each activity would lead to more effective treatments to IRE1 related diseases.

RESULTS

To determine if IRE1 is in fact the nuclease that carries out cleavage of ER localized mRNAs, we incubated *in vitro* transcribed ER localized mRNAs with baculovirally expressed recombinant human IRE1 (hIRE1) containing the cytoplasmic kinase and RNase portion of IRE1. Similar in vitro IRE1 nuclease reactions have been used to examine IRE1 cleavage of either XBP1 or HAC1 mRNA (Sidrauski et al., Cell 1996). We prepared a uniformly radiolabelled ER localized RNA substrate, Blos1 coding for a membrane protein. We found that the intact full-

length *BLOS1* RNA generated cleaved RNA fragments when incubated with hIRE1 (Fig. 1A: lane2). Similarly, we found that Insulin RNA was also cleaved upon IRE1 addition to the reaction. Thus, results of these experiments demonstrated directly that Ire1 can cleave ER localized RNA. It should be noted that the cleavage efficiency was not as robust as the reaction previously reported with immunoprecipitated IRE1 (Han et al., Cell 2009), suggesting the presence of an additional component(s) or associated factors of hIRE1 for enhancement of cleavage activity.

IRE1 is conserved among all the eukaryotes including yeast, and to date, all the features of the hIRE1 RNase reaction with human *XBP1* RNA are well-conserved with yeast IRE1 cleaving *HAC1* RNA. In fact, yIRE1 can cleave XBP1 RNA. Therefore, we wanted to test if yeast IRE1 (yIRE1) is also able to cleave ER localized mRNAs. To this end, we performed *in vitro* nuclease assays using purified recombinant yIRE1 containing both kinase and RNase domains with radiolabelled Blos1 mRNA and we found that yIRE1 was able to cleave Blos1 mRNA even more efficiently than hIRE1 (Fig. 1B: lane2). Similarly, We also tested yIRE1 cleavage of another mammalian target, mouse Insulin2 (mIns2) (Fig. 1B: lane7). The ability of yeast IRE1 to cleave mammalian ER localized RNA points that the decrease in ER-associated RNA during the UPR is also conserved in yeast and that yeast Ire1 can directly cleave ER associated RNA. Thus, we wanted to determine if yIRE1 can cleave a yeast ER localized RNA target. Previous microarray experiments have identified the UPR-induced down-regulation does take place in yeast (Gasch et al., Mol Biol Cell 2000). Thus, we picked and tested DPAPB and alpha Factor, yeast mRNAs localized to the ER and found to be downregulated during ER stress. We found that yIRE1 was also able to cleave these targets which resulted in more cleaved fragments than the mammalian RNA targets (Fig. 1C: lanes2 and 7). However, RNA coding for actin, a cytoplasmic protein, was not cleaved by yIRE1 in vitro (Fig. 1D: lane2), demonstrating that yeast

IRE1 specifically cleaves ER localized mRNAs. This indicates an intrinsic specificity for IRE1 which can differentially degrade an ER associated RNA, but not cytosolic mRNAs.

IRE1 dependent cleavage of *HAC1* or *XBP1* RNA has been shown to require activation of the kinase domain. Thus, we wanted to test if ER localized RNA cleavage requires the kinase domain activity. In order to test this, we first turned to a recent report showing that Quercetin (Qr) can activate IRE1 dependent cleavage for *HAC1* (or *XBP1*) mRNA. Thus, Qr presents us with a unique means of activating IRE1 which is independent of IRE1 kinase activation (Wiseman et al., Mol Cell 2010). Thus, we wanted to use Quercetin to achieve activation of IRE1's nuclease without kinase domain activation to test its effects on ER localized RNA cleavage. Quercetin was able to activate cleavage of Hac1 and XBP1 similar to ADP activation (Fig. 1E: lane5, 1F). In our *in vitro h*IRE1 reaction, we incubated ER localized RNA with Qr instead of ADP, and found that Qr activated hIre1 could cleave the ER localized RNA Blos1. (Fig. 1A: lane3). Similarly, we found that Qr-activated yeast Ire1 cleaved ER localized RNA cleavage (Fig. 1B & 1C: lanes3,8). In addition, Actin mRNA was not cleaved by Quercetin activated yIRE1 (Fig. 1D: lane3), demonstrating the specificity of Qr-induced Ire1 ER localized RNA cleavage. Taken together, these data indicate that IRE1 is the nuclease that cleaves ER localized mRNAs during UPR, and Quercetin activation results in similar ER localized mRNA cleavage by IRE1 as activation through the kinase domain.

To further examine the involvement of the kinase domain function for the Ire1 ER localized RNA cleavage reaction, we generated a D828A kinase dead mutant Ire1 containing an amino acid substitution at D828, which allows for binding of nucleotide to the kinase pocket, but prevents transfer of phosphate of ATP since the active site Asp residue needed to chelate the Mg2+ ion is missing. We have reported previously that Ire1-D828A was able to bind to nucleotide but not transfer phosphate, and that UPR activation of HAC1 RNA splicing did take place, although it is defective in terminating Ire1 RNase once activated *in vivo* (Chalwa, et al.,

2011). In an in vitro reaction, Ire1-D828A was able to cleave HAC1 RNA when activated by ADP, in an equivalent manner as WT (Fig. 1E). We tested Hac1 cleavage by D828A activated by Quercetin, we found that Hac1 was cleaved in a similar manner as ADP activation (Fig. 1E). Since both ADP and Quercetin can activate Hac1 cleavage in the D828A mutant, these results suggest that either nucleotide binding at the kinase pocket or binding of Qr at the Q-Stie, but not phosphorylation, is required for HAC1 RNA cleavage.

We then looked at how ADP and Quercetin activation affected ER localized RNA cleavage in the D828A mutant. When we activated D828A with ADP and looked at ER localized mRNA cleavage, we found that cleavage was severely reduced in the D828A as compared to wild type IRE1 (Fig. 1B: lanes4,9; Fig. 1C: lanes4,9). This result is consistent with the proposal that ER localized RNA cleavage requires an active kinase that can transfer phosphate. However, when we treat with Quercetin, we found that ER localized RNA cleavage activity was equivalent to wild type levels (Fig. 1B: lanes 5,10; Fig. 1C: lanes5,10). This indicates that Quercetin activation of D828A mutant IRE1 bypasses the requirement for the kinase and can activate ER-RNA cleavage, regardless of kinase function.

In addition, we also examined the effect of Quercetin activation for ER localized RNA cleavage in vivo using mouse embryonic fibroblasts (MEFs). We treated MEFs with either thapaisgargin (Tg), an agent that causes ER stress by disturbing calcium levels in the ER, or Quercetin. We found strong XBP1 cleavage with Tg treatement, also, we find that Qr is able to activate XBP1 splicing at a moderate level (Fig. 2A). When we looked at ER localized mRNA decay activity, we found that Blos1 and Scara3, two mRNAs identified as ER localized mRNA decay targets in MEFs (Hollien et al., JCB 2009), were significantly decreased when treated with both Tg and Qr (Fig. 2B). Furthermore, the decrease in mRNA levels correlate with XBP1 splicing activity for both Tg and Qr treatment. BiP expression, a gene upregulated during the UPR, was significantly upregulated by Tg, however, Qr activation resulted in a mild increase in

BiP expression (Fig. 2B). These data showing Quercetin activation of XBP1 and ER localized mRNA decay in mammalian cells is consistent with our in vitro data. We then tested this effect in yeast cells. However, while Tm was able to efficiently activate Hac1 splicing branch of the UPR (Fig 2C), Qr was not able to significantly increase Hac1 splicing (Fig. 2C) presumably through an accessibility issue of Qr in yeast. However, we found that Tm treatment results in a dramatic decrease in both DPAPB and α-Factor mRNA levels (Fig. 2D), consistent with the in vitro cleavage by IRE1, indicating that ER localized mRNA decay also occurs in yeast during UPR activation.

Previously we have shown that an IRE1 RNase inhibitor, irestatin, blocks splicing of XBP1 *in vivo*, and cleavage of XBP1 RNA *in vitro* (Panandreou et al., Blood 2010). We also found that irestatin was able to inhibit the kinase activity of yIRE1 but not hIRE1 (Fig. 3A and 1B). Irestatin was able to inhibit XBP1 splicing when activated by ER stress (Fig. 3D), similar to previous reports (Papandreou et al., Blood 2010). Irestatin was also able to inhibit Hac1 splicing in yeast (Fig. 3C), indicating that Irestatin is a functional IRE1 inhibitor in both yeast and mammalian cells. To test Irestatin's effects on in vitro cleavage of Hac1, we added increasing concentrations of Irestatin to the reaction. Surprisingly, we found that irestatin exhibited differential inhibition of the 5' and 3' splice sites of Hac1 (Fig. 4A). This result has profound implications on the catalytic mechanism of IRE1 cleavage which we are reporting in a separate study. Taken together, Irestatin is able to inhibit ER stress induced XBP1 splicing through Tg and ATP/ADP activation.

Since we found that bypassing the kinase requirement of IRE1 through Quercetin activation is able to activate Hac1/XBP1 splicing and ER localized mRNA decay, we wanted to determine if Irestatin inhibits Quercetin activation of either activation mode. To this end, we started by determining Irestatin inhibition of Quercetin activated Hac1 cleavage in vitro. Upon addition of increasing amounts of Irestatin, we found a similar pattern of inhibition with ADP

activation, where only cleavage of the 5' splice site was inhibited (Fig. 4A: lanes7-11). This indicated that Irestatin inhibits ATP/ADP activation and bypassing the kinase requirement for activation using Quercetin resulted in similar inhibition. We also tested this effect in cells by adding Quercetin to induce XBP1 splicing which resulted in a modest BiP induction (Fig. 5B). Also addition of Irestatin inhibited both XBP1 splicing and BiP induction. This indicates that Irestatin is able to inhibit Quercetin activation of Hac1/XBP1 splicing.

We then wanted to determine Irestatin's effects on ER localized mRNA decay activated by either ER stress/ATP or Quercetin in vitro and in cells. To test inhibition in vitro, we activated yIRE1 with ADP and added increasing amounts of Irestatin to the reaction. We found that Irestatin inhibits ER localized mRNA degradation by IRE1 (Fig. 4B: lanes 1-5; 4C: lanes1-3; 4D: lanes1-5). To test inhibition in cells, we treated MEFs with Tg to induce UPR which activated both XBP1 splicing and ER localized mRNA decay and added Irestatin. We found that Irestatin was able to inhibit decrease in Blos1 and Scara3 mRNA, indicating inhibition of ER localized mRNA decay activity (Fig. 5C). Taken together, Irestatin is able to inhibit both XBP1 splicing and ER localized mRNA decay through ATP/ADP or ER stress activation.

However, when we looked at Irestatin's effects on Quercetin activated ER localized mRNA decay in vitro, interestingly, we found that Irestatin was not able to inhibit Quercetin activated ER localized mRNA decay for ER localized mRNAs (Fig. 4B: lanes6-10; 4C: lanes4-6; 4D: lanes6-10). This was surprising since this indicated that Iresatin can sense whether IRE1 was activated through the kinase domain or not. To show this effect in cells, we treated MEFs with Quercetin to induce ER localized mRNA decay as seen by decrease in RNA levels of Blos1 and Scara3. However, when we inhibited with Irestatin, we did not see a change in Blos1 and Scara3 levels (Fig. 5D). This indicated that Irestatin was unable to inhibit ER localized mRNA decay activity however, it can inhibit XBP1 splicing in cells. This finding allows for

pharmacological manipulation of IRE1's separate nuclease activities since activation of ER localized mRNA decay can be achieved without splicing of XBP1.

DISCUSSION

IRE1 is a critical component of the ER stress response since it has been linked to several cellular pathways. Part of its versatility comes from its unique structural design which allows for multiple modes of activation. For example, its kinase domain is able to bind to factors such as TRAF2 to activate pathways such as JNK (Urano et al., Science 2000), independent of its nuclease activity. Furthermore, its nuclease activity seems to display at least two modes, one which initiates precise splicing of Hac1/XBP1, and another that cleaves ER localized mRNAs. In addition, chemical-genetic manipulation of the kinase domain of IRE1 has suggested that these activities are separable (Hollien et al., JCB 2009; Han et al., Cell 2009). Here, we show that separation of these nuclease activities of IRE1 can be achieved through pharmacological means, making IRE1 a more viable therapeutic target for specific regulation. Degradation of ER localized mRNAs by IRE1 without splicing of XBP1 can be achieved by activation with Quercetin and inhibition by Irestatin. Furthermore, activation of only XBP1 splicing without activation of ER localized mRNA decay can theoretically be achieved by kinase inhibitors which bind to the kinase pocket. This condition is similar to the chemical-genetic system with an extended kinase pocket bound by its new ligand, 1NM-PP1, or our genetic system, the D828A mutant, which allows for ATP/ADP binding but no phosphotransfer activity. These conditions have been shown to specifically activate Hac1/XBP1 cleavage, but not ER localized mRNA decay. Designing molecules similar in structure to pocket binding kinase inhibitors, but tailored for IRE1's kinase pocket would allow for IRE1 specific activation without affecting other kinases. This method of specifically activating the XBP1 pathway only without activating ER

localized mRNA decay, can be substituted for the current genetic or chemical-genetic systems which would require gene therapy to be developed as a treatment to IRE1 related diseases.

Furthermore, we show that yeast IRE1 is able to induce ER localized mRNA decay both in vitro and in vivo, indicating that this function of IRE1 is also conserved. However, we see differences in efficiency between yeast and human IRE1. One explanation is that another factor is required to stabilize human IRE1 in order to efficiently activate ER localized mRNA decay activity. Unilke yeast IRE1, mammalian IRE1 has been found to bind to several proteins which have been shown to regulate IRE1's activity. For example, BAX/BAK has been found to associate with IRE1 and cells lacking BAX/BAK are defective in IRE1 activity (Hetz et al., Science 2006). Also Hsp90, a chaperone, has been found to stabilize IRE1 structure, and inhibition of Hsp90 activity decreases stability of IRE1 (Marcu et al., MCB 2002). Our in vitro reactions using human IRE1 were not as efficient as yeast IRE1 suggesting that immunoprecipitated mammalian IRE1 may contain associated factors that stabilize its structure and increases its efficiency in cleaving ER localized mRNAs (Han et al., Cell 2009). In this manner, our in vitro system may be used to determine factors that affect IRE1 function by addition of those proteins.

The ability to differentially activate ER localized mRNA decay without activating XBP1/Hac1 splicing may provide a mechanism to differentially influence cell fate. In mammalian UPR, sustained activation of IRE1 resulting in sustained XBP1 splicing has been shown to enhance cell survival using a chemical-genetic system (Lin et al., Science 2007), conversely activation of ER localized mRNA decay has been correlated with enhanced cell death (Han et al., Cell 2009). Here we show that we can specifically activate ER localized mRNA decay and not Hac1/XBP1 splicing through pharmacological means which is proposed to result in enhanced cell death. A more potent effect driving cells towards apoptosis could be achieved with

combinatorial treatment of irestatin and quercetin which inhibits survival by inhibiting the XBP1 pathway, and also enhances cell death by leaving ER localized mRNA decay activity intact.

MATERIALS AND METHODS

Constructs and Cloning

Hac1 508 substrate (pCF187) was used from Sidrauski et al (1997). XBP1 444 substrate was made by amplification of cDNA using a forward primer with a T7 promoter. (F) TAATACGACTCACTATAGGGAGAAGAACCAGGAGTTAAGACAGCGC; (R) TAAGACTAGGGGCTTGGTATATATGTG. Templates for ER associated mRNAs were amplified from either mouse cDNA or yeast genomic DNA. Primers contained a T7 promoter and Kpn1 and Sac1 restriction sites for integration into plasmids. Primers are: mouse Insulin2: (F) ATGGTACCTAATACGACTCACTATAGGAAAGCCCTAAGTGATCCGCTACAATC; (R) ATGAGCTCCTCATTCAAAGGTTTTATTCATTGCAG; Blos1: (F) ATGGTACCTAATACGACTCACTATAGGATGCTGTCCCGCCTGC, (R) ATGAGCTCCTAGGATGGTGCAGACTGCAG; DPAPB: (F) ATGGTACCTAATACGACTCACTATAGGGCAGAAAAATGCGACAAAGG; (R) ATGAGCTCTTGAAATGTCTTCCGCCATC.

In vitro Nuclease Assay

In vitro transcription of the ^{32}P labeled Hac1 508 substrate has been described previously (Sidrauski, 1997). For the nuclease assay, hIRE1 or yIRE1 protein (1μg) was incubated with the indicated amount of Irestatin, Quercetin, or DMSO in the nuclease reaction mix: Kinase buffer (100mM Hepes, 50mM MgAcetate, 250mM KOAc, 10mM DTT), RNAse out (Invitrogen), 2mM ADP), and 20,000 cpm of ^{32}P labeled substrates. The reaction was incubated for 30 min at 30°C

or for the indicated amount of time. After, the RNA was extracted with phenol/chloroform, ethanol precipitated and analyzed on a denaturing 6% Urea acrylamide gel. Bands were visualized by autoradiography.

In vitro Kinase Assay

Purified hIRE1 or yIRE1 protein (1μg) was incubated with 5 μCi of ^{32}P-γATP in Kinase Buffer (100mM Hepes, 50mM MgAcetate, 250mM KOAc, 10mM DTT). Irestatin, Irestatin-A, Irestatin-S, or DMSO was also added to the reaction. Samples were incubated for 30 min at 30°C then ran on a 7% SDS-PAGE gel. Autoradiography was used to determine amount of ^{32}P-γATP incorporated.

Cell culture and treatment

MEFs were cultured in DMEM media (Cellgro). All media was supplemented with 10% fetal calf serum (Gibco), 100 U/ml penicillin, and 100ug/ml streptomycin (Mediatech). Cells were grown in 5% CO_2 at 37°C. Cells were treated with 200 nM thapsigargin (Calbiochem), 400μM Quercetin (Sigma), or 60 μM Irestatin for the indicated amount of time.

Northern Blots

Northern blots were performed as previously described (Sidrauski et al., 1997).

RNA extraction, RT, and quantitative PCR

Total RNA was prepared using Trizol (Invitrogen) and treated with RNase free DNase (Promega) according to manufacturer's instructions. One microgram of total RNA was then reverse transcribed using ThermoScript reverse transcriptase (Invitrogen) according to manufacturer's instructions to obtain cDNA. XBP1 splicing was determined as previously described (Durose et al., 2006). For quantitative PCR, 5 ng of input cDNA was analyzed in

triplicate per sample for each primer pair. All reactions were performed using SYBR Green PCR Master Mix (Applied Biosystems) and 400nM of each primer per reaction in a total volume of 25 µl. The reaction was performed using default cycling parameters on an ABI Prism 7200 Sequence Detector. A standard curve composed of five-fold serial dilutions of concentrated cDNA was included in each qPCR run for each primer. Since the SYBR Green system is used, it is important to have a single product being amplified so a melting curve analysis was performed after each run to confirm amplification of a single product. Expression of each gene was normalized to 18S and expressed as fold induction. Values are mean±s.e.m of at least three independent experiments. Primers used for qPCR were from Hollien et al. (2009).

REFERENCES

Acosta-Alvear, D., Zhou, Y., Blais, A., Tsikitis, M., Lents, N.H., Arias, C., Lennon, C.J., Kluger, Y., and Dynlacht, B.D. (2007). XBP1 controls diverse cell type- and condition-specific transcriptional regulatory networks. Mol Cell *27*, 53-66.

Aragon, T., van Anken, E., Pincus, D., Serafimova, I.M., Korennykh, A.V., Rubio, C.A., and Walter, P. (2009). Messenger RNA targeting to endoplasmic reticulum stress signalling sites. Nature *457*, 736-740.

Brunsing, R., Omori, S.A., Weber, F., Bicknell, A., Friend, L., Rickert, R., and Niwa, M. (2008). B- and T-cell development both involve activity of the unfolded protein response pathway. J Biol Chem *283*, 17954-17961.

Credle, J.J., Finer-Moore, J.S., Papa, F.R., Stroud, R.M., and Walter, P. (2005). On the mechanism of sensing unfolded protein in the endoplasmic reticulum. Proc Natl Acad Sci U S A *102*, 18773-18784.

Gasch, A.P., Spellman, P.T., Kao, C.M., Carmel-Harel, O., Eisen, M.B., Storz, G., Botstein, D., and Brown, P.O. (2000). Genomic expression programs in the response of yeast cells to environmental changes. Mol Biol Cell *11*, 4241-4257.

Han, D., Lerner, A.G., Vande Walle, L., Upton, J.P., Xu, W., Hagen, A., Backes, B.J., Oakes, S.A., and Papa, F.R. (2009). IRE1alpha kinase activation modes control alternate endoribonuclease outputs to determine divergent cell fates. Cell *138*, 562-575.

Hetz, C., Bernasconi, P., Fisher, J., Lee, A.H., Bassik, M.C., Antonsson, B., Brandt, G.S., Iwakoshi, N.N., Schinzel, A., Glimcher, L.H., and Korsmeyer, S.J. (2006). Proapoptotic BAX and BAK modulate the unfolded protein response by a direct interaction with IRE1alpha. Science *312*, 572-576.

Hetz, C., and Glimcher, L.H. (2009). Fine-tuning of the unfolded protein response: Assembling the IRE1alpha interactome. Mol Cell *35*, 551-561.

Hollien, J., Lin, J.H., Li, H., Stevens, N., Walter, P., and Weissman, J.S. (2009). Regulated Ire1-dependent decay of messenger RNAs in mammalian cells. J Cell Biol *186*, 323-331.

Hollien, J., and Weissman, J.S. (2006). Decay of endoplasmic reticulum-localized mRNAs during the unfolded protein response. Science *313*, 104-107.

Korennykh, A.V., Egea, P.F., Korostelev, A.A., Finer-Moore, J., Zhang, C., Shokat, K.M., Stroud, R.M., and Walter, P. (2009). The unfolded protein response signals through high-order assembly of Ire1. Nature *457*, 687-693.

Lin, J.H., Li, H., Yasumura, D., Cohen, H.R., Zhang, C., Panning, B., Shokat, K.M., Lavail, M.M., and Walter, P. (2007). IRE1 signaling affects cell fate during the unfolded protein response. Science *318*, 944-949.

Marcu, M.G., Doyle, M., Bertolotti, A., Ron, D., Hendershot, L., and Neckers, L. (2002). Heat shock protein 90 modulates the unfolded protein response by stabilizing IRE1alpha. Mol Cell Biol *22*, 8506-8513.

Papa, F.R., Zhang, C., Shokat, K., and Walter, P. (2003). Bypassing a kinase activity with an ATP-competitive drug. Science *302*, 1533-1537.

Papandreou, I., Denko, N.C., Olson, M., Van Melckebeke, H., Lust, S., Tam, A., Solow-Cordero, D.E., Bouley, D.M., Offner, F., Niwa, M., and Koong, A.C. Identification of an Ire1alpha endonuclease specific inhibitor with cytotoxic activity against human multiple myeloma. Blood.

Romero-Ramirez, L., Cao, H., Nelson, D., Hammond, E., Lee, A.H., Yoshida, H., Mori, K., Glimcher, L.H., Denko, N.C., Giaccia, A.J., Le, Q.T., and Koong, A.C. (2004). XBP1 is essential for survival under hypoxic conditions and is required for tumor growth. Cancer Res *64*, 5943-5947.

Rutkowski, D.T., and Hegde, R.S. Regulation of basal cellular physiology by the homeostatic unfolded protein response. J Cell Biol *189*, 783-794.

Sidrauski, C., and Walter, P. (1997). The transmembrane kinase Ire1p is a site-specific endonuclease that initiates mRNA splicing in the unfolded protein response. Cell *90*, 1031-1039.

Urano, F., Wang, X., Bertolotti, A., Zhang, Y., Chung, P., Harding, H.P., and Ron, D. (2000). Coupling of stress in the ER to activation of JNK protein kinases by transmembrane protein kinase IRE1. Science *287*, 664-666.

Wiseman, R.L., Zhang, Y., Lee, K.P., Harding, H.P., Haynes, C.M., Price, J., Sicheri, F., and Ron, D. Flavonol activation defines an unanticipated ligand-binding site in the kinase-RNase domain of IRE1. Mol Cell *38*, 291-304.

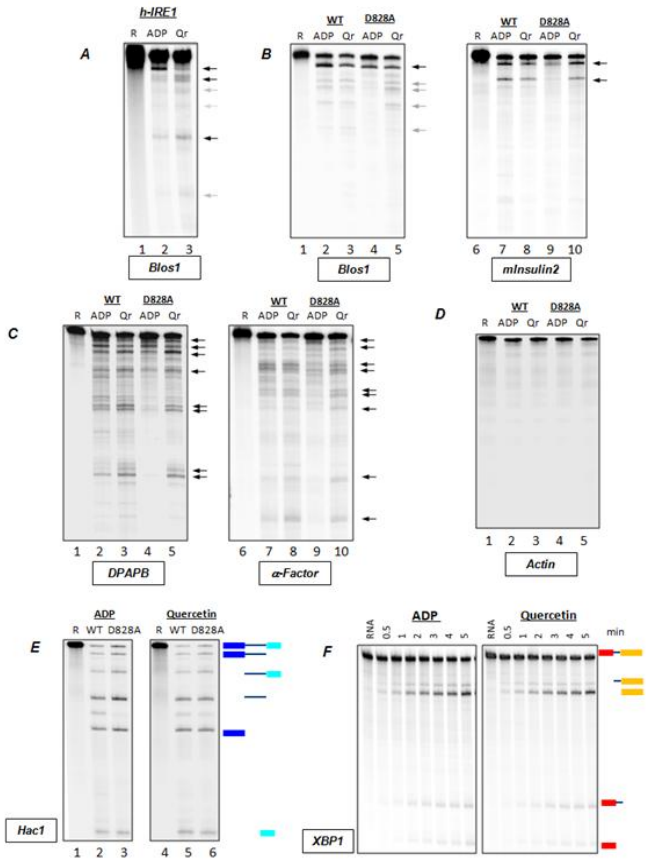

Figure 1. In vitro reconstitution of ER localized mRNA decay activity in yIRE1p.

(A) Human IRE1α shows ER localized mRNA decay activity in vitro. Human IRE1 was incubated with radiolabelled Blos1 mRNA. Cleavage fragments are indicated as arrows.
(B) Yeast IRE1 can cleave mammalian targets with ER localized mRNA decay activity. Either WT or D828A yIRE1 were incubated with either ADP or Qr and Blos1 or mouse Insulin2 radiolabelled RNA. Cleavage fragments are indicated as arrows.
(C) The D828A mutant of Hac1 does not efficiently activate ER localized mRNA decay when activated by ADP, but quercetin efficiently activates ER localized mRNA decay. Either WT or D828A yIRE1 was incubated with ADP or Qr and radiolabelled DPAPB or alpha Factor RNA. Cleavage fragments of the RNA are indicated (arrows).
(D) yIRE1 does not cleave actin RNA. Either WT or D828A yIRE1 was incubated with either ADP or Qr and radiolabelled yeast actin RNA. Neither WT nor D828A IRE1 resulted in cleavage of actin RNA.
(E) ADP and quercetin (Qr) activate Hac1 cleavage of WT or D828A IRE1 equally. Either WT yeast IRE (yIRE1) or D828A, a kinase dead mutant of IRE1, incubated with either ADP or Qr and radiolabelled Hac1. Hac1 is cleaved at two splice sites, the 5' splice site (ss) or 3'ss resulting in a characterized cleavage pattern (Sidrauski et al., Cell 1997) corresponding to intermediates and final cleavage products of Hac1 (blue schematic).
(F) Human IRE1α cleaves XBP1 RNA in vitro activated by ADP and quercetin. Human IRE1 was activated by either ADP or quercetin and incubated with radiolabelled XBP1 RNA. Cleavage fragments are indicated as an orange schematic.

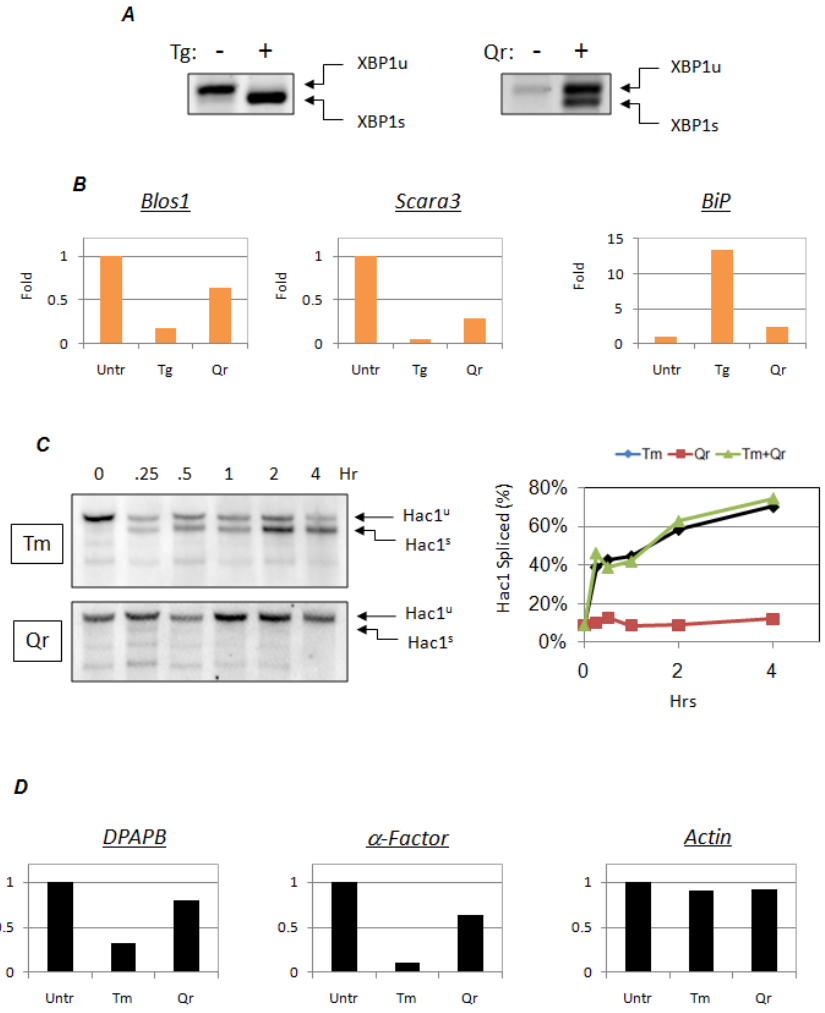

Figure 2. ER localized mRNA decay is active in yeast.
(A) Quercetin activates XBP1 splicing in MEFs. MEFs were treated with either thapsigargin (Tg) or quercetin for 6 hrs and RT-PCR was performed to determine level of XBP1 splicing. Both Tg and Qr induced splicing of XBP1.
(B) Quercetin activates ER localized mRNA decay in MEFs. MEFs were treated with Tg or Qr for 6 hrs. RT-qPCR was performed to determine RNA levels of Blos1 and Scara3, two RNA targets of ER localized mRNA decay activity. Both Tg and Qr show a significant decrease in RNA levels. BiP, a UPR target, was significantly upregulated by Tg, but only a small increase was seen with Qr activation.
(C) UPR activation in yeast; Qr does not splice Hac1. Yeast cells were treated with either tunicamycin (Tm) to induce the UPR, quercetin (Qr). Northern blots show Hac1 splicing by differentiating between the unspliced form (Hac1u) and the spliced form (Hac1s). Tm induces Hac1 splicing, however, quercetin does not. Quantitation is shown (right panel).
(D) DPABP and α–Factor mRNA levels decrease during UPR. Yeast cells were treated with either Tm or Qr. RNA was extracted and reverse transcribed, and quantitative real time PCR was performed. DPAPB and a-Factor RNA was significantly reduced during Tm treatment while only a very mild decrease was seen with quercetin treatment. Actin RNA levels did not change during treatment.

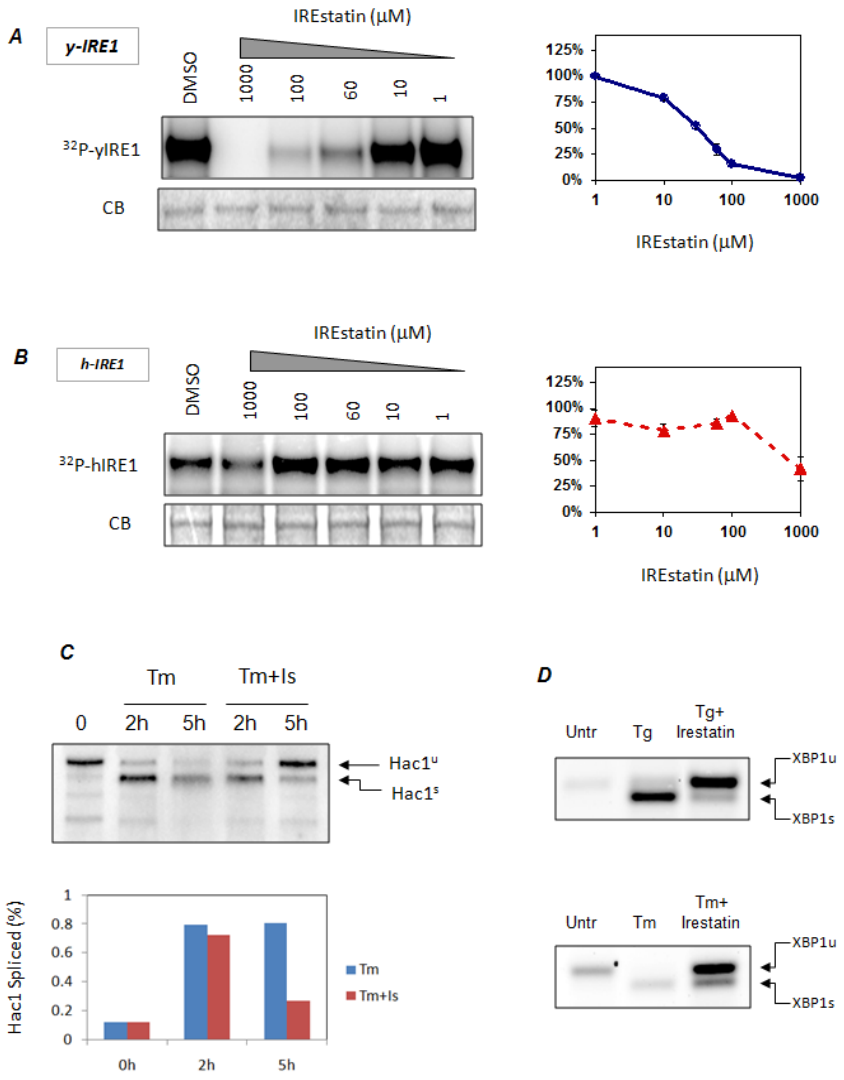

Figure 3. Characterization of Irestatin

A.) Irestatin inhibits kinase activity of yeast IRE1. To test for autophosphorylation, yIRE1 was incubated with gP32-ATP and run on as SDS-PAGE, and autoradiography determined levels of phosphorylated IRE1 (32P-yIRE1). Commassie Blue (CB) staining shows equal loading of protein.

B.) Irestatin does not inhibit kinase activity of human IRE1. hIRE1 was incublated with g-P32 ATP to test trans-autophosphorylation of IRE1. Samples were run on as SDS PAGE and kinase activity was determined by autoradiography. Commassie blue (CB) staining shows equal loading of protein.

C.) Irestatin inhibits UPR in yeast. Yeast was treated with Tm for either 2h or 5h with or without irestatin. Hac1 splicing was determined by northern blot. Addition of irestatin results in decreased Hac1 splicing at 5 hrs. Quantitation is shown (bottom panel).

D.) Irestatin inhibits UPR in MEFs. MEFs were treated with either Tg or Tm with or without irestatin. XBP1 splicing was determined by RT-PCR. Treatment with irestatin resulted in a reduction of XBP1 splicing.

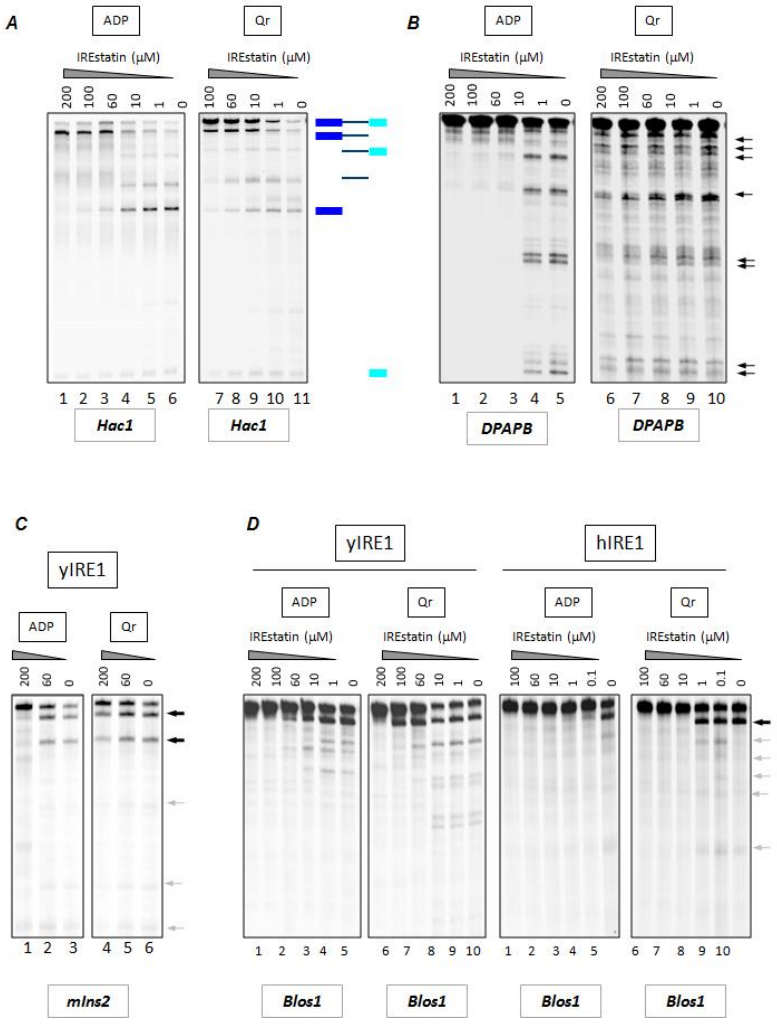

Figure 4. Differential inhibition of ER localized mRNA decay and Hac1 splicing by Irestatin.

(A) Irestatin inhibits ADP and Qr activation of yeast IRE1 equally. yIRE1 was activated by ADP or Qr and incubated with radiolabelled Hac1 RNA. Increasing amounts of irestatin was added to the reaction. Addition of irestatin resulted in differential inhibition of the 5' and 3' splice sites of Hac1 for both ADP and Qr activation, indicating equal inhibition by irestatin.

(B) Irestatin differentially inhibits ER localized mRNA decay. yIRE1 was activated by ADP or Qr and incubated with radiolabelled DPAPB RNA. Increasing concentrations of irestatin was added to the reaction. Irestatin shows strong inhibition of ER localized mRNA decay by ADP activated IRE1, however, activation of ER localized mRNA decay by Qr was minimally inhibited by irestatin.

(C) yIRE1 was activated by ADP or Qr and incubated with radiolabelled mouse Insulin 2 RNA. Increasing concentrations of irestatin was added to the reaction. Irestatin shows differential inhibition of ADP and Qr activation of ER localized mRNA decay.

(D) Irestatin differentially inhibits ER localized mRNA decay in yeast and human IRE1. Either yeast or human IRE1 was activated by either ADP or Qr, and incubated with radiolabelled Blos1 mRNA. Increasing amounts of irestatin was added to the reaction. For both yeast and human IRE1, irestatin showed stronger inhibition towards ADP activated IRE1 than Qr activated IRE1.

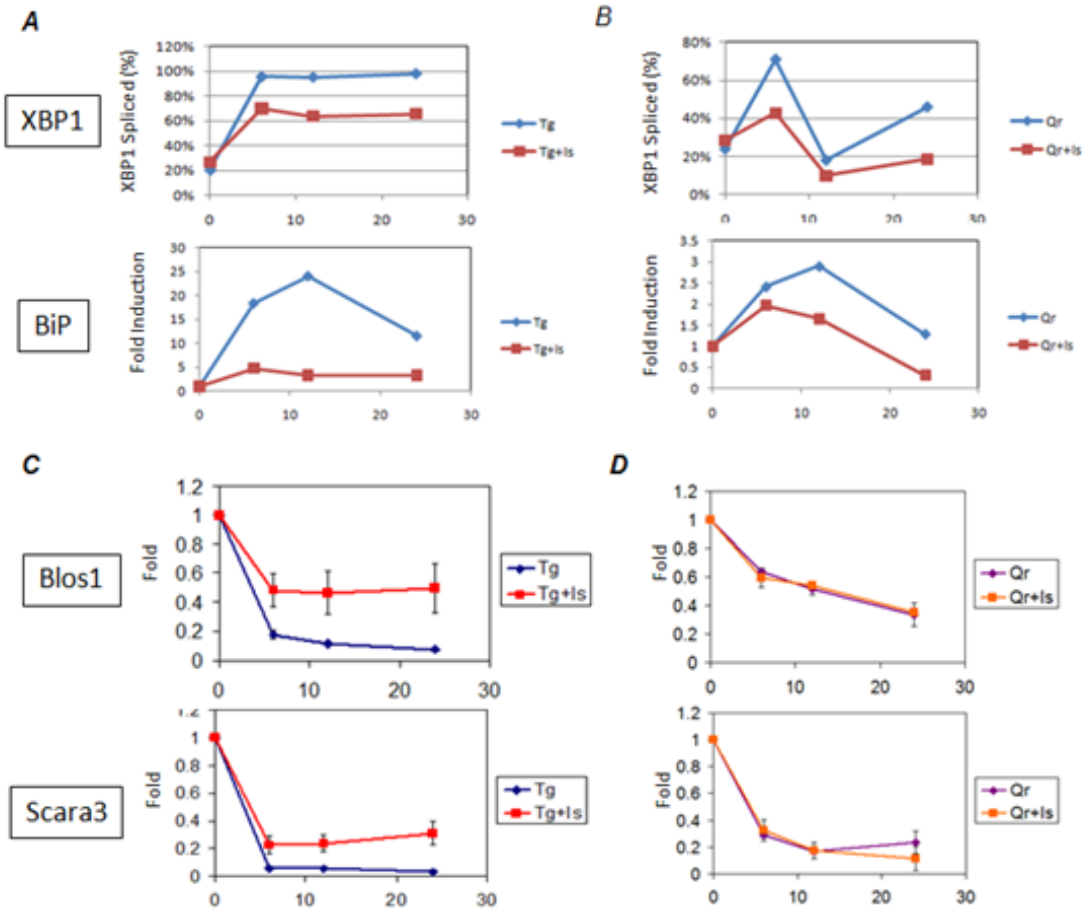

Figure 5. Differential inhibition of XBP1 splicing and ER localized mRNA decay by Irestatin in mammalian cells.

(A) Inhibition of XBP1 signaling during the UPR by irestatin. MEFs were treated with Tg with or without irestatin for up to 24 hours. XBP1 splicing was determined by RT-PCR, and BiP mRNA levels were determined by quantitative real time PCR. Addition of irestatin results in a decrease in both XBP1 splicing and BiP activation.

(B) Inhibition of XBP1 signaling from quercetin activation of IRE1 by irestatin. MEFs were treated with Qr for up to 24 hours and XBP1 splicing and BiP mRNA levels were determined. Both XBP1 splicing and BiP activation were activated with quercetin activation, but at a lower level than Tg treatment. Addition of irestatin resulted in a decrease in both XBP1 splicing and BiP activation.

(C) Inhibition of UPR activated ER localized mRNA decay by irestatin. MEFs were treated with Tg for up to 24 hours and mRNA levels of Blos1 and Scara3 were determined by real time qPCR. Tg treatment of cells resulted in a significant decrease in both Blos1 and Scara3 mRNA demonstrating activation of ER localized mRNA decay. Addition of irestatin resulted in inhibition of ER localized mRNA decay since a reduction of both Blos1 and Scara3 mRNA was seen.

(D) Irestatin does not inhibit ER localized mRNA decay activated by quercetin. MEFs were treated with Qr for up to 24 hours and mRNA levels of Blos1 and Scars3 were determined by real time qPCR. Reduction of both mRNAs were seen with Qr activation, however, addition of irestatin did not inhibit the decrease of mRNA.

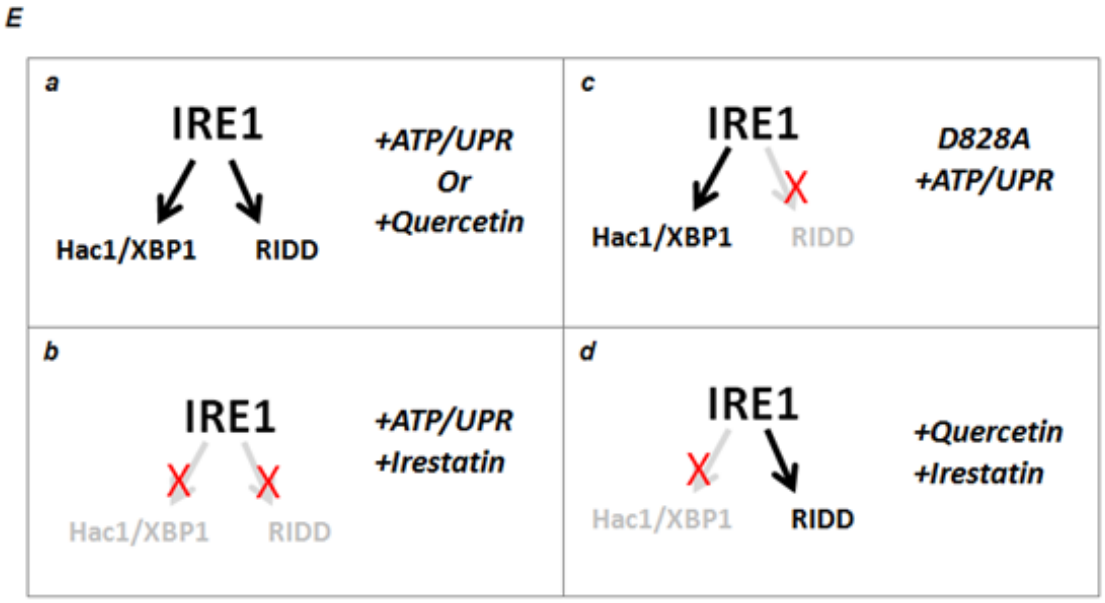

Figure 5. Continued

(E) Manipulation of IRE1's nuclease activities. a) Both UPR/ATP activation and Quercetin treatment is able to activate both the Hac1/XBP1 splicing and ER localized mRNA decay activities of IRE1. b) Irestatin inhibits both Hac1/XBP1 splicing and ER localized mRNA decay activities when activated by UPR/ATP. c) Specific activation of only Hac1/XBP1 splicing but not ER localized mRNA decay can be achieved by the D828A mutant of yIRE1 when activated with UPR/ATP. d) Activation of only ER localized mRNA decay but not Hac1/XBP1 can be achieved by activation with Quercetin and inhibition by irestatin.

Chapter 5

DISCUSSION

Manipulating IRE1 Functions to Study Physiology and Disease

Ever since its discovery, the UPR has been implicated in the pathology of certain diseases. In particular, IRE1 has been found to be a major player in the progression of diabetes and cancer. In light of our findings, we now have the tools to tease apart the individual contributions of XBP1 splicing versus ER localized mRNA decay which may be playing opposite roles in determining cell fate. Among the different signals from the UPR, XBP1 splicing has been implicated in activities that promote cell survival since its main functions are to upregulate ER chaperones and increase ER size. Furthermore, the function of ER localized mRNA decay is thought to be detrimental to the cell, and may perhaps be a temporary solution to increased ER load, but prolonged degradation of ER localized mRNA decay presumably results in a drastic decrease in secretory and membrane proteins. Therefore, it would be interesting to determine the relative kinetics of XBP1 splicing versus ER localized mRNA decay. It has been shown that prolonged ER stress activated all three components, ATF6, PERK and IRE1, however, XBP1 splicing was the earliest signal that was terminated (Lin et al., Science 2007). Furthermore, ectopic, prolonged expression of XBP1 splicing resulted in more cell survival, indicating an importance of XBP1 in cell fate. Since we now have an opposing nuclease activity of IRE1, determining the kinetics of ER localized mRNA decay would be critical for determining IRE1's role in cell fate during the UPR. For example, ER localized mRNA decay may only be transiently activated at the start of ER stress while XBP1 splicing persists allowing it to prevent cell death. The more interesting possibility is that ER localized mRNA decay persists even when XBP1 splicing is terminated. This would suggest a mechanism for explaining cell death during prolonged ER stress. Li and colleagues (2010) show that XBP1 splicing, in conjunction with IRE1 phosphorylation and foci formation, declines after 6-8 hrs during activation of UPR with

either Thapsigargin or Tunicamycin. Although we also see that ER localized mRNAs are degraded during the first 6 hrs of UPR activation, we see that the levels of mRNA remain low up to 24 hrs, suggesting that even though IRE1 is inactivated, levels of ER localized mRNAs such as insulin are still missing, which may lead to defective secretion. A situation such as this has implications in disease states where chronic ER stress is an issue such as in the case of high fat diets and chronic glucose exposure during diabetes. Currently, IRE1 has been implicated in the development of diabetes through both death of insulin secreting pancreatic β cells and through insulin resistance. Furthermore, a compilation of several studies suggest that different activities of IRE1 play distinctive roles in the pathogenesis of diabetes. (Lipson et al., Plos One 2008; Oslowski et al., Curr Opin Cell Biol 2010; Lipson et al., Cell Metab 2006)

Pancreatic beta cells are professional secretory cell responsible for secreting insulin when stimulated by glucose, and a key factor in development of diabetes is loss of function and death of β cells. IRE1 has been shown to contribute to cell death in pancreatic beta cells, in particular, chronic high glucose levels have been found to activate the UPR and lead to β cell dysfunction and death (Lipson et al., Cell Metab 2006). Interestingly, these conditions are reported to lead to a degradation of insulin mRNA in an IRE1 dependent manner, indicating degradation of ER localized mRNAs (Lipson et al., Plos One 2008), however, high glucose did not result in the splicing of XBP1 (Lipson et al., Cell Metab 2006), suggesting a physiological condition may exist that differentiates between IRE1 active modes by degrading ER localized mRNAs but not XBP1 splicing. One important problem we can answer using this system is the difference between transient ER stress and chronic ER stress if they are indeed correct. Specifically, in pancreatic β cells, how do each of IRE1's activities react to transient and chronic ER stress. Seemingly, the physiological function of the UPR is to deal with transient perturbations in ER homeostasis, since the main purpose of the UPR is to restore ER function and folding capacity. This function is consistent with roles associated with XBP1. However, prolonged ER stress such

as in the case of chronic high glucose, lead to degradation of insulin mRNA and cell death, roles consistent with ER localized mRNA decay. Conditions of transient ER stress may lead to the XBP1 pathway overcoming ER localized mRNA decay while, if the stress is prolonged, we may see that only the ER localized mRNAs are degraded while XBP1 is not spliced, driving the cells to apoptosis. This can be determined experimentally by treating pancreatic β cells under conditions of both transient ER stress and prolonged ER stress and determine activation of both pathways. Furthermore, we can manipulate these by activation of only XBP1 through kinase inhibitiors which activate splicing but not ER localized mRNA degradation and hypothetically increase cell survival. Conversely, treating with quercetin and inhibiting with Irestatin results in only activation of ER localized mRNA decay leading to cell death. Therefore, developing a targeted IRE1 activator that can specifically activate XBP1 but not ER mRNA decay, may be used to prevent diabetes in patients exhibiting signs of pancreatic β cell death.

IRE1 has also been implicated in progression of diabetes through obesity and insulin resistance, and in this case, the kinase activity of IRE1 may be important for this phenotype. Insulin resistance results from the inability of cells to sense and responds to blood insulin levels. Mice fed a high fat diet were shown to have the UPR activated in liver cells (Ozcan et al., Science 2004), also, JNK was found to be phosphorylated in an IRE1 dependent manner which led to phosphorylation of insulin receptor substrate 1 (IRS1) which led to reduced insulin receptor signaling. Presumably, this mode of IRE1 activation comes from its kinase function since TRAF2 association with IRE1 during ER stress leads to JNK activation (Urano et al., Science 2000). Again, development of an targeted IRE1 theraputic that only binds to the specific kinase pocket of IRE1 and not other kinases, will result in prevention of the kinase mediated insulin resistance, while also activating XBP1 which allows the cells to survive. Therefore, being able to pharmacologically manipulate each of these activities gives us an instrument to dissect IRE1's involvement in the pathology of diabetes and allow us to develop targeted therapeutics.

One physiological area where IRE1 activity is critical in B cell development. Both IRE and XBP1 are required for plasma cell development and XBP1 has been found to be activated in early B cell development (Brunsing et al., JBC 2008; Zhang et al., JCI 2005). However, however the separation of individual IRE1 activities is not clear, so manipulation of each activity may yield interesting insights. For example, in B cell lymphopoesis, cells lacking the cytosolic portion of IRE1 were not able to fully develop into plasma cells, however, a kinase dead or nuclease dead mutant of IRE1 was able to develop to Ig secreting mature B cells (Zhang et al., JCI 2005). This shows that the presence of the cytoplasmic domain of IRE1 is necessary, but not the kinase or nuclease activities. Since our finding suggests that IRE1 posses multiple modes of activation, this system may require a unique manner of IRE1 activation. Using conditions to manipulate IRE1's nuclease activities, we can test which activity is involved in differentiation of B cells. We know that XBP1 splicing is required for B cell development, but we still do not know if ER localized mRNA decay is involved. It would seem counterproductive for a B cell to degrade ER localized mRNA when trying to expand the ER and increase protein folding capacity, so there is a possibility that during B cell development, only XBP1 is active and not ER localized mRNA decay. We can determine this by monitoring XBP1 splicing and degradation of ER localized mRNAs during B cell development. If only XBP1 is active, then we can ectopically express ER localized mRNA decay by activating with Quercetin, or specifically activate ER localized mRNA decay and inhibit XBP1 splicing by treating with Quercetin and inhibiting with Irestatin. This will demonstrate the role of each pathway in determining B cell fate during differentiation.

Misregulated IRE1 function has been implicated as a key factor in the development of multiple myeloma, a type of cancer resulting from the malignant transformation of plasma cells. XBP1 was initially found to be overexpressed in multiple myeloma cells (Reimold et al., J Exp Med 1996) and subsequently, patients with this disease expressed high levels of spliced XBP1

(Carrasco et al., Cancer Cell 2007). Interestingly, mice that were engineered to overexpress spliced XBP1 specifically in B cells, developed symptoms similar to those seen in human multiple myeloma patients such as bone lesions (Carrasco et al., Cancer Cell 2007). Also proteasome inhibitors such as Bortezomib was shown to inhibit XBP1 splicing and resulted increased ER stress induced apoptosis in myeloma cell lines (Lee et al., PNAS 2003). In fact, irestatin was initially developed as a potential treatment since it exhibits cytotoxic effect in human multiple myeloma (Papandreou et al., Blood 2010). Since we are able to manipulate differential IRE1 activities, one implication is that we can further drive the survival or apoptotic pathways by pharmacological manipulation, and in the case of multiple myeloma, for example, combined treatment with irestatin and quercetin should result in exclusive inhibition of XBP1 while activating ER localized mRNA decay. Since high levels of spliced XBP1 maintain survival in myeloma cells, specific inhibition of XBP1 while degrading ER localized RNAs through ER localized mRNA decay should result in higher rates of cell death. Using quercetin and irestatin is useful to show the concept of differential inhibition of IRE1, however this can be used to develop more potent agents or derivatives which show the same effects but at lower concentrations.

Multiple Modes of IRE1 Activation

Regulation of ER homeostatis has been found to have wide-ranging consequences on cellular function including transcriptional and translational regulation, activation of several signal transduction pathways, and determination of cell fate. The ER components IRE1, PERK, and ATF6 are responsible for initiating multiple signals which is inclusively called the UPR. However, initial studies of the UPR revealed opposing effects in areas such as cell fate. For example, general UPR activation resulted in activation of both pro and anti-apoptotic pathways. Like any other complex pathway, UPR activation consists of competing signals from individual components, so determination of these individual signals allow for a more precise understanding

of the ER stress response. IRE1 has been characterized to have distinct activities which have separate cellular consequences. Activation of IRE1's kinase function result in initiation of signal transduction pathways, and is independent of IRE1' nuclease function. Also, two distinct RNase modes have been identified for IRE1, initiation of a non-conventional splicing of a cytoplasmic mRNA coding for a bZIP transcription factors and ER localized mRNA decay. Here, we have revealed novel consequences for each of these activities of IRE1. Furthermore, we have identified tools which manipulate the individual activities of IRE1, allowing for a more precise understanding of the ER stress response.

Activation of IRE1's kinase domain has been linked to activation of several cellular pathways. During ER stress, the adaptor protein TRAF2 was found to associate with the cytoplasmic domain of IRE1 and activate cJun N-terminal Kinase (JNK) (Urano et al., Science 2000), additionally, IRE1 missing the nuclease domain was still able to bind TRAF2, indicating that this activity is independent of IRE1's nuclease activity. TRAF2 binding has also been shown to activate Apoptosis Signal-regulating Kinase 1 (ASK1) which contributes to cell death in neurons (Nishitoh et al., Genes Dev, 2002). Here, we show that IRE1 is able to maintain basal IKK activity and ensure efficient NF-κB activation during ER stress. This activity of IRE1 was found to be independent of the nuclease function of IRE1 since a nuclease dead IRE1 rescues the decrease in NF-κB activation. This finding adds evidence to the idea that IRE1 is able to interact and maintain cellular proteins in a homeostatic manner. One example where this is illustrated is the relationship between IRE1 and Bax/Bak, two proteins involved in general apoptotic signaling. Bax/Bak was found to interact with IRE1 in the ER and maintain its function since cells lacking Bax/Bak have deficient IRE1 activation and UPR signaling (Hetz et al., Science 2006). In a similar manner, IKK function is maintained by IRE1 and has consequences on general NF-κB activation since cells lacking IRE1 but not PERK have defective TNFa induced NF-κB signaling. This adds to the importance of the ER and UPR signaling as central players in general stress

responses. Furthermore, we reveal a function for NF-κB activation during the UPR by increasing transcription of a subset of UPR target genes including ER chaperones such as BiP. This shows that signaling from the kinase of IRE1 has some contribution to the UPR transcription profile, independent of XBP1 activation demonstrating an even more diverse role for IRE1.

The most well-characterized function of IRE1 is its ability to non-conventionally splice mRNA of a bZIP transcription factor. In budding yeast, IRE1 splices a 252nt intron from Hac1, while in metazoans, a 26nt intron is excised from XBP1. Activation of the resulting transcription factor results in initiation of a gene transcription profile that has effects on multiple cellular functions. This method of transcription factor activation has also been conserved from yeast to humans, indicating its evolutionary importance. However, while IRE1 was conserved, there has been variation of IRE1's substrate. Initial studies of Hac1 and XBP1 show that Hac1 has a long intron and metazoan substrates have a short intron leading to the assumption that other species of yeast have substrates similar to budding yeast (S. cerevisiae). Upon close examination of IRE1 substrates, we find that several yeast species have a short intron similar to XBP1, however, we find divergent secondary structure of the 3' splice site between S. cerevisiae Hac1, yeasts with Hac1 containing a small intron, and XBP1. In fact, our structural studies of the interaction between IRE1 and its substrate indicate a divergence in the 3' splice site recognition by IRE1. Conversely, the 5' splice site structure appears to be conserved through species, and correlating with this, IRE1 recognition of the 5' splice site is conserved since both yeast and human IRE1 are able to cleave the 5' splice site of both Hac1 and XBP1. This study also demonstrates an asymmetric mode of IRE1 activation since IRE1 is able to differentially recognize the 5' and 3' splice sites of its substrate. This finding allows for the possibility that IRE1 is able to cleave other substrates, and in fact, may help explain the specificity of ER localized mRNA decay which cleaves at sites similar to known Hac1 and XBP1 splice site loops (Han et al., Cell 2009). Also,

the asymmetric manner in which IRE1 cleaves its substrate allows for distinct modes of activation and opens the possibility for IRE1 being differentially regulated.

Recently, a distinct nuclease activity of IRE1, regulated IRE1 dependent decay of ER localized mRNA, has been identified which results in cleavage of ER localized mRNAs in drosophila and mammalian systems (Hollien et al., JCB 2009; Han et al., Cell 2009). Interestingly, ER localized mRNA decay and XBP1 splicing was able to be differentiated by a chemical-genetic system where a mutation in IRE1's kinase pocket (I642G) prevents ATP from binding, however, another small molecule 1NM-PP1, is able to bind to the genetically modified pocket but not able to transfer phosphate. When IRE1 is activated in this manner, only XBP1 splicing occurs. These studies were done using immunoprecipitated IRE1 from cells, allowing for the possibility that an associated nuclease may be the factor that catalytically cleaved ER localized mRNAs. However, we were able to directly recapitulate this effect in vitro using a mutated yeast IRE1 where a mutation of the kinase (D828A) is able to bind to ATP, but not able to transfer phosphate. The D828A mutant of IRE1 was only able to efficiently cleave Hac1, but not ER localized mRNAs. Furthermore, we demonstrate that Quercetin (Qr), a naturally occurring favanol, is able to activate both Hac1/XBP1 splicing activities of IRE1 and ER localized mRNA decay. Interestingly, Qr activation of ER localized mRNA decay does not require kinase activity since the D828A kinase dead mutant is able to induce ER localized mRNA decay when activated by Qr. The fact that there are naturally occurring compounds that can activate IRE (Wiseman et al., Mol Cell 2010) suggest that in physiological conditions, the nuclease activities of IRE1 may be activated regardless of the state of the ER. Aside from upregulating ER chaperones, XBP1 activation by IRE1 affects myogenic differentiation, immune cell development, hepatic lipogenesis, and determination of cell fate (Acosta-Alvear et al., Mol Cell 2007; Lee et al., Science 2008; Iwakoshi et al., Nat Immunol 2003), making XBP1 splicing by IRE1 more than just a response that increases folding capacity of the ER. Regulation of IRE1 activities by

naturally occurring ligands may provide an explanation of how IRE1 is activated in the absence of overt ER stress such as in the case of B-cell differentiation (Zhang et al., JCI 2005). Furthermore, we demonstrate that we can pharmacologically manipulate IRE1's distinct activites using an IRE1 inhibitor, irestatin. We find that irestatin specifically inhibits Hac1/XBP1 activation, and not ER localized mRNA decay, when IRE1 is activated through Qr. This approach has high potential value as compared to the chemical-genetic approach since the previous method requires genetic manipulation of an organism to study IRE1's function. Using pharmacological means, we can study distinct IRE1 functions in organisms by simple treatment, making this approach faster. In addition, pharmacological manipulation also allows IRE1 to be a viable therapeutic target for conditions including diabetes and cancer.

REFERENCES

Acosta-Alvear, D., Zhou, Y., Blais, A., Tsikitis, M., Lents, N.H., Arias, C., Lennon, C.J., Kluger, Y., and Dynlacht, B.D. (2007). XBP1 controls diverse cell type- and condition-specific transcriptional regulatory networks. Mol Cell *27*, 53-66.

Brunsing, R., Omori, S.A., Weber, F., Bicknell, A., Friend, L., Rickert, R., and Niwa, M. (2008). B- and T-cell development both involve activity of the unfolded protein response pathway. J Biol Chem *283*, 17954-17961.

Carrasco, D.R., Sukhdeo, K., Protopopova, M., Sinha, R., Enos, M., Carrasco, D.E., Zheng, M., Mani, M., Henderson, J., Pinkus, G.S., Munshi, N., Horner, J., Ivanova, E.V., Protopopov, A., Anderson, K.C., Tonon, G., and DePinho, R.A. (2007). The differentiation and stress response factor XBP-1 drives multiple myeloma pathogenesis. Cancer Cell *11*, 349-360.

Corbett, J.A. (2006). Insulin biosynthesis: the IREny of it all. Cell Metab *4*, 175-176.

Han, D., Lerner, A.G., Vande Walle, L., Upton, J.P., Xu, W., Hagen, A., Backes, B.J., Oakes, S.A., and Papa, F.R. (2009). IRE1alpha kinase activation modes control alternate endoribonuclease outputs to determine divergent cell fates. Cell *138*, 562-575.

Hetz, C., Bernasconi, P., Fisher, J., Lee, A.H., Bassik, M.C., Antonsson, B., Brandt, G.S., Iwakoshi, N.N., Schinzel, A., Glimcher, L.H., and Korsmeyer, S.J. (2006). Proapoptotic BAX and BAK modulate the unfolded protein response by a direct interaction with IRE1alpha. Science *312*, 572-576.

Hollien, J., Lin, J.H., Li, H., Stevens, N., Walter, P., and Weissman, J.S. (2009). Regulated Ire1-dependent decay of messenger RNAs in mammalian cells. J Cell Biol *186*, 323-331.

Hu, C.C., Dougan, S.K., McGehee, A.M., Love, J.C., and Ploegh, H.L. (2009). XBP-1 regulates signal transduction, transcription factors and bone marrow colonization in B cells. Embo J *28*, 1624-1636.

Lee, A.H., Iwakoshi, N.N., Anderson, K.C., and Glimcher, L.H. (2003). Proteasome inhibitors disrupt the unfolded protein response in myeloma cells. Proc Natl Acad Sci U S A *100*, 9946-9951.

Lin, J.H., Li, H., Yasumura, D., Cohen, H.R., Zhang, C., Panning, B., Shokat, K.M., Lavail, M.M., and Walter, P. (2007). IRE1 signaling affects cell fate during the unfolded protein response. Science *318*, 944-949.

Lipson, K.L., Ghosh, R., and Urano, F. (2008). The role of IRE1alpha in the degradation of insulin mRNA in pancreatic beta-cells. PLoS One *3*, e1648.

Nishitoh, H., Matsuzawa, A., Tobiume, K., Saegusa, K., Takeda, K., Inoue, K., Hori, S., Kakizuka, A., and Ichijo, H. (2002). ASK1 is essential for endoplasmic reticulum stress-induced neuronal cell death triggered by expanded polyglutamine repeats. Genes Dev *16*, 1345-1355.

Ozcan, U., Cao, Q., Yilmaz, E., Lee, A.H., Iwakoshi, N.N., Ozdelen, E., Tuncman, G., Gorgun, C., Glimcher, L.H., and Hotamisligil, G.S. (2004). Endoplasmic reticulum stress links obesity, insulin action, and type 2 diabetes. Science *306*, 457-461.

Papandreou, I., Denko, N.C., Olson, M., Van Melckebeke, H., Lust, S., Tam, A., Solow-Cordero, D.E., Bouley, D.M., Offner, F., Niwa, M., and Koong, A.C. Identification of an Ire1alpha endonuclease specific inhibitor with cytotoxic activity against human multiple myeloma. Blood.

Reimold, A.M., Ponath, P.D., Li, Y.S., Hardy, R.R., David, C.S., Strominger, J.L., and Glimcher, L.H. (1996). Transcription factor B cell lineage-specific activator protein regulates the gene for human X-box binding protein 1. J Exp Med *183*, 393-401.

Urano, F., Wang, X., Bertolotti, A., Zhang, Y., Chung, P., Harding, H.P., and Ron, D. (2000). Coupling of stress in the ER to activation of JNK protein kinases by transmembrane protein kinase IRE1. Science *287*, 664-666.

Wiseman, R.L., Zhang, Y., Lee, K.P., Harding, H.P., Haynes, C.M., Price, J., Sicheri, F., and Ron, D. Flavonol activation defines an unanticipated ligand-binding site in the kinase-RNase domain of IRE1. Mol Cell *38*, 291-304.

Zhang, K., Wong, H.N., Song, B., Miller, C.N., Scheuner, D., and Kaufman, R.J. (2005). The unfolded protein response sensor IRE1alpha is required at 2 distinct steps in B cell lymphopoiesis. J Clin Invest *115*, 268-281.